BIOLANALYTICAL METHODS DEVELOPMENT FOR THE STUDY OF REGULATION IN TRANSCRIPTION ELONGATION

Robert Daniel Brodnick

A thesis submitted to the faculty of the University of North Carolina at Chapel Hill in partial fulfillment of the requirements for the degree of Doctor of Philosophy in the Department of Chemistry.

Chapel Hill
2008

Approved by:

Advisor: Dr. Dorothy Erie

Dr. Linda Spremulli

Dr. James Jorgenson

Dr. Richard Superfine

Dr. Michael Ramsey

ABSTRACT

ROBERT D. BRODNICK: Bioanalytical Methods Development for the Study of Regulation in Transcription Elongation
(Under the direction of Dr. Dorothy A. Erie)

Previous biochemical data has shown that transcription by multisubunit RNA polymerases is heavily regulated by the interactions between the ternary elongation complex and catalytic and non-catalytic templated NTPs. While kinetics studies and crystal structures have aided in the generation of mechanistic models for nucleotide incorporation with stalled elongation complexes (SEC), quantitative observation of NTP-SEC binding properties has not been achieved. The primary limitation in NTP-SEC binding analysis is the lack available methods capable of measuring binding when only low nanomolar amounts of protein acceptor (in this case, the SECs) are available.

In this work, I developed a number of purification techniques for the study of NTP-SEC binding, including novel approaches in electrodialysis, microfiber dialysis, gel electrophoresis and other phase separations. I report that some of these methods show promise for universal application in small molecule-protein binding assays. One method termed reversible matrix assisted phase partitioning (RevMAPP) facilitated the direct capture of NTP-SEC occupancies (stoichiometries), and many other binding properties. I was able to increase the signal to noise ratio in radiochemical binding analyses by using a monomeric avidin coated matrix to synthesize and purify biotinalated SECs.

I have determined that subsequent to SEC purification, a high occupancy of non-templated nucleotides remain bound to the enzyme, exhibiting very slow passive (non-

competitive) rates of dissociation. Parts of our previous mechanistic models for regulation in transcription elongation by allosteric NTP binding will need minor adjustments to fit these new data.

In addition to NTP-SEC binding studies and method development, I present a myriad of glass surface preparation protocols for the purpose of conducting atomic force microscopy on multimeric biological complexes. Conducting biological AFM on glass will streamline the combination of high resolution single molecule fluorescence (SMF) techniques with AFM to bolster the structure-function information we are capable of currently capturing with the each microscopy technique by itself. Molecular alignment on DNA on glass is the primary limitation in conducting structure-function AFM studies. For AFM imaging on glass, I present a minimal force deposition method for preparing DNA samples in a way that does not stretch or align the DNA molecules. I present the first high resolution AFM images of protein-DNA complexes deposited onto smoothed glass under physiological conditions.

For Mom and Dad, who gave me everything and asked for nothing in return.

ACKNOWLEDGEMENTS

I would first like to thank my advisor, Dorothy Erie, for giving me a fair shake when others would not. I have learned many valuable lessons under her guidance and I have her to thank for many of the opportunities before me. Dorothy was always willing to help me when I needed it, yet she gave me the freedom to creatively explore in my research. I also appreciate her honesty for when my wanderings lead me in the wrong direction. Thank you.

I would also like to recognize my committee and several others of the faculty, many of whom are directly responsible for giving me the opportunity to succeed in graduate school when I faced adversity.

I owe a debt of gratitude to my Erie lab colleges as well; you are a wonderful group of people to work alongside. In particular, I would like to thank Candi Cunningham for critically editing many of my manuscripts, and of course for making the best pot pie in the world. Erika Borgerding conducted outstanding undergraduate researcher under my direction; some of the results in my AFM chapter are thanks to her. Scott Kennedy has also been a valuable college in science, roommate and friend. I may not have gotten interested in transcription if it were not him. *You*, Scott, are number one.

Finally, thanks to those whose opinions matter most to me. I especially thank Kara Diamond for her unending support and unconditional care. My family falls in the same category. I truly appreciate everything, and I am just as proud of you.

TABLE OF CONTENTS

LIST OF TABLES

LIST OF FIGURES

LIST OF ABBREVIATIONS

CHAPTER 1: AN INTRODUCTION TO TRANSCRIPTION.....1

1.1 Introduction.....1

1.1.1 Transcription……..……..……3

1.1.2 The Transcription Cycle.....3

1.1.3. RNAP and Elongation Complex Structure.....6

1.1.4 The Conformational States of Ternary Elongation Complexes.....12

1.1.5 The Regulation of States in Transcription Elongation by External Factors.....14

1.1.6 The Hierarchy of Pathways in Transcription Elongation.....16

1.1.7 NTP Incorporation Mechanisms.....18

1.1.8 The Putative Location and Function of the Allosteric Site.....22

1.2 Development of Bioanalytical Methods for Transcription: A Project Précis..24

1.2.1 Novel Methods for Capturing NTP-Elongation Complex Binding Information.....24

BIBLIOGRAPHY.....27

CHAPTER 2: BACKGROUND METHODS....32

2.1 Ligand Binding....32

2.1.1 The Binding Function....33

2.1.2 Interpreting Binding Data....34

2.1.3 Non-Specific Adsorption....35

2.1.4 The Limitations of Common Binding Techniques in Transcription Elongation....37

2.1.5 Common Binding Assays....37

2.1.5.1 Phase Separations....38

2.1.5.2 Spectral Studies....39

2.1.5.3 Mobility Methods....40

2.1.5.4 Calorimetric Measurements....41

2.1.5.5 Biosensors, Competitive Binding Assays and Ion Selective Electrodes....42

2.1.6 Previous Work Attempts to Assay NTP-SEC Binding....42

2.2 Atomic Force Microscopy....43

2.2.1 AFM Function....43

2.2.2 Selected Previous RNAP-DNA Complex Analyses with AFM....46

2.2.3 Physical Limitations of AFM Imaging....49

BIBLIOGRAPHY....51

CHAPTER 3: CHARATERIZATION OF NUCLEOTIDE – TRANACRIPTION ELONGATION COMPLEX INTERACTION....54

3.1 NTP-TEC Binding and Regulation in Transcription Elongation....54

3.1.1 Previous NTP-SEC Ratio Assays....57

3.2 Methods....68

3.2.1 RevMAPP Method: SEC Synthesis and Purification.....58

3.2.2 Determination of the Minimum Required Washes.....61

3.2.3 Determination of NTP-SEC Stoichiometries.....61

3.2.4 Determination of NTP-SEC Dissociation Rates.....61

3.2.5 Competition Assays Using dNTPs.....64

3.2.6 Detection of NTP Displacement Related to Catalysis.....66

3.2.7 GTP Binding Affinity Assay.....68

3.3 Results.....70

3.3.1 Approximately 7-10 Washes are Required to Remove Non-Specific Background.....70

3.3.2 The Tight NTP-SEC Stoichiometry is Roughly 2.....73

3.3.3 The NTP-SEC Rates of Dissociation are Slow.....75

3.3.3 ATP, GTP and UTP are Displaced Differently by dATP and dCTP.....79

3.3.4 Catalysis Completely Displaces UTP and ATP, but not GTP, from Purified SECs.....82

3.3.4 GTP Binds to Purified SECs at Equilibrium with an Affinity of 26μM.....86

3.4 Discussion.....88

3.4.1 The RevMAPP Protocol is a Major Addition to the Transcription Analysis Toolbox.....88

3.4.2 UTP is Locked into the Catalytic Site in the Absence of CTP.....90

3.4.3 ATP May Occupy the Catalytic Site of SECs not binding UTP.....97

3.4.4 GTP Binding May Be Magic.....98

3.5 Future Direction with NTP-SEC Binding Dynamics.....101

BIBLOGRAPHY.....103

CHAPTER 4: DEVELOPMENT OF NOVEL HIGH EFFICIENCY PHASE SEPARATIONS FOR LIGAND BINDING STUDIES.....106

4.1 The Development of Novel Phase Separations.....106

4.1.1 Small Volume Electrodialysis.....107

4.1.2 Reverse Microfiber Dialysis.....107

4.1.3 Short Travel Gel Electrophoresis.....109

4.2 Materials and Methods.....110

4.2.1 SVED Design.....110

4.2.2 Reverse Microfiber Dialysis Design.....112

4.2.3 STaGE Design.....114

4.3 Novel Method Characterizations.....116

4.3.1 SVED Experimental and Results.....116

4.3.2 Reverse Microfiber Dialysis Experimental and Results.....120

4.3.3 STaGE Experimental and Results.....124

4.4 Novel Phase Separation Discussion.....131

4.4.1 SVED.....131

4.4.2 Microfiber Dialysis.....132

4.4.3 STaGE.....136

4.4.4 Future Directions in Novel Phase Separation.....137

BIBLIOGRAPHY.....139

CHAPTER 5: ATOMIC FORCE MICROSCOPY OF BIOLOGICAL MARCOMOLECUAR COMPLEXES DEPOSITED ONTO ULTRA SMOOTH GLASS.....141

5.1 Addressing a Limitation of Atomic Force Microscopy.....141

5.1.1 AFM Imaging of DNA on Mica.....144

5.1.2 Imaging DNA with AFM on Glass.....144

5.1.3 Previous Work Involving AFM of DNA on Glass.....145

5.2 Depositing DNA onto Glass.....147

5.2.1 The Minimal Force Deposition and Rinsing Method.....147

5.2.2 Minimal Force Method Results.....150

5.2.3 Minimal Force Method Discussion.....152

5.3 DNA on Smoothed Glass.....154

5.3.1 Glass Modification Protocols.....154

5.3.1.1 Sonication.....154

5.3.1.2 Chemical Modifications.....155

5.3.1.3 Plasma Cleaning.....155

5.3.1.4 PVK Polymer Coating.....156

5.3.2 Surface Characterization: Roughness and DNA Affinity.....156

5.3.2.1 Corning No1. Out-of-the-Box.....159

5.3.2.2 Sonication.....159

5.3.2.3 Plasma Cleaning.....161

5.3.2.4 PVK Polymer Coating.....163

5.3.2.5 Chemical Modifications.....165

5.3.2.6 O_2-Plasma Cleaned TMS Monolayers.....167

5.3.2.7 Combined Cleaning.....169

5.3.3 Discussion of Glass Surface Preparations.....170

5.3.4 Glass Surface Preparation Conclusions.....173

5.4 The First High Resolution AFM Images of Unstretched Protein-DNA Complexes Deposited onto Smoothed Glass under Physiological Conditions....174

5.4.1 Sample Preparation....175

5.4.2 Results....175

5.4.3 Discussion....177

5.5 Topics Unique to AFM on Glass....178

5.5.1 A Growing Problem: Static Charges Can Accumulate with Oscillating AFM on Glass....178

5.5.2 Phase Imaging: Seeing Samples Differently....181

5.5.2.1 Phase Imaging on Glass....182

5.5.2.2 Our use of Phase Imaging on Glass....182

5.5.2.3 The Future Use of Phase Imaging on Glass....184

5.5.3 The Future of Glass Preparation Protocols....184

5.5.4 The Future of AFM on Glass....186

BIBLIOGRAPHY....187

APPENDIX A: SOURCES OF PROTEINS AND TEMPLATE DNA 190

A.1 Proteins and DNA....190

BIBLIOGRAPHY....191

APPENDIX B: RevMAPP CONTROLS....192

B.1 Boiling Control....192

B.2 RNAP(-) Controls....194

B.4 Staggered Gel Loading and Transcript Distribution Controls....197

B.4 Equilibrium Binding Control....200

BIBLIOGRAPHY....201

LIST OF TABLES

Table 3.1 NTP:SEC Stoichiometry Consensus.....74

Table 3.2 The Passive and Active Dissociation Rate of NTP-SEC Complexes.....78

Table 3.3 Competition dNTPs Selectively Displace NTPs from SECs.....81

Table 5.1 Summary of Methods that Smoothed Corning No.1 Glass Cover Slips.....158

LIST OF FIGURES

Figure 1.1 The Central Dogma of Molecular Biology.....2

Figure 1.2 The Transcription Cycle.....5

Figure 1.3 Space Filled Model of the *T. thermophilus* Elongation Complex Highlighting the "Crab Claw" Structure Made by the β and β' Subunits.....9

Figure 1.4 Partial Space Filled Structure of the *T. thermophilus* Elongation Complex.....10

Figure 1.5 Important mobile structures in the catalytic core of *S. cerevisiae RNAP* II Elongation Complexes.....11

Figure 1.6 Ternary Complex Conformations Governing the States of Elongation.....17

Figure 1.7 The Multitude of Pathways Followed During Transcription Elongation.....21

Figure 1.8 A Kinetic Model for NTP Incorporation Based on the Rapid Equilibrium on the Pre- and Post-translocated States.....20

Figure 1.10 The Putative Allosteric Site is Comprised of Typical NTP Binding Site Motifs.....23

Figure 2.1 Non-specific Adsorption Noise can Limit Binding Analysis.....36

Figure 2.2 Schematic of Atomic Force Microscopy.....45

Figure 2.3 Examples of Direct Structural Analysis of Transcription Complexes with AFM.....47

Figure 2.4 Physical Limitations in Topographic Imaging by AFM.....50

Figure 3.1 A Cartoon Model Showing Multiple Template Dependant NTP Binding Locations....56

Figure 3.2 The Fundamental Steps of the RevMAPP Protocol....60

Figure 3.3 Diagram of NTP-SEC Dissociation Rate Experiments....63

Figure 3.4 Diagram of the dNTP competitive Assay....65

Figure 3.5 Diagram of CTP Catalysis Assay for NTP Displacement....67

Figure 3.6 Diagram of the GTP-SEC Binding Affinity Assay....69

Figure 3.7 RevMAPP Removes Non-Specific Background in about 7 Washes....71

Figure 3.8 Direct Calculation of All Non-Templated NTP-SEC Stoichiometries....73

Figure 3.9 GTP-SEC Ratio Decay is Unaffected by a Cold Competitor....76

Figure 3.10 ATP-SEC Ratio Decay is Affected by the Presence of Cold Competitor....77

Figure 3.11 An Example of a dNTP Competitive Assay: GTP is Displaced by dCTP....80

Figure 3.12 UTP is Displaced Due to a Single Nucleotide Incorporation Event; GTP is only Partially Displaced....83

Figure 3.13 Partial Catalysis Equivalently Displaces ATP from SECs....84

Figure 3.14 ATP Completely Dissociates from SECs during Catalysis and GTP Does Not....85

Figure 3.15 The GTP-SEC Dissociation Constant is 26μM....87

Figure 3.16 Access to the Secondary Channel is Regulated by the Trigger Loop....94

Figure 3.17 A Previously Proposed Model for Activated State Misincorporation....95

Figure 3.18 A New Proposed Mechanism for NTP Misincorporation....96

Figure 4.1 Small Volume Electrodialysis Design....111

Figure 4.2 The Reverse Microfiber Dialysis Apparatus....113

Figure 4.3 The Short Travel Gel Electrophoresis Design....115

Figure 4.4 Electrical Current Aids in the Mass Transport of Nucleotides
to the Surface of a Semi-permeable Membrane.....119

Figure 4.5 Reverse Microfiber Dialysis Repeatably Purifies a
Nucleotide Diluate Solution in just 4 to 5 Minutes.....122

Figure 4.6 Microfiber Dialysis Purification of SECs is
More Effective than Magnetic Affinity Beads.....123

Figure 4.7 Electrophoretic Filtering by Agarose and Polyacrylamide STaGE Gels.....126

Figure 4.8 Polyacrylamide STaGE Captures ATP bound to *Taq*MutS.....128

Figure 4.9 ATP-*Taq*MutS Binding Analysis Determined by STaGE Purification.....130

Figure 4.9 Comparison of Microfiber and Well Design Dialysis Geometries.....134

Figure 5.1 One Strategy for Combined AMF-SMF Microscopy.....143

Figure 5.2 The Minimal Force Rinsing Protocol.....149

Figure 5.3 The Minimal Force Deposition Method Does Not
Stretch or Align DNA on Ethanol Sonicated Glass.....151

Figure 5.4.The Nanoscale Surface Effect of Sonicating
Corning No.1 in Absolute Ethanol.....160

Figure 5.5 Surface Heterogeneity Appears with Longer
O_2-Plasma Cleaning Exposure.....162

Figure 5.6 Spin Coated PVK on Corning No.1 is Very
Heterogeneous on the Nano-Scale.....164

Figure 5.7 Liquid APTES and HMDS are Microscopically Insoluble.....166

Figure 5.8 TMS Monolayers on Glass are Drastically Changed
with Increasing Exposure to O_2-Plasma.....168

Figure 5.9 The First High Resolution AFM Images of Protein-DNA Complexes
Deposited onto Smoothed Glass Under Physiological Condition.....176

Figure 5.10 An Electrostatic Build Up Between Tip and Surface
can be Deleterious to AFM Imaging on Glass.....180

Figure 5.11 Phase Imaging with AFM Selectively Reveals Biological
Constructs and Not Background topography.....183

Figure B.1 Over Boiling Thermally Degrades NTPs.....193

Figure B.2 The RNAP- Control Validates the RevMAPP Protocol.....196

Figure B.3 Simultaneous Analysis of RNA Chain Length
Distribution and NTP-SEC ratios.....198

LIST OF ABBREVIATIONS

%	percent
~	approximately
<	less than
>	greater than
°	degrees
3’	three prime end
^{32}P	radio-active phosphorus isotope (32)
3-D	three dimensional
5’	five prime end
α	alpha
α	alpha phase
α	alpha subunit in RNAP
β	beta subunit in RNAP
β	beta phase
β’	beta prime subunit in RNAP
γ	gamma
μ	solution density
μ	micro
v_s	average fluid velocity
π	pi bond
ρ	solution viscosity

σ	sigma subunit in RNAP
Ω	ohm
ω	omega subunit in RNAP
A	acceptor molecule
A-	acceptor negative control
A	adenosine monophosphate
A	area
AFM	atomic force microscopy
AMPcPP	adenosine-5'-[(α,β)-methyleno]-triphosphate
APTES	3-aminopropyltriethoxysilane
Ar	argon
AS	acceptor-ligand complex
*AS**	acceptor-radiolabeled ligand complex
ATP	adenosine-5'-triphosphate
bp	base pair
BSA	bovine serum albumin
C	Celsius
c	centi
C	cytidine monophosphate
Ci	curie
CISMM	computer-integrated systems for microscopy and manipulation
CTP	cytidine-5'-triphosphate
$\overline{C_A}$	total acceptor concentration

C_S	equilibrium free ligand concentration
$\overline{C_S}$	total ligand concentration
$(\overline{C_s} - C_s)$	equilibrium bound ligand concentration
Da	Dalton
ddI H_2O	distilled deionized water
DE13	DNA with the DE13 sequence
DMF	dimethylfuran
DNA	deoxyribonucleic acid
DSC	differential scanning calorimetry
DTT	dithiotheitol
E. coli	*Escherichia coli*
ED	electrodialysis
EDTA	ethylenediamine tetra-acetic acid
ELISA	enzyme linked immunosorbent assay
EtOH	ethanol
eV	electron volt
FIONA	fluorescence imaging with one nanometer accuracy
FRET	fluorescence resonance energy transfer
g	gram
G	Giga
G	guanosine monophosphate
GFC	gel filtration chromatography
GTP	guanosine-5'-triphosphate

H_2O	water
HEPES	*4*-(2-hydroxyethyl)-1-piperazineethanesulfonic acid
HMDS	1,1,1,3,3,3-hexamethyldisilazane
Hz	hertz
in vitro	outside of a living organism
in vivo	inside of a living organism
ITC	isothermal titration calorimetry
K^+	potassium ion
K_D	dissociation constant
K_M	Michalis-Menten Constant
k_{off}	off rate
k_{on}	on rate
L	characteristic flow path
L	liter
LC/MS	liquid chromatography/mass spectrometry
m	milli
m	meter
M	molar
Mg^{+2}	magnesium ion
$MgCl_2$	magnesium chloride
min	minute
MMR	mismatch repair
mol	mole

MWCO	molecular weight cut off
n	nano
N	iteration number
N_2	nitrogen
NaOAc	sodium acetate
NaOH	sodium hydroxide
NMR	nuclear magnetic resonance
No.	number
NTP	nucleoside-5'-triphosphate
NTP*	radiolabeled nucleoside-5'-triphosphate
NtrC	nitrogen regulatory protein C
O_2	oxygen
OPC	open promoter complex
p	number of binding sites
p	pico
PAGE	polyacrylamide gel electrophoresis
PCR	polymerase chain reaction
PES	polyethersulfone
PET	polyester
PFM	pulsed force mode
ppp	triphosphate
PP_i	pyrophosphate
PTFE	polytetraflouroethelene

PVK	polyvinylcarbazole
r	binding function
Re	Reynolds number
RevMAPP	reversible matrix assisted phase partitioning
RMS	root mean squared
RNA	ribonucleic acid
RNAP	RNA polymerase
RNAP·σ	holoenzyme
RPM	revolutions per minute
Rq	RMS roughness
S	substrate
S°	standard entropy
S. cerevisiae	Saccharomyces cerevisiae
SEC	stalled elongation complex
sec	second
SFM	scanning force microscopy
Si	silicon
SMF	single molecule fluorescence
STaGE	short travel gel electrophoresis
SVED	small volume electrodialysis
T. aquaticus	*Thermus aquaticus*
T. thermophilus	*Thermus thermophilus*
TAE	tris base, acetic acid, EDTA buffer

Taq	*Thermus aquaticus*
TEC	ternary elongation complex or transcription elongation complex
TLC	thin layer chromatography
TMS	trimethylsilyl
U	uridine
UTP	uridine-5’-triphosphate
V	voltage
V	volume
vs	versus
W	watts
w	weight
wt	wild type
XRD	x-ray diffraction

CHAPTER 1:

AN INTRODUCTION TO TRANSCRIPTION

1.1 Introduction

Francis Crick postulated in 1958 (and clarified in 1970) a likely cascade for how information essential to a cell's life is transferred. The central dogma of molecular biology (as he called it) states that genomic DNA is transcribed into RNA *via* a polymeric biochemical alphabet, or sequence (Crick, 1970). Functional three dimensional proteins are then translated from the RNA. DNA can also be replicated for cell division, as can RNA in lower life forms. Figure 1.1 is an illustration of the central dogma. The process of gene expression described by Crick has been unanimously accepted, and can now be considered the central dogma of *life*. In cellular life, the most heavily regulated step in gene expression is transcription.

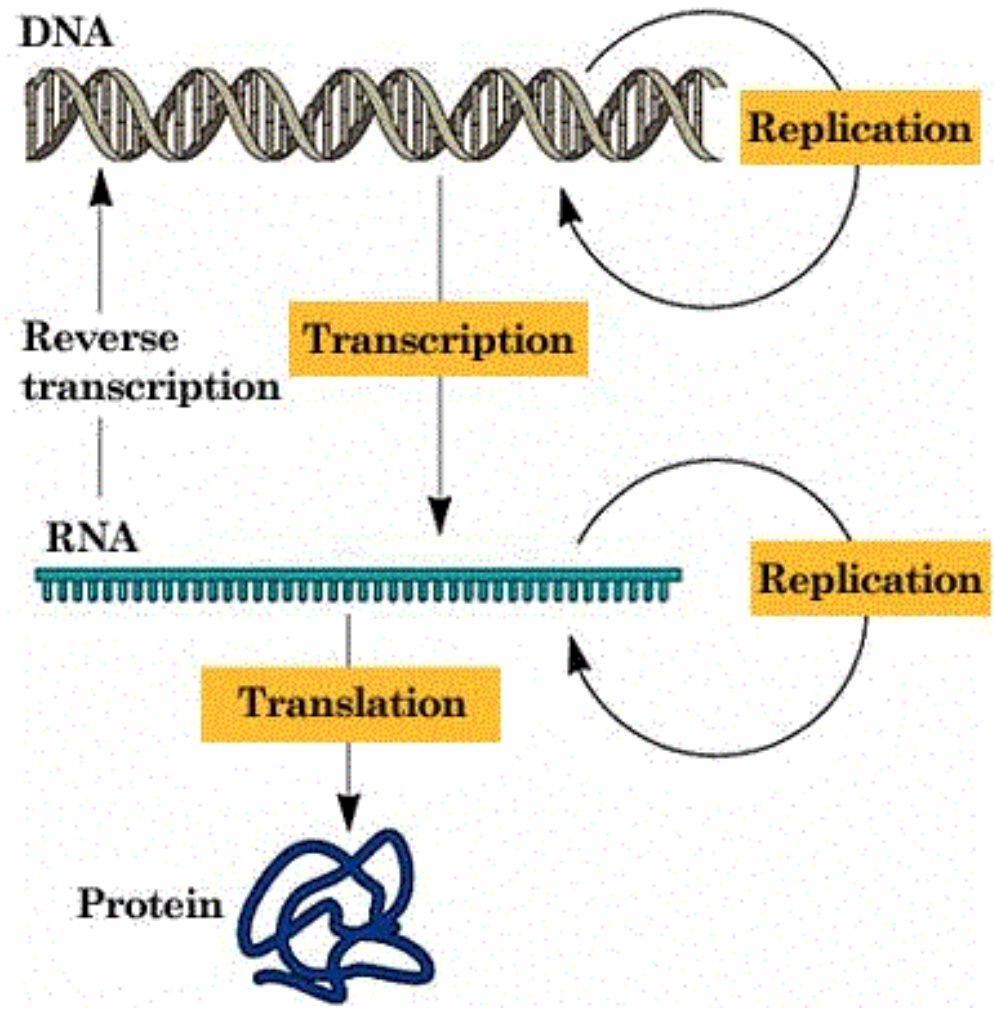

Figure 1.1 The Central Dogma of Molecular Biology. Shown here is the process of gene expression first described by Francis Crick. The central dogma dictates that only the processes in orange boxes can be carried out by life forms. Important to note is that RNA replication only takes place in lower life forms.

1.1.1 Transcription

Transcription is the most complicated and highly regulated process involved in gene expression. Conversion of genomic DNA into RNA is carried out by a highly conserved enzyme called RNA polymerase (RNAP). All cellular life forms primarily use multisubunit RNAPs for transcription, although single subunit RNA polymerases exist in eukaryotic chloroplasts and mitochondria, functioning similarly to DNA polymerases. In prokaryotes, core RNA polymerases are roughly 450 kDa and are comprised of five subunits: two α, β, β' and ω. RNAP reads the template DNA and incorporates nucleotides into a nascent, complementary RNA strand in a 5' to 3' manner. Transcription is governed by a host of RNAP interactions, including nucleoside triphosphate (NTP) binding, interactions with sequence elements in the template DNA and nascent RNA chain, and interactions with several accessory proteins (Chan *et al.*, 1994; Pasman *et al.*, 2000; Severinov, 2000; Artsimovitch *et al.*; Ederth *et al.*, 2002; Erie, 2002; Holmes *et al.*, 2003; Artsimovitch *et al.*, 2004; Perederina *et al.*, 2004). Regulatory interactions cause conformational changes in RNAP that shift transcription between inactive states and various productive states with different kinetics of RNA synthesis and levels of fidelity. The characterization of RNA synthesis mechanisms and regulatory pathways in transcription provides insight into one of the most fundamental processes in cellular life.

1.1.2 The Transcription Cycle

Transcription is characterized by four major phases: Open promoter complex (OPC) formation, initiation, elongation, and termination (Figure 1.2). In prokaryotes, transcription begins with the assembly of the holoenzyme, comprised of the additional subunit sigma (σ),

and core RNAP. OPCs are formed when the holoenzyme binds to the conserved -35 and -10 box promoter sequences on the DNA that indicate the location of a gene to be transcribed. Promoter recognition and binding by RNAP leads to the melting of the DNA into template and non-template strands, forming a transcription bubble. The transcription initiation phase begins with the annealing of an NTP complementary to the first base on the template strand of the gene. Initiation is characterized by the addition of six to nine nucleotides into a nascent RNA chain in a 5' to 3' manner. Until the RNAP releases σ and escapes the promoter region, several rounds of abortive initiation may occur, characterized by the release of short RNA chains (Straney *et al.*, 1987). RNAP enters into the elongation phase when σ dissociates from the enzyme due to interactions with the growing nascent transcript (Kapanidis *et al.*, 2006). Elongation is processive, meaning that if the complex should dissociate prior to reaching the end of the gene, RNAP must rebind σ, locate the promoter, and begin again. Synthesis of the RNA chain continues until the termination phase, marked by the release of the nascent RNA. Termination is sometimes caused by an intrinsic interaction with a RNA hairpin formed at a specific termination sequence. Alternatively, extrinsic termination can occur *via* interactions with a termination factor, Rho (Richardson, 1993). Transcription's total processivity implies that the regulation of RNA synthesis must be efficient to allow the complete transfer of genetic information at a reasonable rate with high fidelity to sustain healthy life.

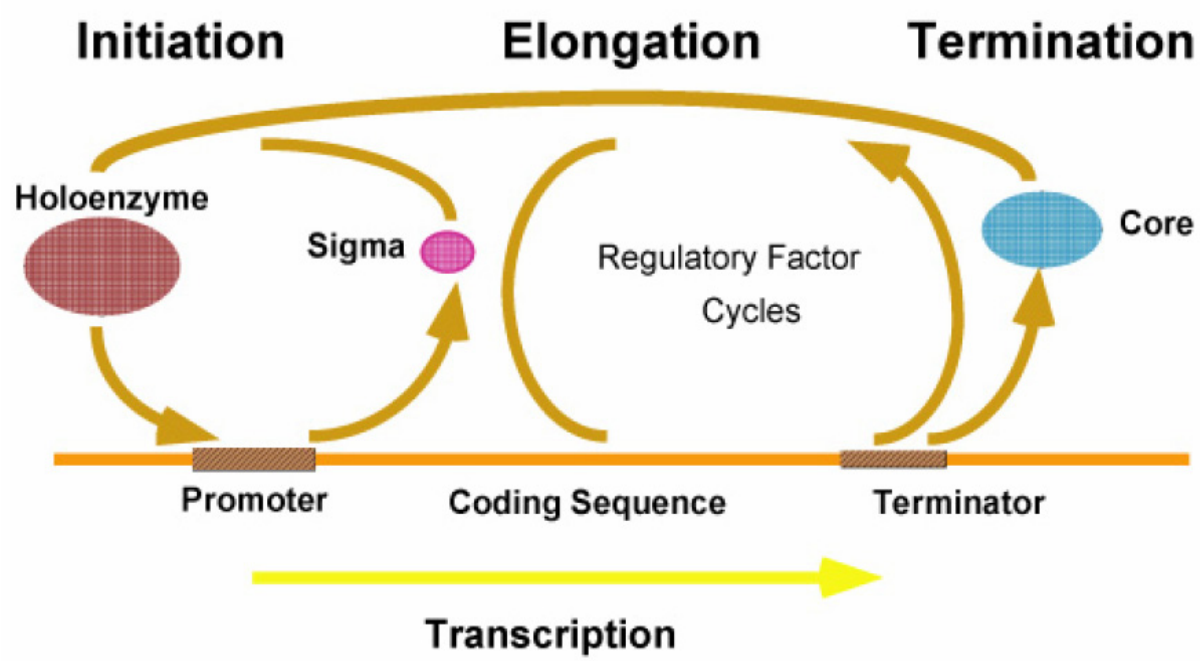

Figure 1.2 The Transcription Cycle.

1.1.3 RNAP and Elongation Complex Structure

While one homologue of RNAP exists in prokaryotes, eukaryotic transcription is typically carried out by the enzyme RNAP I for ribosomal RNA synthesis, RNAP II for messenger RNA, and RNAP III synthesizes transfer RNA (Sweetser *et al.*, 1987). The exterior surfaces of RNAPs vary greatly, however the sequence of the catalytic core residing in the cleft of the β and β' subunits of prokaryotic and eukaryotic enzymes are highly conserved (Allison *et al.*, 1985; Biggs *et al.*, 1985; Sweetser *et al.*, 1987). As a result, several functional similarities exist between lower and higher order life form RNAPs. Eukaryotic RNAP III functions similarly to prokaryotic RNAPs during initiation and termination of transcription, while RNAP I, II and III function much like eubacteria RNAPs during elongation. Due to the extensive structural and functional conservation of multisubunit RNAPs throughout biology, the study of RNAP from prokaryotes divulges information about transcription in all life forms (Sweetser *et al.*, 1987).

RNA polymerase crystal structures from *Saccharomyces cerevisiae, Thermus aquaticus,* and *Thermus thermophilus* have been solved and have aided in the construction of models describing nucleotide incorporation and conformational fluctuations associated with the regulation of transcription (Zhang *et al.*, 1999; Campbell *et al.*, 2001; Bushnell *et al.*, 2002; Vassylyev *et al.*, 2002; Artsimovitch *et al.*, 2004; Temiakov *et al.*, 2005; Vassylyev *et al.*, 2007). In 2006, Roger Kornberg was awarded the Nobel Prize in Chemistry for his work with in the structure of eukaryotic RNAP II.

The model of *T. thermophilus* RNAP bound to DNA and RNA, shown in Figure 1.3, reveals the general attributes of RNAP. The β and β' subunits form a "crab claw" structure; the cleft junction of β and β' form what is known as the main channel. In Figure 1.4, various

views of the *T. thermophilus* elongation complex are depicted. As seen in Figure 1.4, DNA is melted into template and non-template strands at the βD loop I (fork loop 2) for form the transcription bubble; the βD loop I is visible through the main channel. The template stand lies across main channel making contacts with the catalytic center of RNAP while the non-template stand resides outside the main channel. As RNA is synthesized in the main channel, it is base paired with the template DNA until it is extruded from the main channel near the rudder structure, and the upstream template DNA is rejoined with the non-template stand (Figure 1.4) (Korzheva *et al.*, 2000; Kettenberger *et al.*, 2004; Vassylyev *et al.*, 2007). Several important conserved features on RNAP are in close proximity to the template DNA and the NTP catalytic site. Shown in Figure 1.3 is a Mg^{+2} ion binding site located at a cluster of three aspartic acid residues (Zhang *et al.*, 1999). The bridge helix (F-helix) (Figures 1.4 and 1.5) spans the entire main channel and probably plays a role in translocation signal transduction (Epshtein *et al.*, 2002; Artsimovitch *et al.*, 2003; Bar-Nahum *et al.*, 2005; Temiakov *et al.*, 2005; Tuske *et al.*, 2005). Displayed in Figure 1.5 is the putative allosteric NTP binding site on the βD loop I (fork loop 2) (Foster *et al.*, 2001; Kennedy, 2007). The trigger loop (Figure 1.5) is also located under the bridge helix, and is necessary for nucleotide incorporation (Temiakov *et al.*, 2005).

In the presence of the DNA-RNA hybrid, Figures 1.4 and 1.5 show that there is very little room for NTPs to gain direct access to the catalytic site *via* the main channel. Another important conserved feature on RNAP is the secondary channel, which can be seen clearly on the right in Figure 1.4. Located on the back side of the β' subunit, the secondary channel leads to the catalytic site. Roughly 12Å wide and 45Å long, the secondary channel is thought to be the primary route that NTPs take to the active center (Zhang *et al.*, 1999; Korzheva *et*

al., 2000; Cramer *et al.*, 2001; Vassylyev *et al.*, 2002; Batada *et al.*, 2004; Kettenberger *et al.*, 2004; Westover *et al.*, 2004; Temiakov *et al.*, 2005), although there is some evidence that NTPs may also enter though the main channel (Burton *et al.*, 2005; Kennedy *et al.*, 2008).

Figure 1.5 is close up view of the catalytic core in an elongation complex with *S. cerevisiae* RNAP II. A GTP molecule (light purple) is shown bound to the catalytic site. On the other side of the bridge helix (orange), fork loop 2 (βD loop I) is shown in several opened-to-closed conformations (yellow, green and light blue, respectively). Kennedy and Erie (2007, 2008) show that an allosteric NTP bound to fork loop 2 can accelerate the rate of nucleotide incorporation, and that the bound NTP can be shuttled into the catalytic site *via* the main channel. The mobility of the trigger loop is shown in the open (green) and closed (magenta) conformations (Figure 1.5). The mobility of fork loop 2 and the trigger loop likely play an important signal transduction role between the allosteric and catalytic site, as discussed later.

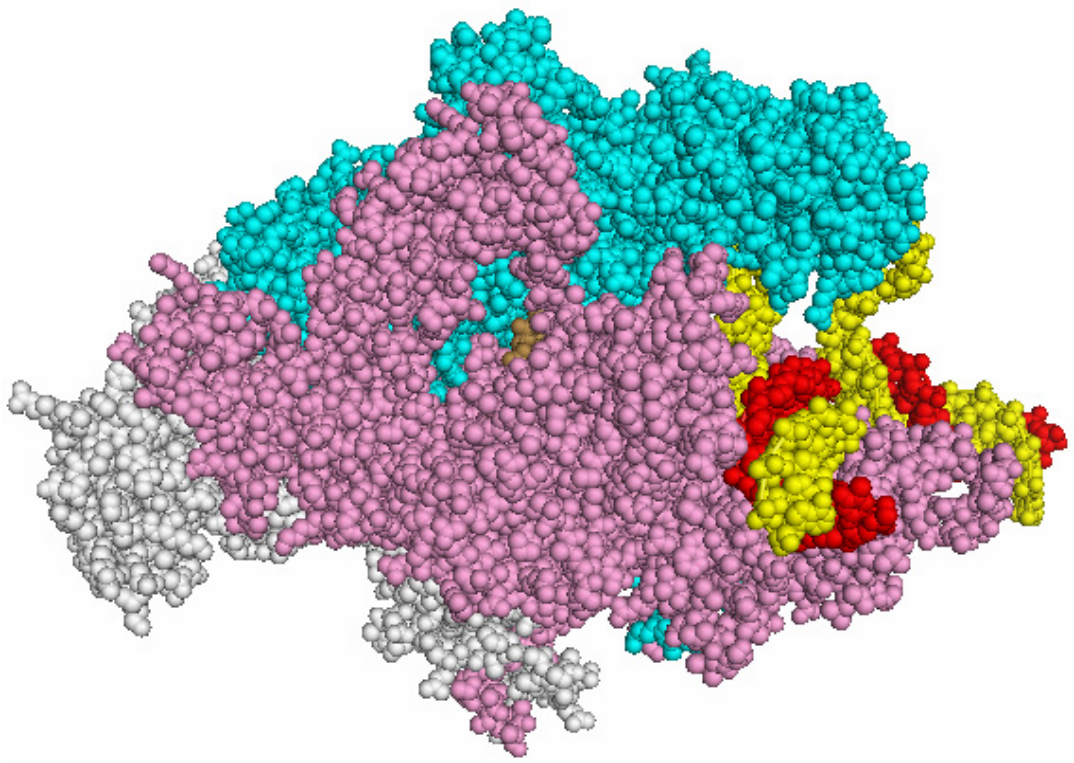

Figure 1.3 Space Filled Model of the *T. thermophilus* Elongation Complex Highlighting the "Crab Claw" Structure Made by the β and β' Subunits (Korzheva *et al.*, 2000). The major features displayed here are found in all multisubunit RNAPs. Shown in grey are the two α subunits (left) and the ω subunit (bottom). The β and β' subunits are shown in cyan and magenta, respectively. Portions of the DNA template strand (red) and non-template strand (yellow) can be seen lying across the main channel. The nascent RNA chain is displayed in brown and is barely visible through the main channel on β'. PDB ID: 2PPD

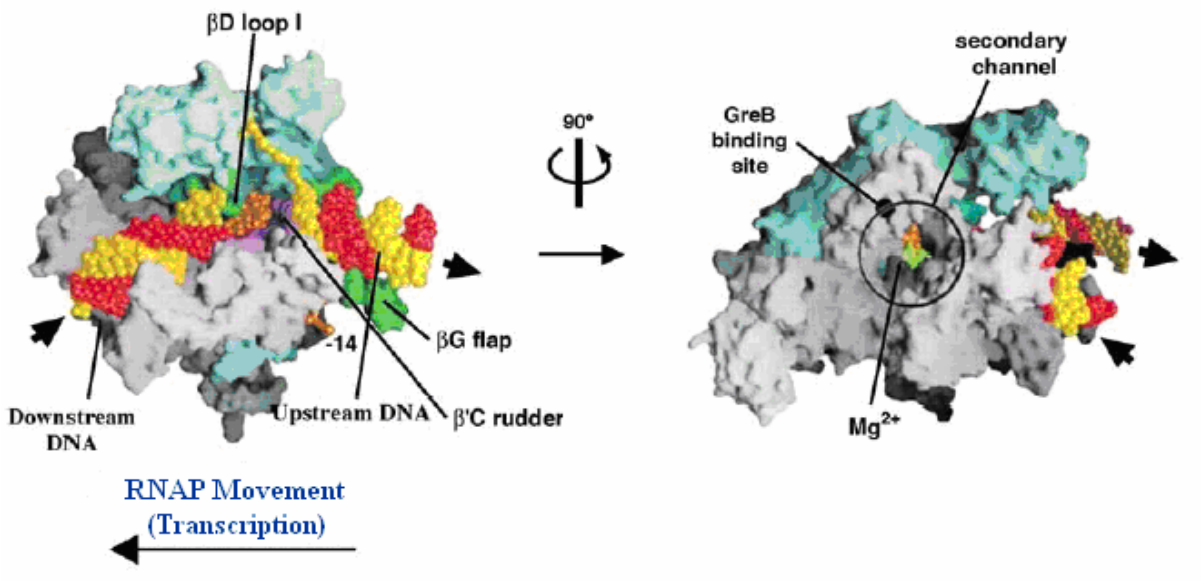

Figure 1.4 Partial Space Filled Structure of the *T. thermophilus* Elongation Complex (Korzheva *et al.*, 2000). Highlighted in this model is the location of the secondary channel on β' (magenta). β is displayed in cyan. The main channel is occupied by the template DNA (red) and RNA (brown). The non-template DNA strand is shown in yellow. The nascent RNA chain is extruding from the main channel near the βG flap in the upper left image. Also visible are various sites important to transcription function and regulation. The catalytic site and the Mg^{+2} binding site are visible through the main channel on the upper right image. A GreB binding site is located near the entrance to the secondary channel. PDB ID: 2PPD.

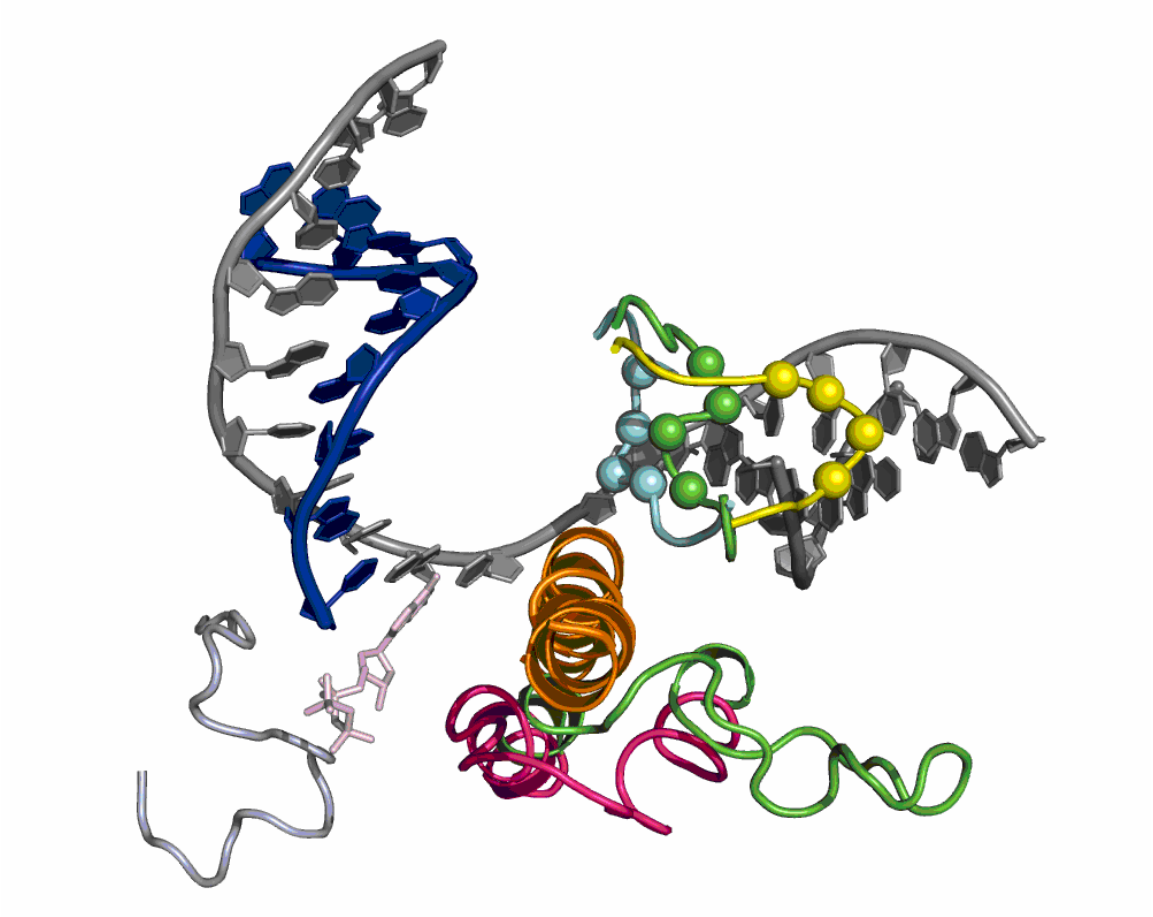

Figure 1.5 Important mobile structures in the catalytic core of *S. cerevisiae* RNAP II Elongation Complexes. The template and non-template DNA are shown in grey and dark blue respectively. The RNA (red), bound GTP (light purple) and bridge helix (orange) are also shown. The trigger loop shown in two conformations: open (green) and closed (magenta). Fork loop 2 is shown in three conformations: open (yellow), partially closed (green), and closed (light blue). PDB IDs: 2E2H, 1Y77, 1Y1V and 2E2I (Kennedy *et al.*, 2008).

1.1.4 The Conformational States of Ternary Elongation Complexes

A multitude of ternary (RNAP-DNA-RNA) complex conformations direct a plethora of states in transcription. Shown in Figure 1.6, the DNA-RNA hybrid may shift with respect to the catalytic site. During productive synthesis, the 3' end of the RNA exists in the pre-translocated state after one round of nucleotide incorporation. The RNA then moves to the post-translocated state to make room for an incoming NTP. However, the RNA may translocate by more than one base position, known as the hyper-translocated state (Figure 1.6). During productive synthesis, pausing can occur when RNA polymerase encounters certain sequence elements (pause sites) and may lead to the hyper-translocation of the RNA. Hyper-translocation is believed to be a pathway toward termination (Toulokhonov *et al.*, 2007).

Alternatively, the RNA may become backtracked through the enzyme such that the RNA is reverse translocated and extruded into the secondary channel (Boukhov *et al.*, 1992), as shown in Figure 1.6. In backtracked states, cleavage may occur that removes the 3' end of the transcript so that the RNAP may restart synthesis at the registered template position (Figure 1.6). Intrinsic cleavage may occur when the RNAP cleaves the backtracked portion of the transcript to generate a new 3' terminus, or external protein factors may extrinsically cause RNAP to cleave the backtracked transcript (Komissarova *et al.*, 1997); (Surratt *et al.*, 1991; Boukhov *et al.*, 1992; Izban *et al.*, 1992).

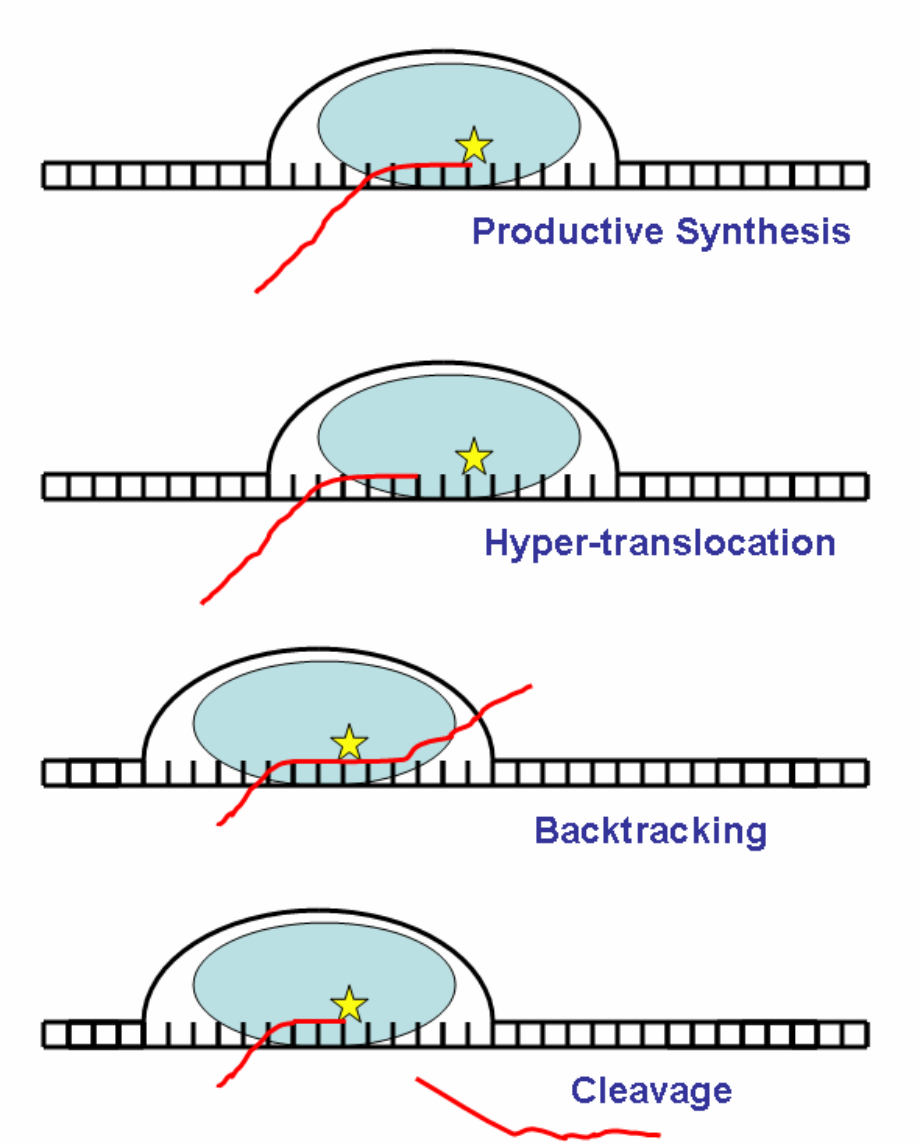

Figure 1.6 Ternary Complex Conformations Governing the States of Elongation. Shown in cyan is RNAP; the catalytic site is depicted by a yellow star. The red lines represent the nascent RNA chain and the black lines depict the DNA. Aside from the productive synthesis conformation, show here is the hyper-translocated state that may lead to termination, and the backtracked state that may either result in an irreversible dead-end state or may undergo cleavage for *via* a rescue pathway.

1.1.5 The Regulation of States in Transcription Elongation by External Factors

The states of transcription can be broken up into productive synthesis states, regulatory (paused) states, and errant (dead-end) states. Regulation in transcription is controlled by conformational changes in RNAP (and the ternary structure) that shift transcription into, or rescue the enzyme from the various conformational states. The conformational state changes are mitigated by RNAP's interactions with nucleic acid sequence elements and by external interactions with small molecules and proteins co-factors. The complexity and shear number of general transcription factors (GTFs), core promoter elements, and other co-factors that regulate eukaryotic transcription is staggering (Thomas *et al.*, 2006). To illustrate the importance and complexity of the regulatory co-factor machinery, a few relevant examples of external regulation in bacterial transcription are presented below.

Prokaryotic co-factors including GreA and GreB have been shown to bind into the secondary channel on RNAP (Opalka *et al.*, 2003; Sosunova *et al.*, 2003; Perederina *et al.*, 2004). GreA and GreB can rescue RNAP from back tracked states by inducing cleavage (Komissarova *et al.*, 1997; Opalka *et al.*, 2003; Sosunova *et al.*, 2003; Perederina *et al.*, 2004), and may do so by delivering a catalytic aspartic acid to the active center via the secondary channel (Sosunova, Sosunov *et al.*, 2003). Transcript cleavage by GreA and GreB have also been shown to reduce abortive initiation (Hsu *et al.*, 1995) and misincorporation (Erie *et al.*, 1993) during initiation. Not only may GreA rescue transcription from dead-end states, but it may also play an important role in controlling the fidelity of prokaryotic transcription *via* regulation of various active synthesis pathways (Erie *et al.*, 1993).

Stringent control of transcription is required during periods of amino acid starvation and NTP deprivation. Unique nucleotides know as magic spot I and II [guanosine tetraphosphate (ppGpp) and guanosine pentaphosphate (pppGpp), respectively] help to pause elongation in the absence of NTPs (Krummel *et al.*, 1992). DksA has been shown to stabilize the interaction between ppGpp and RNAP to regulate transcription initiation (Perederina *et al.*, 2004). DksA shares some attributes with GreA: it binds to the secondary channel and inhibits elongation arrest; but, DskA does not induce transcript cleavage (Perederina, Svetlov *et al.*, 2004).

The Nus family has also been identified as important cofactors in transcription, especially in controlling termination. NusG is completely essential to cell vitality and has been found to inhibit the termination activity of RNAP (Burova *et al.*, 1995; Pasman *et al.*, 2000). NusA, when acting on it own with elongation complexes, induces termination and pausing. However in the presence of the lambda-related phage 82 anti-terminator, Q(82), pausing is antagonized and the suppression of termination is enhanced (Shankar *et al.*, 2007). Shankar *et al.* (2007) postulate that both NusA and Q(82) bind somewhere near the β-flap; their data suggest that anti-termination and anti-pausing are related to the regulation of an RNA occlusion mechanism. Additionally, NusG and NusB have been shown to regulate the rates of transcription elongation (Zellars *et al.*, 1999).

1.1.6 The Hierarchy of Pathways in Transcription Elongation

The rate and fidelity of successive nucleotide incorporation during transcription elongation is dependant on the fluctuations between RNAPs conformational states. Figure 1.7 illustrates the observable relationships between the various conformationally controlled pathways and the how the states compare to each other energetically.

Shown in the light purple box (Figure 1.7), two productive synthesis pathways exist: unactivated and activated. The active pathway (shown in blue) represents the faster, low fidelity cycle of nucleotide addition. The normal addition of NTPs is carried on the active pathway (Foster *et al.*, 2001; Holmes *et al.*, 2003). Transcription may decay into the slower, higher fidelity unactivated pathway (show in green, Figure 1.7) (Foster *et al.*, 2001; Holmes *et al.*, 2003). Only from the unactivated state of synthesis may a number of errant backtracked states (yellow) arise. Brought on by NTP deprivation or sequence elements, some backtracked states my lead to an arrested state (red) (Krummel *et al.*, 1992). Alternatively, some of the errant backtracked states may be rescued by cleavage as described earlier (Surratt *et al.*, 1991; Boukhov *et al.*, 1992). From the unactivated state, the transcript may decay into a hyper-translocated state that will most likely lead to termination, but can return to the unactivated pathway via regulatory pathways (Toulokhonov *et al.*, 2007).

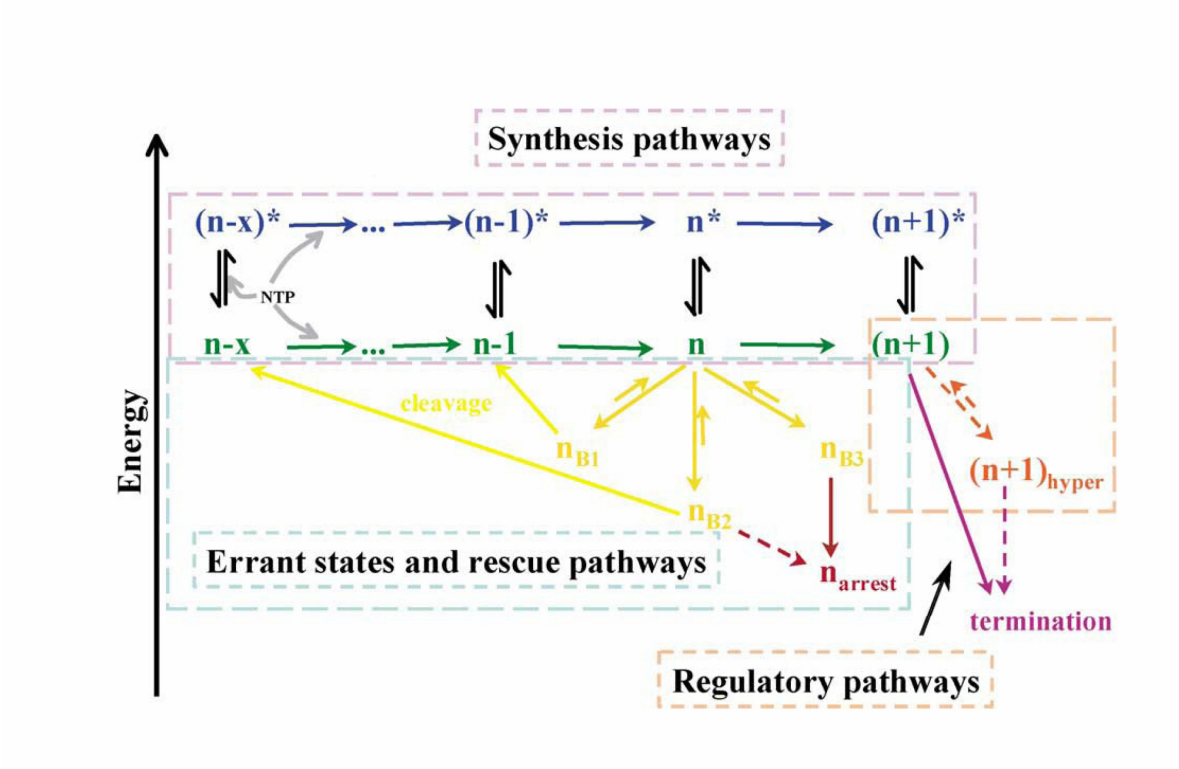

Figure 1.7 The Multitude of Pathways Followed During Transcription Elongation. Transcription normally follows the high energy, activated pathway (blue), with occasional visits into an unactivated pathway (green). NTP deprivation, sequence elements or external factors may give rise to conformations that further decay transcription into regulated (yellow/orange) or errant states (red).

1.1.7 NTP Incorporation Mechanisms

RNAP's interactions with non-catalytic NTPs also play a very important role in the regulation of transcription elongation pathways. In our laboratory, transient state kinetic experiments have revealed that a template specific allosteric site must exist in the main channel of RNAP during elongation that drives transcription into the activated pathway upon NTP binding (Foster *et al.*, 2001; Holmes *et al.*, 2003).

Figures 1.8 and 1.9 represent two kinetically indistinguishable models for NTP incorporation. In both models, the green boxes represent RNAP in the unactivated (n) synthesis pathway, and the blue boxes represent activated (n*) synthesis. The catalytic and allosteric sites are shown as red and magenta boxes, respectively. The product terminus (post-translocated transcript) binding site is shown in tan. The connecting lines between N's (bases) imply that those nucleotides have been incorporated into the nascent RNA chain. The PP_i is short for pyrophosphate. A base bound to the catalytic site is represented by NTP_C, and NTP_A symbolizes allosteric binding.

Figure 1.8 is a mechanistic model for nucleotide incorporation that assumes a rapid equilibrium between the pre- and post-translocated states. An NTP may first bind to the allosteric site which shifts the enzyme into the activated state [(n-1)*:NTP_A]. On the activated pathway, the next NTP to be incorporated enters the catalytic site [(n-1)*:NTP_A:NTP]. Pyrophosphate is released as synthesis takes place (n*:NTP_A:PPi). Alternatively, the first NTP may bind to the catalytic site [(n-1):NTP], leaving the enzyme on the unactivated pathway. With the allosteric site unoccupied, nucleotide incorporation may still take place, but at a slower rate (n:PPi) (Holmes *et al.*, 2003).

Figure 1.9 shows a mechanism for nucleotide incorporation where the ternary complex heavily favors the pre-translocated state [(n-1)] until binding the allosteric NTP drives translocation [(n-1):NTP_A]. On the unactivated pathway, the NTP in the allosteric site can be shuttled into the catalytic site [(n-1):NTP_C]. Instead, the allosteric NTP bound may remain bound after translocation and a second NTP can bind to the catalytic site [(n-1):NTP_A:NTP_C] and be incorporated on the activated pathway (Holmes *et al.*, 2003).

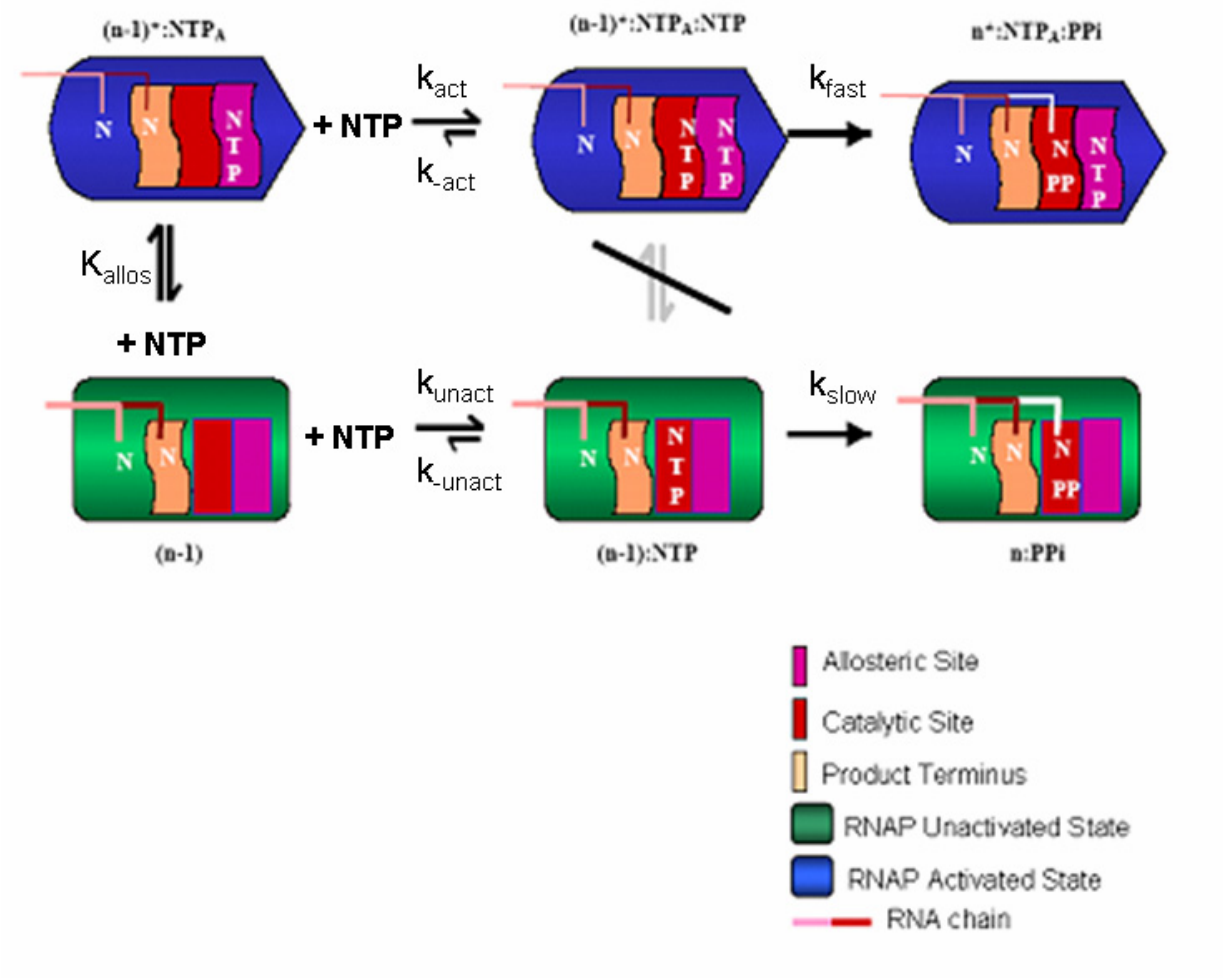

Figure 1.8 A Kinetic Model for NTP Incorporation Based on the Rapid Equilibrium on the Pre- and Post-translocated States. The model displayed here assumes that an equilibrium exists between the pre- and post-translocated states.

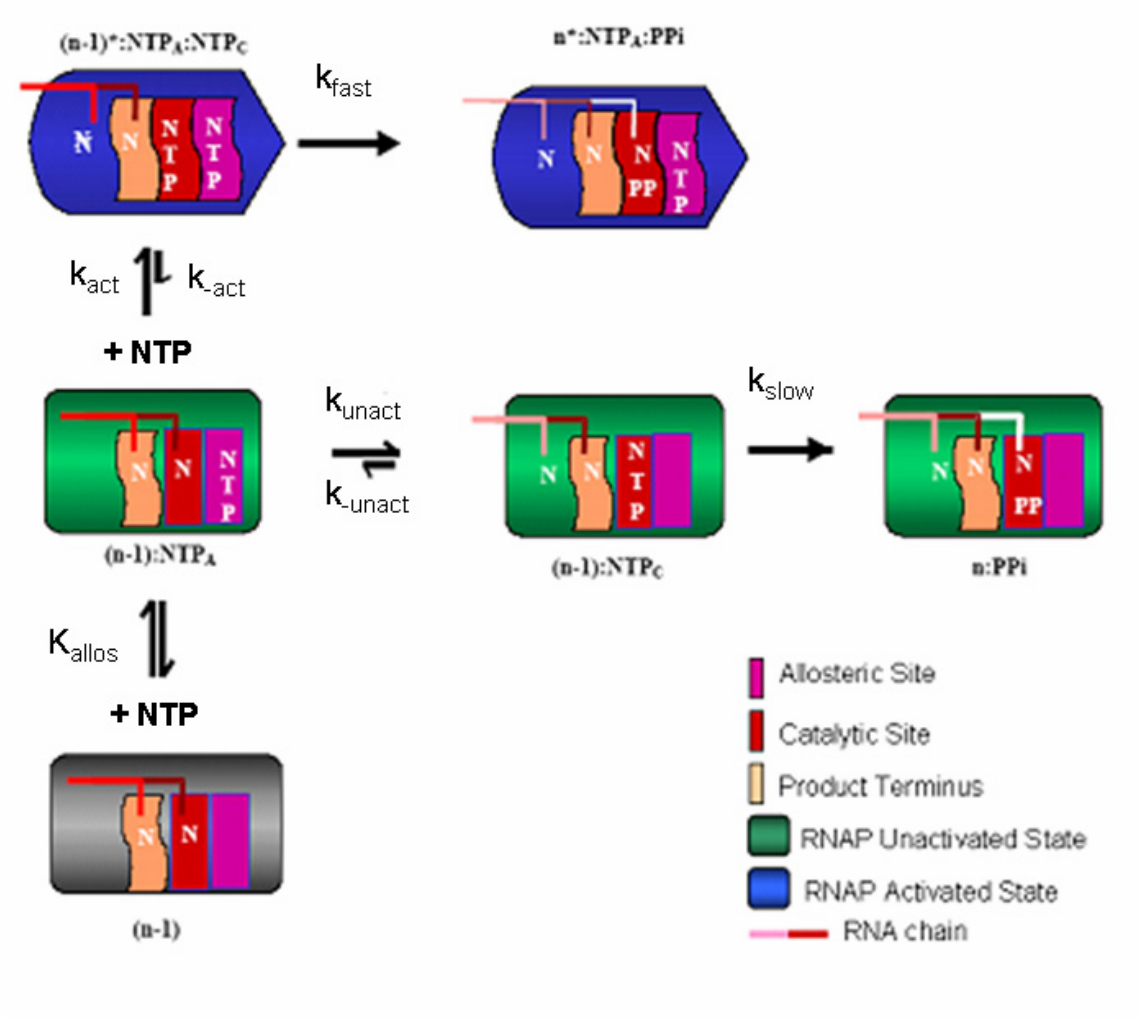

Figure 1.9 A Kinetic Model for NTP Incorporation where Allosteric NTP Binding Drives Translocation. The model shown here begins in the pre-translocated state, and is mathematically indistinguishable from the model shown in figure 1.8.

1.1.8 The Putative Location and Function of the Allosteric Site

The allosteric site (shown in Figures 1.5 and 1.10) is comprised of several elements that are typical of an NTP binding site. The flexible fork loop 2 (βD-loop I) is flanked by α-helices on one side a β-sheet on the other. Fork loop 2 is glycine-rich, much like "P-loops" found in many other NTP binding sites (Walker *et al.* 1982; Kull *et al.* 1998; Via *et al.* 2000; Leipe *et al.* 2002). A totally conserved Walker B motif at the back of the loop can indirectly interact with the γ-phosphate of NTPs (Walker *et al.* 1982; Via *et al.* 2000). An NTP bound to the putative allosteric site would be 5-6 Å from the DNA, poised to interact with the downstream (i+2) DNA template position.

Considering the attributes of the putative allosteric site and the mechanism put forth previously (Figures 1.8 and 1.9) Holmes and Erie proposed a ratchet model for translocation (Holmes, 2002). According to the model, the mobile fork loop 2 undergoes a conformation al change upon allosteric NTP binding. The change in fork loop 2 conformation signals other movements on RNAP that contact the DNA-RNA hybrid, driving translocation *via* a ratchet motion (Holmes, 2002). Further kinetic studies in our laboratory suggest that binding to the allosteric site drives translocation, and opens NTP access to the catalytic site through the secondary channel *via* "gate keeper" interactions with the mobile trigger loop (Kennedy, 2007).

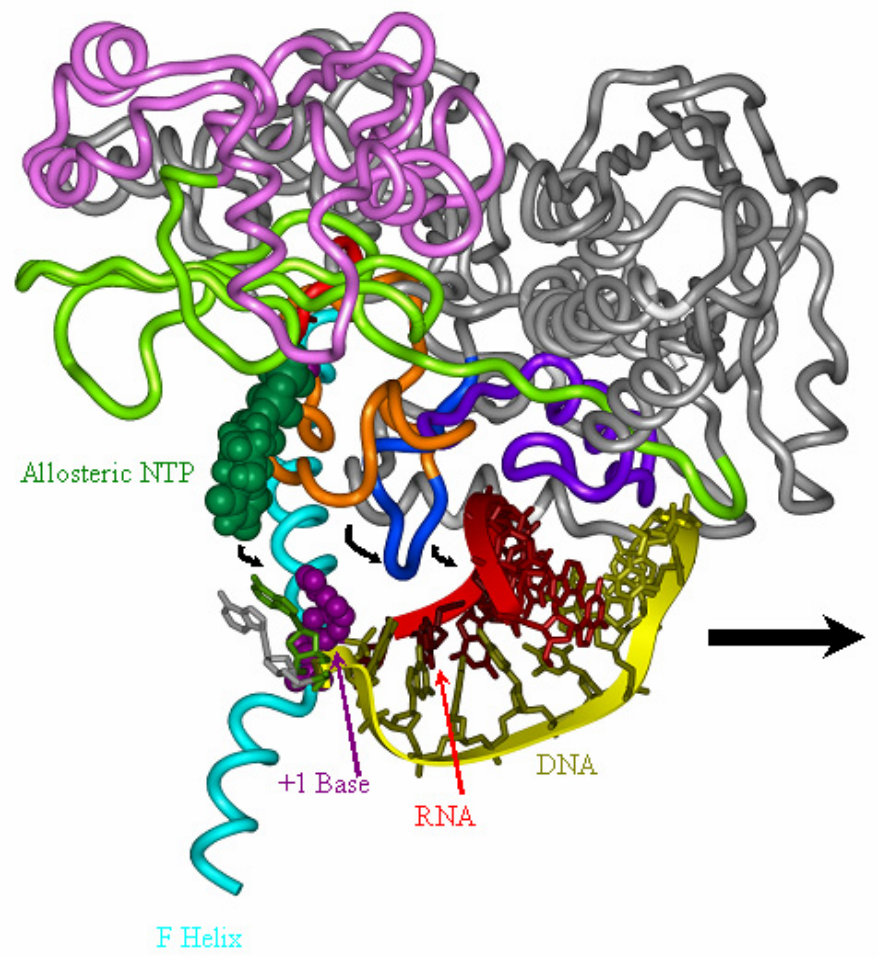

Figure 1.10 The Putative Allosteric Site is Comprised of Typical NTP Binding Site Motifs. The DNA template strand is shown in yellow, the nascent RNA chain is displayed in red. The Bridge helix (F-helix) colored in cyan, fork loop 2 is shown in orange, the β-sheet and α-helices on either site of the putative allosteric site are shown in light green and pink, respectively. A UTP molecule is shown modeled into the allosteric site (dark green). The downstream DNA base is displayed in purple [figure as reported previously (Holmes, 2002)].

1.2 Development of Bioanalytical Methods for Transcription: A Project Précis

Transient state kinetic measurements, crystal structures and mutagenesis of RNAP have been the primary tools in discerning regulatory and synthesis mechanisms in transcription. However, crystal structures and kinetic data can only indirectly describe the presence of certain molecular interactions. Bioanalytical methods aimed at obtaining direct evidence of selected macromolecular and small molecule interactions with RNAP will further bolster the development of mechanistic and regulatory models of transcription.

1.2.1 Novel Methods for Capturing NTP-Elongation Complex Binding Information

The binding of templated and non-templated nucleotides to transcription elongation complexes is not fully understood. Our laboratory has hypothesized that two NTP binding sites exist that effect transcription: a catalytic site and an allosteric site (Foster *et al.*, 2001; Holmes *et al.*, 2003; Kennedy, 2007). But are there actually two NTPs bound tightly to transcription elongation complexes? If so, we specifically need more information concerning the nucleotide occupancies of catalytic and allosteric sites, the rates of NTP dissociation (k_{off}) and the NTP binding affinities (K_D). We also want to find out if an active displacement mechanism is in place for NTP binding to the catalytic and putative allosteric sites.

We sought to provide the means to address the boundaries limiting the direct quantitative assessment of NTP-transcription elongation complex (TEC) interactions. Chapter 2 outlines the general analytical limitations of existing binding assays and describes the need for new methods that can facilitate the capture of NTP-TEC stoichiometries. Chapter 3 describes the use of a novel separation technique that we developed specifically for transcription experiments. In Chapter 3, we go on to present our current data concerning

nucleotide binding. We disclose information about the stoichiometric occupancies of non-templated NTP on TECs and the NTP off rates, we characterize the change in NTP-TEC stoichiometry during catalysis and non-specific ligand competition, and we determine binding the affinities for non-templated NTPs. Finally, we propose a synthesis mechanism for misincorporation in transcription.

In Chapter 4 we describe our genesis of other novel equilibrium binding techniques to quantitatively measuring NTP-TEC interactions. Some of the methods outlined in Chapter 4 show potential for universal applications outside of transcription. A versatile, universal method that requires 10-fold less protein than filter binding is presented.

1.2.2 Opening the Door for Combined Microscopies to Study Regulation in Transcription

Complicated macromolecular interactions are crucial in transcription regulation. We would like to characterize some of the specific structure-function attributes of RNAP-accessory protein complexes. Single molecule studies with transcription complexes interacting with accessory proteins may identify transitions between regulatory states not observable in bulk studies. Atomic Force Microscopy (AFM) and Single Molecule Fluorescence (SMF) techniques are powerful tools for answering some of the structure-function questions in molecular biology; however, the combination of AMF and SMF will amplify the data capture from each technique individually.

We outline in Chapter 5 the progression of biological AFM, and discuss the combination of AFM with SMF techniques. One critical step in the generation of combined AFM-SMF is the ability to image biological constructs on glass that has been made ultra-smooth and conducive to biological sample depositions under physiological conditions. In

Chapter 5, we present a number of protocols for the preparation glass surface, and identify a method to deposit transcription complexes onto smooth glass without distorting their macromolecular structures.

BIBLIOGRAPHY

Allison, L. A., M. Moyle, Michael Shales and C. J. lngles (1985). "Extensive Homology among the Largest Subunits of Eukaryotic and Prokaryotic RNA Polymerases." Cell **42**(2): 599.

Artsimovitch, I. and R. Landick (2002). "The transcriptional regulator RfaH stimulates RNA chain synthesis after recruitment to elongation complexes by the exposed nontemplate DNA strand." Cell **109**(2): 193.

Artsimovitch, I., V. Patlan, S.-i. Sekine, M. N. Vassylyeva, T. Hosaka, K. Ochi, *et al.* (2004). "Structural Basis for Transcription Regulation by Alarmone ppGpp." Cell **117**(3): 299.

Artsimovitch, I., V. Svetlov, K. S. Murakami and R. Landick (2003). "Co-overexpression of Escherichia coli RNA Polymerase Subunits Allows Isolation and Analysis of Mutant Enzymes Lacking Lineage-specific Sequence Insertions." J Biol Chem **278**(4): 12344.

Bar-Nahum, G., V. Epshtein, A. E. Ruckenstein, R. Rafikov, A. Mustaev and E. Nudler (2005). "A Ratchet Mechanism of Transcription Elongation and Its Control." Cell **120**(2): 183.

Batada, N. N., K. D. Westover, D. A. Bushnell, M. Levitt and R. D. Kornberg (2004). "Diffusion of Nucleoside Triphosphates and Role of the Entry Site to the RNA Polymerase II Active Center." Proc Natl Acad Sci U S A **101**(50): 17361.

Biggs, J., L. L. Sesrles and A. L. Greenleaf (1985). "Structure of the Eukaryotic Transcription Apparatus: Features of the Gene for the Largest Subunit of Drosophila RNA Polymerase II." Cell **42**(2): 611.

Boukhov, S., A. Polyakov, V. Nikiforov and A. Goldfarb (1992). "GreA Protein: A Transcription Elongation Factor from *Escherichia coli*." Proc Natl Acad Sci U S A **89**(19): 8899.

Burova, E. and M. E. Gottesman (1995). "NusG overexpression inhibits Rho-dependent termination in Escherichia coli." Mol Microbiol **17**(4): 633.

Burton, Z. F., M. Feig, X. Q. Gong, C. Zhang, Y. A. Nedialkov and Y. Xiong (2005). "NTP-Driven Translocation and Regulation of Downstream Template Opening by Multi-Subunit RNA Polymerases." Biochem Cell Biol **83**: 486.

Bushnell, D. A., P. Cramer and R. D. Kornberg (2002). "Structural Basis of Transcription: α–Amanitin-RNA Polymerase II Cocrystal at 2.8 Å Resolution." Proceedings of the National Academy of Sciences **99**(3): 1218.

Campbell, E. A., N. Korzheva, A. Mustaev, K. Murakami, S. Nair, A. Goldfarb*, et al.* (2001). "Structural Mechanism for Rifampicin Inhibition of Bacterial RNA Polymerase." Cell **104**(6): 901.

Chan, C. L. and R. Landick (1994). New Perspectives on RNA chain elongation and termination by E. coli RNA polymerase. Transcription: Mechanisms and Regulation. R. C. Conaway and J. W. Conaway. New York, Raven Press, Ltd.**:** 297.

Cramer, P., D. A. Bushnell and R. D. Kornberg (2001). "Structural Basis of Transcription: RNA Polymerase II at 2.8 Ångstrom Resolution." Science **292**(5523): 1863.

Crick, F. (1970). "Central Dorma of Molecular Biology." Nature **227**(8): 561.

Ederth, J., I. Artsimovitch, L. A. Isaksson and R. Landick (2002). "The downstream DNA jaw of bacterial RNA polymerase facilitates both transcriptional initiation and pausing." J Biol Chem **277**(40): 37456.

Epshtein, V., A. Mustaev, V. Markovtsov, O. Bereshchenko, V. Nikiforov and A. Goldfarb (2002). "Swing-Gate Model of Nucleotide Entry into the RNA Polymerase Active Center." Mol Cell **10**(3): 623.

Erie, D. A. (2002). "The many conformational states of RNA polymerase elongation complexes and their roles in the regulation of transcription." Biochim Biophys Acta **1577**(2): 224.

Erie, D. A., O. Hajiseyedjavadi, M. C. Young and P. H. von Hippel (1993). "Multiple RNA Polymerase Conformations and GreA: Control of the Fidelity of Transcription." Science **262**(5135): 867.

Foster, J. E., S. F. Holmes and D. A. Erie (2001). "Allosteric Binding of Nucleoside Triphosphates to RNA Polymerase Regulates Transcription Elongation." Cell **106**: 243.

Holmes, S. (2002). Downstream DNA Sequence Effects on Transcription Elongation: NTP Binding Induces Translocation Via A Ratchet Motion. Chemistry. Chapel Hill, University of North Carolina at Chapel Hill. **Ph.D.**

Holmes, S. F. and D. A. Erie (2003). "Downstream DNA Sequence Effects on Transcription Elongation: Allosteric Binding of Nucleoside Triphosphates Facilitates Translocation Via a Ratchet Motion." J Biol Chem. **278**(37): 35597.

Hsu, L. M., N. V. Vo and M. J. Chamberlin (1995). "Escherichia coli Transcript Cleavage Factors GreA and GreB Stimulate Promoter Escape and Gene Expression in vivo and in vitro." Proc Natl Acad Sci U S A. **92**(25): 11588.

Izban, M. G. and D. S. Luse (1992). "The RNA Polymerase II Ternary Complex Cleaves the Nascent Transcript in a 3'→5' Direction in the Presence of Elongation Factor SII." Genes Dev **6**(7): 1342.

Kapanidis, A. N., E. Margeat, S. O. Ho, E. Kortkhonjia, S. Weiss and R. H. Ebright (2006). "Initial Transcription by RNA Polymerase Proceeds Through a DNA-Scrunching Mechanism." Science **314**(5802): 1144.

Kennedy, S. R. (2007). Modulation of Transcription Elongation via the Main Channel in Eschericia coli RNA Polymernase. Chemistry. Chapel Hill, NC, University of North Carolina at Chapel Hill. **Ph.D.:** 162.

Kennedy, S. R. and D. A. Erie (2008). "A Non-catalytic Nucleoside Triphosphate Binding Site on RNA Polymerase Regulates Transcription." submitted to Cell March, 2008: 32.

Kettenberger, H., K.-J. Armache and P. Cramer (2004). "Complete RNA Polymerase II Elongation Complex Structure and Its Interactions with NTP and TFIIS." Mol Cell **16**(6): 955.

Komissarova, N. and M. Kashlev (1997). "Transcriptional Arrest: *Escherichia coli* RNA Polymerase Translocates Backward, Leaving the 3'-end of the RNA Intact and Extruded." Proc Natl Acad Sci U S A **94**(5): 1755.

Korzheva, N., A. Mustaev, M. Kozlov, A. Malhotra, V. Nikiforov, A. Goldfarb*, et al.* (2000). "A Structural Model of Transcription Elongation." Science **289**: 619.

Krummel, B. and M. J. Chamberlin (1992). "Structural Analysis of Ternary Complexes of *Escherichia coli* RNA Polymerase Individual Complexes Halted along Different Transcription Units Have Distinct and Unexpected Biochemical Properties." J Mol Biol **225**(2): 221.

Opalka, N., M. Chlenov, P. Chacon, W. J. Rice, W. Wriggers and S. A. Darst (2003). "Structure and Function of the Transcription Elongation Factor GreB Bound to Bacterial RNA Polymerase." Cell **114**(3): 335.

Pasman, Z. and P. H. von Hippel (2000). "Regulation of rho-dependent transcription termination by NusG is specific to the Escherichia coli elongation complex." Biochemistry **39**(18): 5573.

Perederina, A., V. Svetlov, M. N. Vassylyeva, T. H. Tahirov, S. Yokoyama, I. Artsimovitch*, et al.* (2004). "Regulation through the Secondary Channel—Structural Framework for ppGpp-DksA Synergism During Transcription." Cell **118**: 297.

Richardson, J. P. (1993). "Transcription Termination." Crit Rev Biochem Mol Biol **28**(1): 126.

Severinov, K. (2000). "RNA polymerase structure-function: insights into points of transcriptional regulation." Curr Opin Microbiol **3**(2): 118.

Shankar, S., H. A. and R. JW. (2007). "A Transcription Antiterminator Constructs a NusA-dependent Shield to the Emerging Transcript." Mol Cell **9**(6): 914.

Sosunova, E., V. Sosunov, M. Kozlov, V. Nikiforov, A. Goldfarb and A. Mustaev (2003). "Donation of Catalytic Residues to RNA Polymerase Active Center by Transcription Factor Gre." Proc Natl Acad Sci U S A **100**(26): 15469.

Straney, D. C. and D. M. Crothers (1987). "A Stressed Intermediate in the Formation of Stably Initiated RNA Chains at the *Escherichia coli lac* UV5 Promoter." J Mol Biol **193**(2): 267.

Surratt, C. K., S. C. Milan and M. J. Chamberlin (1991). "Spontaneous Cleavage of RNA in Ternary Complexes of *Escherichia coli* RNA Polymerase and its Significance for the Mechanism of Transcription." Proc Natl Acad Sci U S A **88**(18): 7983.

Sweetser, D., M. Nonet and R. A. Young (1987). "Prokaryotic and eukaryotic RNA polymerases have homologous core subunits." Proc Natl Acad Sci U S A **84**(5): 1192.

Temiakov, D., N. Zenkin, M. N. Vassylyeva, A. Perederina, T. H. Tahirov, E. Kashkina*, et al.* (2005). "Structural Basis of Transcription Inhibition by Antibiotic Streptolydigin." Molecular Cell **19**(5): 655.

Thomas, M. C. and C.-M. Chiang (2006). "The General Transcription Machinery and General Cofactors." Crit Rev Biochem Mol Biol **41**(3): 105.

Toulokhonov, I., J. Zhang, M. Palangat and R. Landick (2007). "A Central Role of the RNA Polymerase Trigger Loop in Active-Site Rearrangement during Transcriptional Pausing." Cell **227**(3): 406.

Tuske, S., S. G. Sarafianos, X. Wang, B. Hudson, E. Sineva, J. Mukhopadhyay*, et al.* (2005). "Inhibition of Bacterial RNA Polymerase by Streptolydigin: Stabilization of a Straight-Bridge-Helix Active-Center Conformation." Cell **122**: 541.

Vassylyev, D. G., S. Sekine, O. Laptenko, J. Lee, M. N. Vassylyeva, S. Borukhov*, et al.* (2002). "Crystal structure of a bacterial RNA polymerase holoenzyme at 2.6 A resolution." Nature **417**(6890): 712.

Vassylyev, D. G., M. N. Vassylyeva, A. Perederina, T. H. Tahirov and I. Artsimovitch (2007). "Structural Basis for Transcription Elongation by Bacterial RNA Polymerase." Nature **448**(7150): 157.

Westover, K. D., D. A. Bushnell and R. D. Kornberg (2004). "Structural Basis of Transcription: Nucleotide Selection by Rotation in the RNA Polymerase II Active Center." Cell **119**(4): 481.

Zellars, M. and C. L. Squires (1999). "Antiterminator-dependent modulation of transcription elongation rates by NusB and NusG." Mol Microbiol **32**(6): 1296.

Zhang, G., E. A. Campbell, L. Minakhin, C. Richter, K. Severinov and S. A. Darst (1999). "Crystal Structure of *Thermus aquaticus* Core RNA Polymerase at 3.3 Å Resolution." Cell **98**(7): 811.

CHAPTER 2:

BACKGROUND METHODS

2.1 Ligand Binding

The interactions between ligands and acceptors in biology play important roles in the function of cellular processes, genomic regulation, neurotransmission, and hormonal responses (Winzor *et al.*, 1995). Ligand binding to an acceptor (cell membranes, proteins, oligonucleotides, etc) can be described by fundamental parameters including equilibrium binding affinities, binding stoichiometries, and cooperativity with other binding events. For an acceptor with one binding site ($p = 1$), the law of mass action is as follows:

$$S + A \underset{koff}{\overset{kon}{\rightleftharpoons}} AS \qquad (2.1)$$

where S is a ligand (substrate), A is a single site acceptor, and AS is the ligand-acceptor complex binding with a 1:1 stoichiometry. In this simple case, ligand binding to the acceptor occurs noncovalently and reversibly. Association (k_{on}) and dissociation (k_{off}) rates ($min^{-1} \cdot M^{-1}$ and min^{-1}, respectively) are not observed in equilibrium binding studies. Instead, the ligand and acceptor are allowed to reach equilibrium, and dissociation constant K_D (M) is measure. K_D is the free ligand concentration at equilibrium when 50% of the acceptor has been bound by a ligand.

2.1.1 The Binding Function

Equilibrium binding has been studied by a myriad of techniques, ranging from simple separations, to sophisticated spectral studies, titrations, immunoassays, biosensors and specialized purifications. Each technique aims to decipher the Ligand-Acceptor complex formation dependence on the free ligand concentration. The binding function, *r* (Klotz, 1946) is as follows:

$$r = (\overline{C_s} - C_s) / \overline{C_A} \tag{2.2}$$

where $\overline{C_s}$ is the total molar concentration of ligand in solution, C_s is the molar equilibration concentration of free ligand, and $\overline{C_A}$ is the total molar concentration of acceptor. Consequently, $(\overline{C_s} - C_s)$ is the ligand concentration bound to *A* at any of its *p* sites (Klotz, 1946; Scatchard, 1949; Winzor *et al.*, 1995). By definition, an individual site may only bind a single ligand; ergo, $0 \leq r/p \leq 1$. r/p is the fractional saturation of acceptor with ligand. Complexation can be measured by directly observing the formation of *AS*, or alternatively assaying the remainder of free ligand present subsequent to reaching equilibrium. The nomenclature found in much of literature describing the fundamentals of ligand binding can become cumbersome and hard to follow; for the remainder of this manuscript the following expression will be used to describe the binding function:

$$r = \frac{[bound]}{[acceptor]} \tag{2.3}$$

Explicitly, *[bound]* is the amount of ligand bound to an acceptor, and *[acceptor]* is the total amount of acceptor in solution. In the scope of this discussion, the acceptors we are interested in are enzymes, and the ligands are nucleotides. Specifically, we are interested in transcription elongation complexes with RNAP; the ternary elongation complex is considered

our *acceptor*, not the free enzyme. Nucleotides are negatively charged ligands, which will become relevant in our coming discussions of electrophoretic techniques.

2.1.2 Interpreting Binding Data

Binding curves are generated by plotting the free ligand concentration at equilibrium versus the binding function (*eqs.* 2.2, 2.3). If a ligand-acceptor pair's p sites are equivalent, and the occupancy of one site has no effect on the binding to another, the overall binding can be described in terms of a single intrinsic association or dissociation constant and the data will fit to a single rectangular hyperbolic expression (Klotz, 1946). In homogeneous site binding, 50% of the saturation concentration is an approximation of the binding affinity. K_D is explicitly determined by fitting the binding data to a rectangular hyperbolic expression. When an acceptor contains multiple, independent sites with unique affinities for a specific ligand, the binding data are the sum of the independent rectangular hyperbolic expressions (Perrin *et al.*, 1975). Acceptor site heterogeneity can by inspected by plotting the $1/r$ vs. $1/C_s$ (double reciprocal), r vs. r/C_s (Scatchard Plot), or C_s vs. C_s/r (Hames Plot); linear responses indicate a single type of interaction, whereas non-linearity indicates site heterogeneity (Winzor *et al.*, 1995). When multiple, heterogeneous binding sites are present, ligand binding to one site may have a positive or negative effect on the binding affinity of another site, known as cooperativity or anti-cooperativity, respectively. In proteins, binding cooperativity is due to conformational changes that take place at or near the second site upon binding to the first site. Sigmoidality in the binding data indicates positive or negative cooperativity between sites, and can be characterized by Scatchard analysis.

2.1.3 Non-Specific Adsorption

Nonspecific adsorption of free ligands to filters, tube walls, biological membranes, support matrices, and/or biological matter can add an unsaturatable, linear component to the *r* dependence on free ligand concentration. Non-specific adsorption of labeled ligands (radioactive, fluorescent or otherwise) leads to noisy data in most binding experiments (Winzor *et al.*, 1995). While some amount of nonspecific binding may be impossible to eliminate in binding experiments, it may be identified and subtracted. Through the proper use of acceptor-negative (*A*-) controls and non-labeled free ligand competitive assays, the nonspecific component of the raw binding curve can be characterized and mathematically removed. Figure 2.1a is a graphical representation of binding data that may be seen in the presence of some acceptable amount of non-specific adsorption. In the situation portrayed in Figure 2.1a, a hyperbolic curve fit to the data can tease out an accurate K_D. However, if non-specific adsorption is high, the signal to noise can too high to achieve accurate binding affinity information (Figure 2.1b). When the dependence of free ligand concentration on nonspecific adsorption is stronger than that of the actual ligand-acceptor interaction, the specific interaction of interest is undetectable over the noise of the experiment. It is important to recognize and quantify nonspecific adsorption. Inherently, low concentrations of acceptor produce less binding signal. For binding assays limited by the signal to noise ratio, the researcher is left with two strategies: either identify and reduce the sources of nonspecific adsorption, or produce a technique with lower limits of detection. In transcription experiments, the limited concentration of elongation complexes that can be observed prevents the use of most common binding techniques due to the low signal to noise ratio, as detailed in the next section.

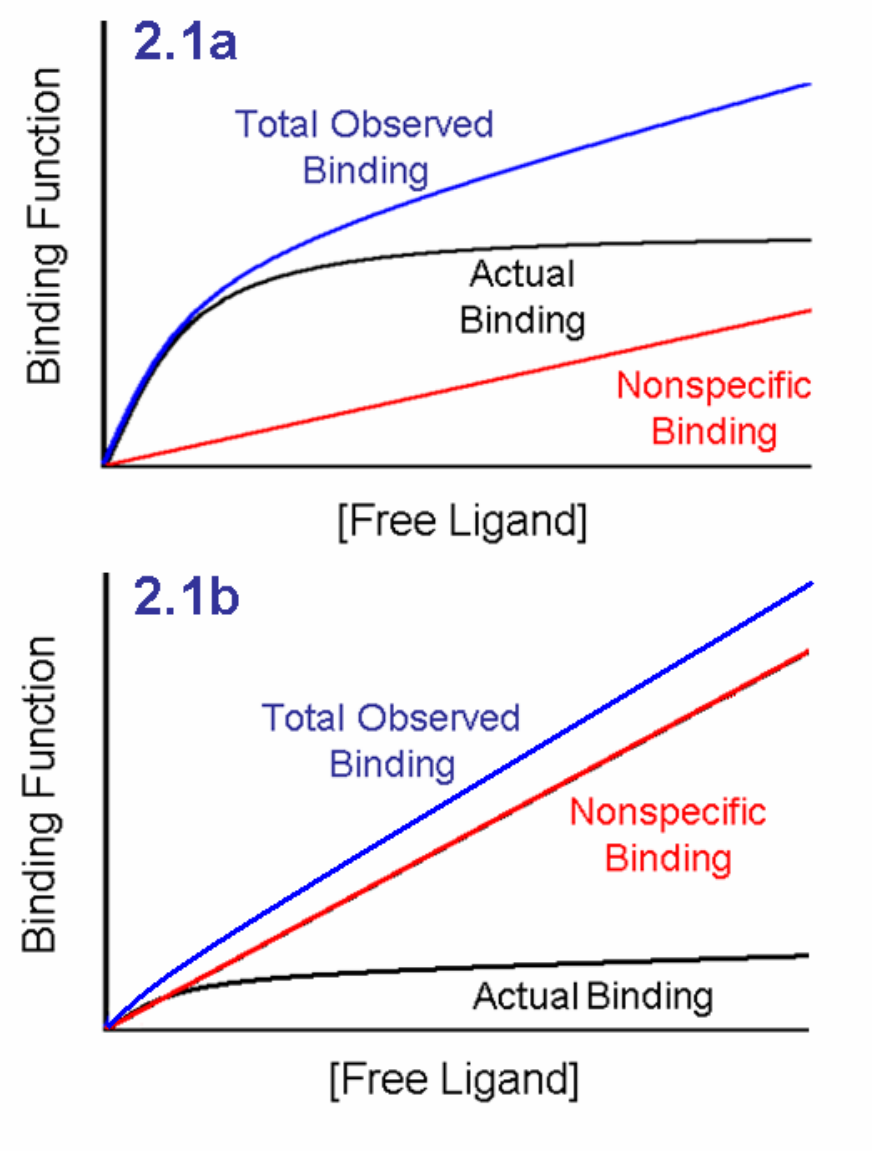

Figure 2.1 Non-specific Adsorption Noise can Limit Binding Analysis. In 2.1a, the linear rise of non-specific noise is partially observable in the collected data. However, fitting the data and probing the binding affinity is still possible. The representation also shows how the linear (unsaturatable) portion of the observed data can be subtracted to reveal the true binding. Figure 2.1b show a situation with high non-specific noise and/or low signal from the bound ligand and acceptor. The ability to capture binding affinity is reduced or eliminated, as the blue curve may appear completely linear in the worst of cases.

2.1.4 The Limitations of Common Binding Techniques in Transcription Elongation

Transcription elongation complexes (TECs) bind NTPs and incorporate NMPs into a nascent RNA chain in a DNA-dependant manner. Analysis of nucleotide binding to TECs is difficult for one fundamental reason: TECs are not a typical protein acceptor. Stalled elongation complexes (SECs) (Krummel *et al.*, 1992) are comprised of DNA, RNAP and RNA. SECs must be purified to halt transcription at a specific synthetic state in the elongation phase, eliminate free RNAP, and remove misincorporable free NTPs. In our laboratory, efficient synthesis and purification of SECs typically yield nanomolar concentrations of elongation complexes. We have also noted that SECs cannot survive indefinitely once synthesized; within a few hours the complexes will dissociate or become inactive catalytically, even when stored on ice. The low concentration of highly complicated, somewhat unstable SEC acceptors severely limits the applicability of common binding analysis techniques.

2.1.5 Common Binding Assays

Several approaches are available for measuring equilibrium ligand binding to proteins, or alternatively, the residual free ligand concentration after equilibration has been reached. Both strategies produce a value for *[bound]* (eq. 2.3). Several binding analysis methods can be characterized as phase separations, spectral studies or competitive binding assays (Winzor *et al.*, 1995). Other methods separate ligands, acceptors and complexes via migration through gravimetric or electrophoretic fields. Furthermore, electrochemical and calorimetric methods exist that don't quite fall into one of these categories, but are certainly

worth mentioning. The ensuing text will illustrate the inability of existing common techniques to investigate NTP binding parameters in transcription elongation complexes.

2.1.5.1 Phase Separations

Equilibrium and Steady State Dialysis techniques employ semi-permeable membranes to separate free ligand from complexes and acceptor (Svensson, 1946; Colowick *et al.*, 1969; Ford *et al.*, 1984). These techniques are troubled by charge effects inducing osmotic flow across a semi-permeable membrane, long dialysis times. Faster steady state dialysis techniques do exist however.

Diafiltration follows a concept similar to dialysis. Diafiltration utilizes pressure differentiation to force analyte through a filter, a process that takes minutes rather than hours (Sophianopoulos *et al.*, 1978). Sample volume reductions occur during the experiment, therefore changes in effective ligand or acceptor concentrations must be accounted for.

Ultrafiltration, also referred to as filter binding, functions similarly to diafiltration but offers higher throughput by making use of a centrifuge to force analyte solution past a membrane. In the case of protein-nucleotide interactions, filtering techniques retain both proteins and protein-ligand complexes as free radiolabeled ligands (S^*) are washed away. Analytical signal originates from the radiolabeled ligand now bound to acceptor (AS^*), captured on the filter. As with most binding analyses, filtration method performance is limited by the signal to noise ratio at low acceptor quantities. Attaining binding parameters for weak interactions (mid- micromolar and above K_D) is difficult when far less than micromolar concentrations of acceptor are available. Even at saturating NTP concentrations

(probably high micromolar), NTP*-SEC formation is probably not observable with filtration methods due to presence of nonspecific NTP* adsorption to the filter materials.

Other phase separation techniques include liquid-liquid (Goodman, 1958) and liquid-solid (Ford *et al.*, 1981) partitioning studies. These methods rely on solubility differences between ligand and acceptor under controlled conditions (i.e. pH, temperature, ionic strength, etc). The solubility requirements of common partition equilibrium techniques are not compatible with SEC stability and catalytic activity.

In gel filtration chromatography (GFC) (Nichol *et al.*, 1964), affinity information is gained via the same principles of equilibrium dialysis. Observation of the effluent volume required to reach a C_S plateau from columns that have been equilibrated with acceptor and varying ligand concentrations. Compared to other phase separations, GFC is not limited by solubility issues or ligand permeability through a dialysis membrane. GFC does, however, require large amounts of material to fill one column volume with practical concentration of acceptor. Additionally, GFC experiments are complicated by concentration gradients produced within the column, lowering K_D accuracy. Hummel and Dreyer developed a lower sample volume method for GFC (Hummel *et al.*, 1962), but still require far more acceptor material than available with SECs.

2.1.5.2 Spectral Studies

Analysis of colorimetric, NMR, ESR, fluorescence anisotropy or X-ray diffraction (XRD) spectral changes subsequent to equilibrium binding can be a useful way to obtain both stoichiometric and binding affinity parameters (Winzor *et al.*, 1995). Spectral studies are commonly preformed as continuous ligand titrations while chemical shift data are recorded.

Spectral techniques require high sample purity to avoid signal heterogeneity and/or interference. The inherent sensitivities of the spectral methods limit their ability to detect physiochemical changes induced by binding. Differing from the concentration constraints of phase techniques, the efficacy of spectral techniques to assay binding parameters is highly dependant on the nature and intensity of measurable chemical/physical behavior, modified by acceptor-ligand complexation. For example, in an anisotropy titration, a large, multisubunit protein acceptor molecule like RNAP will incur little or no change in solution re-polarization due to small ligand (eg. nucleotide) binding. Fluorescently labeled nucleotides cannot be used since they are much different ligands than naturally occurring NTPs. In NMR, ESR and XRD, the spectra of NTP-SEC complexes are likely too convoluted to produce observable or practical peak shifts.

2.1.5.3 Mobility Methods

Several specialized techniques take advantage of changes in analyte mobility subsequent to ligand binding. Ligand binding that significantly changes the molecular weight or cross-section of an acceptor may increase the viability for the ultracentrifugation techniques in transcription analysis: sedimentation velocity (Chanutin *et al.*, 1942; Velick *et al.*, 1953) and sedimentation equilibrium (Van Holde *et al.*, 1958). If a ligand changes that charge of the acceptor, then affinity electrophoresis can be a powerful tool (Takeo *et al.*, 1972). A version of affinity electrophoresis is widely used for protein-DNA interactions, commonly referred to as a band shift assay (Garner *et al.*, 1981). However, mobility techniques are generally not applicable to NTP-SEC interactions, as NTP binding does not dramatically effect SEC interactions with the surrounding solution under gravimetric or

electric fields. Conversely, bound and unbound labeled NTPs would be highly susceptible to mobility methods. As with filtering techniques, non-specific adsorption of free labeled ligand would become the primary limiting factor. Capillary affinity electrophoresis (Nakajima *et al.*, 2006) has been used to separate complex biological mixtures and assay binding. However, this technique utilizes fluorescence detection and is probably not conducive to transcription analysis.

2.1.5.4 Calorimetric Measurements

Ligand binding is often a thermodynamically controlled event that is governed by the solution's energy landscape. Perhaps one of the most information rich methods for probing ligand-acceptor interactions is isothermal titration calorimetry (ITC). ITC measures the heat that flows to or from a microcalorimetric cell with a fixed amount of acceptor as ligand is titrated (Freire *et al.*, 1990). The temperature of the cell is held constant to a cell containing only acceptor. Basic thermodynamic relationships allow one to use the heat that flows to calculate binding stoichiometry, K_D, and other thermodynamic properties including the molar enthalpies, entropies and Gibbs free energies ($\Delta H°$, $\Delta S°$, & $\Delta G°$ respectively). Binding experiments can also be performed by making heat capacity measurements using differential scanning calorimetry (DSC) (Robert *et al.*, 1988). ITC and DSC require that the acceptor concentration, is near K_D; a common limiting factor in many binding analyses. Specifically, the heat that flows from NTP binding to the available quantities of SECs relative to calorimeter sensitivity is far too low.

2.1.5.5 Biosensors, Competitive Binding Assays and Ion Selective Electrodes

Generally speaking, biosensors, ion selective electrodes, and competitive binding assays such as radioimmunoassays, affinity chromatography and enzyme-linked immunosorbent assays (ELISA) are specifically designed for the ligand acceptor pairs of interest. These are categorically indirect techniques; each depends on a cascade of events directly related to ligand binding to facilitate analytical signal transduction (Winzor *et al.*, 1995). To reiterate, transcription is highly complex, and very sensitive to solution conditions and composition. Indirect techniques do not currently exist to specifically assay NTP-SEC binding.

2.1.6 Previous Work Attempts to Assay NTP-SEC Binding

Previous attempts have been made to analyze the nucleotide content of SECs using two-dimensional thin layer chromatography (TLC) (Holmes, 2002). Using apyrase to scavenge free NTPs, Holmes *et. al.* were able to directly compare bound NTPs to a radiolabeled transcript. Since the concentration of the purified complex was very low, any source of NTP background grossly overestimated the actual stoichiometry. The apyrase was not totally effective in removing all free NTPs. Also, the beads used to purify the transcription complexes are highly susceptible to nonspecific NTP adsorption. The SEC purification protocol, not the TLC technique, was the primary source of background interference in these experiments.

2.2 Atomic Force Microscopy

Scanning force microscopy (SFM), now more commonly referred to as atomic force microscopy (AFM), was a modification to scanning tunneling microscopy (Binnig *et al.*, 1986). Since its origination, AFM has facilitated a multitude of biological investigations under physiologically relevant conditions (i.e. samples need not be rendered conductive as with STM) (Bustamante *et al.*, 1994; Bustamante *et al.*, 1995). The dynamics and structure-function relationships of single biomolecules and multimeric-macromolecular complexes have been probed in air and under buffered solution with AFM. It has been shown that a protein's molecular volume as measured by AFM can be related to its molecular weight; hence, information such as protein-protein association constants and oligomerization states can be accessed (Ratcliff *et al.*, 2001). The divalent cation enhanced interaction between the sugar phosphate backbone of DNA and a negatively charged, atomically flat mica deposition surface allow DNA to be immobilized onto the scanning surface facilitating the acquisition of "snapshot" views of solution DNA conformations (Bustamante *et al.*, 1996; Pastre *et al.*, 2003). When deposited with proteins that bind to and act on the DNA's macromolecular structure, the images generated can include qualitative and quantitative information on wrapping, kinking and bending of the DNA (Yang *et al.*, 2003). Recently, dramatically dynamic protein conformational changes induced by small molecules have been recorded by AFM as well (Sacho *et al.*, 2008).

2.2.1 AFM Function

In contact mode AFM, a sharp tip attached to a flexible cantilever, usually made of silicon nitride, is brought into contact with the surface. The deflection of the cantilever is

measured as a laser diode's reflection off of the back of the cantilever is measured on a position sensitive photo diode. More commonly with soft biological samples, a silicon cantilever is vibrated at its characteristic resonant frequency, and intermittent contact is made with the surface. Known as oscillating or tapping™ mode, the amplitude of oscillation is held constant and the cantilever's oscillation amplitude is clipped by interaction with the surface. The stage is scanned in x-y dimensions. As the probe encounters topography on the surface, the degree at which the cantilever's amplitude is clipped changes. A feed back loop adjusts the stage height to restore the fixed clipping value. The z-movement of the stage is then plotted versus the x-y position to generate false color images. Figure 2.2 is a schematic of the basic AFM function.

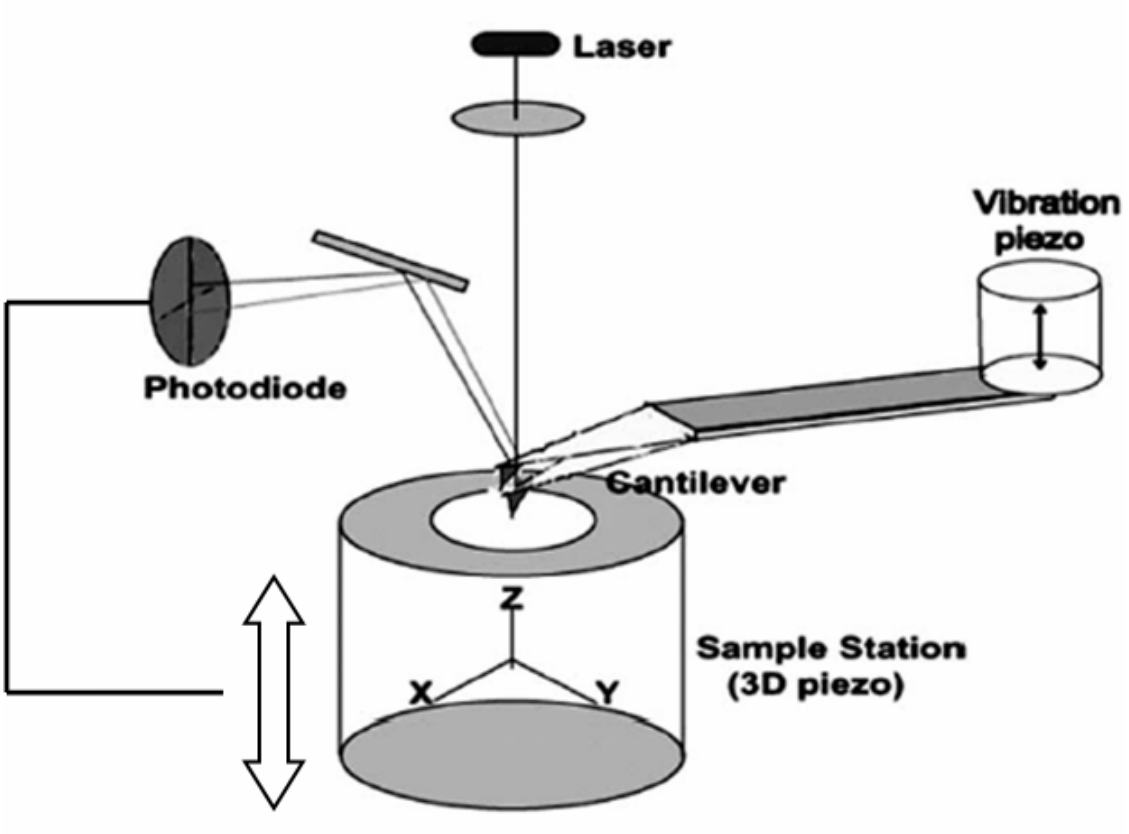

Figure 2.2 Schematic of Atomic Force Microscopy.

2.2.2 Selected Previous RNAP-DNA Complex Analyses with AFM

Atomic Force Microscopy (AFM) (Binnig *et al.*, 1986) is a powerful tool for studying ternary structure and macromolecular interactions in transcription (Rees *et al.*, 1993; Guthold *et al.*, 1994; Rippe *et al.*, 1997; Schulz *et al.*, 1998). Much structure-function information has been gained by the use of AFM in transcription. Figure 2.3 is a montage of images published by groups interested in the overall structure of transcription complexes. In Figure 2.3a, stalled elongation complexes (SECs) are observable by AFM where the extrusion of RNA can be observed; this work also indicated that multiple RNAPs can sometimes interact with the DNA in elongation complexes (Rivetti, Codeluppi *et al.*, 2003). Rippe *et al.* (1997) used AFM to analyze the DNA dependant interactions of RNAP·σ with a constitutively active mutant of nitrogen regulatory protein C (NrtC) from *Salmonella* (Figure 2.3b). Rees *et al.* (1993) have suggested that bend angle of DNA near RNAP can indicate whether or not the complex is in the open or closed promoter conformation (Figure 2.3c). Guthold *et al*. (1994) have been able to follow the assembly of transcription of complexes while imaging under solution conditions.

The structure-function attributes of multi-macromolecular transcription complexes could be better understood by including more direct evidence of interactions with accessory proteins. In the images published by Rippe *et al.* (1997) (*e.g.* Figure 2.3b), it is clear that DNA wraps around both RNAP and the NtrC activator protein, and that the interaction of the enzymes induces looping. However, it is impossible to identify which structure on the surface is RNAP, and which is NtrC.

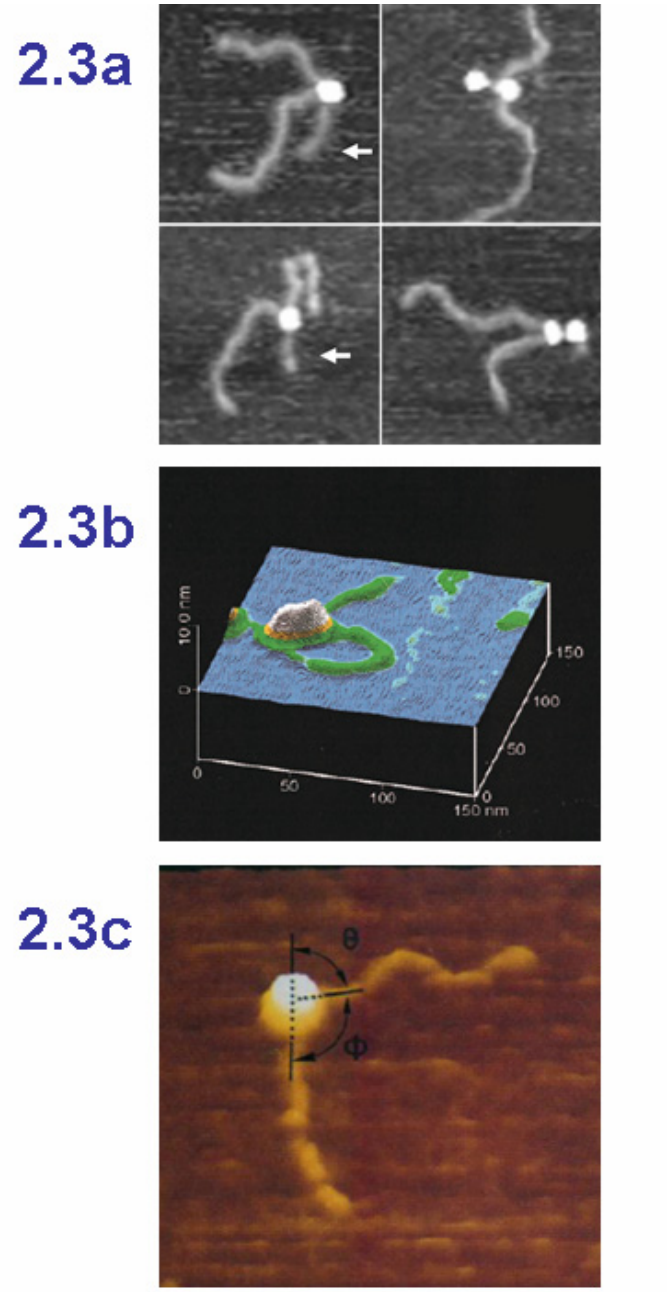

Figure 2.3 Examples of Direct Structural Analysis of Transcriptions Complexes with AFM. All images are approximately 200 nm^2. In these false color images, the lighter colored areas are higher topographic areas. In 2.3a, four selected images display the capability of AFM to visualize the extrusion of RNA from the *E. coli* TEC ternary structure (left). The arrows point to the nascent RNA chain. The two images on the right show that

multiple enzymes often bind the same DNA molecule (Rivetti, Codeluppi *et al.*, 2003). AFM is used to compose a 3D rendering of RNAP from *E. coli* and NtrC (*Salmonella*) simultaneously; the DNA wrap the enzymes (Figure 2.3b). Also noticeable is the loop structure in this image, caused by the "activation complex" interaction of RNAP and NtrC (Rippe *et al.*, 1997). In Figure 2.3c, AFM is used to measure the bend angle of single promoter complexes (shown in 3D). In this work, AFM is used to elucidate the transition between initiation and elongation stages as suggested by the distribution of DNA bend angles (Rees *et al.*, 1993).

2.2.3 Physical Limitations of AFM Imaging

In Figure 2.3b, is clear that AFM cannot assign the identities of similarly sized adjacent bodies. Another problem with AFM imagining involves the detection of small constructs in close proximity to large bodies. The physical geometry of the AFM probe limits the resolution of imaging. Figure 2.4 is a generic cartoon model of how AFM detects protein structures on a surface. The cartoon illustrates how two globular proteins of similar size and geometry are not distinguishable in topographic AFM images (Figure 2.4a). It is also clear how small accessory proteins, such as the ~20 kDa NusG, or ~19 kDa GreB, may not be detectable *via* AFM when interacting with the relatively massive RNAP (~450kDa); see Figure 2.4b.

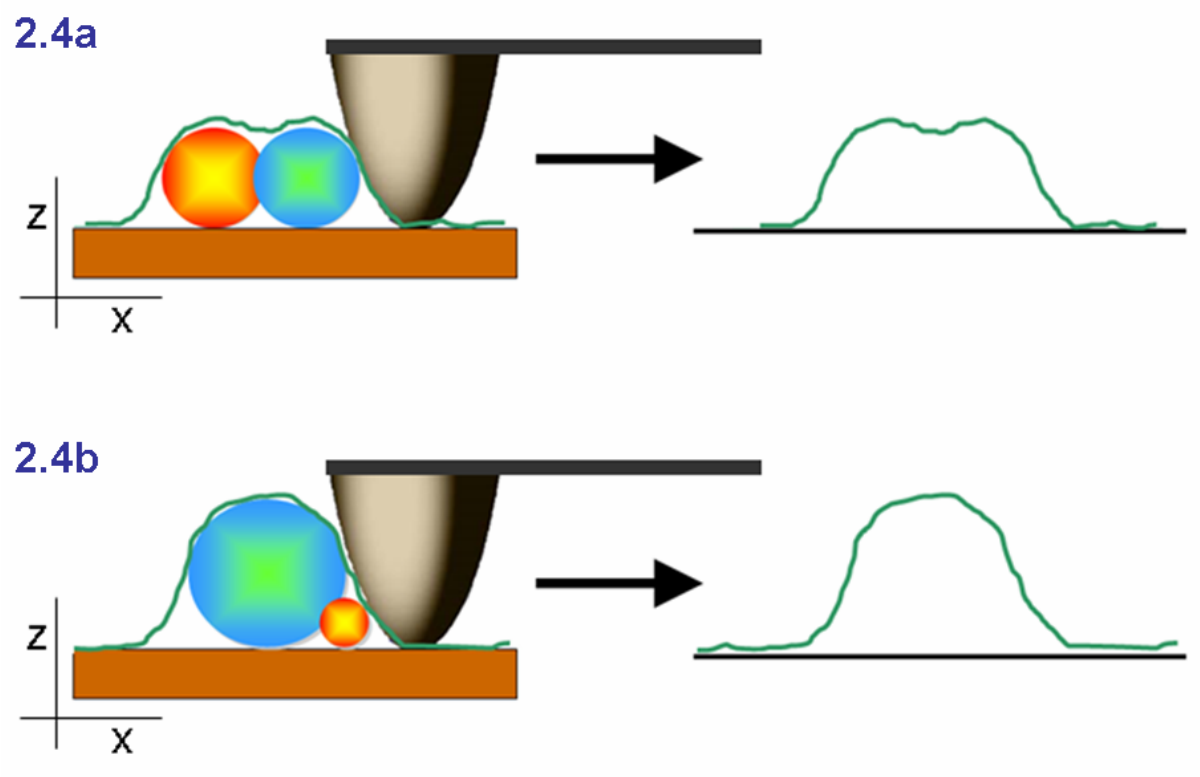

Figure 2.4 Physical Limitations in Topographic Imaging by AFM. In Figure 2.4a, the grey AFM probe encounters two proteins (orange and blue) as it is scanned across a single line in the x dimension. The green trace to the right is the resulting single line of data that would make up part of a topographic AFM image. Since the proteins are similar in size and geometry, AFM cannot distinguish between them. In Figure 2.4b, it is clear how the geometry of the AFM probe cannot detect the tiny orange protein adjacent to a large blue protein. The green trace to the right shows the detection of only one large body.

BIBLIOGRAPHY

Binnig, G., C. F. Quate and C. Gerber (1986). "Atomic Force Microscope." Phys Rev Lett **56**: 930.

Bustamante, C., D.A.Erie and D. Keller (1994). "Biological and Structural Applications of Scanning Force Microscopy." Curr Opin Struct Biol **4**(5): 750.

Bustamante, C. and D. Keller (1995). "Scanning Force Microscopy in Biology." Physics Today **48**: 32.

Bustamante, C. and C. Rivetti (1996). "Visualizing protein-nucleic acid interactions on a large scale with the scanning force microscope." Annu Rev Biophys Biomol Struct **25**: 395.

Chanutin, A., S. Ludewig and A. V. Masket (1942). "Studies on the Calcim-Protein Relationship with the aid of the Ultracetrifuge." J. Biol. Chem. **143**: 737.

Colowick, S. P. and F. C. Womack (1969). "Binding of diffusible molecules by macromolecules: rapid measurement by rate of dialysis." J. Biol. Chem. **244**: 774.

Ford, C. L. and D. J. Winzor (1981). "A recycling gel partition technique for the study of protein-ligand interactions: the binding of methyl orange to bovine serum albumin." Anal. Biochem. **114**: 146.

Ford, C. L., D. J. Winzor, L. W. Nichol and M. J. Sculley (1984). "Effects of thermodynamic nonideality in ligand binding studies." Biophys. Chem. **18**: 1.

Freire, E., O. L. Mayorga and M. Straume (1990). "Isothermal Titration Calorimetry." Anal. Chem **62**: 950A.

Garner, M. M. and A. Revzin (1981). "A gel electrophoresis method for quantifying the binding of proteins to specific DNA regions: application to components of the Escherichia coli lactose operon regulatory system." Nucleic Acids Res. **9**: 3047.

Goodman, D. S. (1958). "The Distribution of Fatty Acids between n-Heptane and Aqueous Phosphate Buffer." J. Am. Chem. Soc. **80**: 3887.

Guthold, M., M. Bezanilla, D. A. Erie, B. Jenkins, H. G. Hansma and C. Bustamante (1994). "Following the assembly of RNA polymerase-DNA complexes in aqueous solutions with the scanning force microscope." Proc Natl Acad Sci U S A. **91**(26): 12927.

Holmes, S. (2002). Downstream DNA Sequence Effects on Transcription Elongation: NTP Binding Induces Translocation Via A Ratchet Motion. Chemistry. Chapel Hill, University of North Carolina at Chapel Hill. **Ph.D.**

Hummel, J. P. and W. J. Dreyer (1962). "Measurement of protein-binding phenomena by gel filtration." Biochim. Biophys. Acta **63**: 530.

Klotz, I. M. (1946). "The application of the law of mass action to binding by proteins. Interactions with calcium." Arch. Biochem. **9**: 109.

Krummel, B. and M. J. Chamberlin (1992). "Structural Analysis of Ternary Complexes of *Escherichia coli* RNA Polymerase Individual Complexes Halted along Different Transcription Units Have Distinct and Unexpected Biochemical Properties." J Mol Biol **225**(2): 221.

Nakajima, K., M. Kinoshita, N. Matsushita, T. Urashima, M. Suzuki, A. Suzuki*, et al.* (2006). "Capillary Affnity Electrophoresis using Lectins for the Analysis of Milk Oligosaccharide Structure and its Application to Bovine Colostrum Oligosaccharides." Anal Biochem. **348**(10): 105.

Nichol, L. W. and D. J. Winzor (1964). "The determination of equilibrium constants from transport data on rapidly reacting systems of the type A + B.dblharw. C." J. Phys. Chem. **68**: 2455.

Pastre, D., O. Pietrement, S. Fusil, F. Landousy, J. Jeusset, M.-O. David*, et al.* (2003). "Adsorption of DNA to Mica Mediated by Divalent Counterions: A Theororetical and Experimental Study." Biophysical Journal **85**(10): 2507.

Perrin, J. H., J. J. Vallner and D. A. Nelson (1975). "Some Quantitative Investigations of the Binding to and the Displacement of Bishydroxycoumarin from Human Serum Albumin." Biochem Pharmacol. **24**(7): 769.

Ratcliff, G. C. and D. A. Erie (2001). "A novel single-molecule study to determine protein--protein association constants." J Am Chem Soc **123**(24): 5632.

Rees, W. A., R. W. Keller, J. P. Vesenka, G. Yang and C. Bustamante (1993). "Evidence of DNA Bending in Transcription Complexes Imaged by Scanning Force Microscopy." Science **260**: 1646.

Rippe, K., M. Guthold, P. H. von Hippel and C. Bustamante (1997). "Transcriptional activation via DNA-looping: visualization of intermediates in the activation pathway of E. coli RNA polymerase x sigma 54 holoenzyme by scanning force microscopy." J Mol Biol **270**(2): 125.

Robert, C. H., S. J. Gill and J. Wyman (1988). "Quantitative Analysis of Linkage in Macromolecules When One Ligand Is Present in Limited Total Quantity." Biochemistry **27**: 6829.

Sacho, E. J., F. A. Kadyrov, P. Modrich, T. Kunkel and D. A. Erie (2008). "Direct Visulaization of Asymmetric Adnine Nucleotide-Induced Conformational Changes in MutLa." Mol Cell **29**(1): 112.

Scatchard, G. (1949). "The Attractions of Proteins for Small Molecules and Ions." New York Acad. Sci. (51): 660.

Schulz, A., N. Mucke, J. Langowski and K. Rippe (1998). "Scanning force microscopy of Escherichia coli RNA polymerase.sigma54 holoenzyme complexes with DNA in buffer and in air." J Mol Biol **283**(4): 821.

Sophianopoulos, J. A., S. J. Durham, A. J. Sophianopoulos, H. L. Ragsdale and W. P. Cropper (1978). "Ultrafiltration is theoretically equivalent to equilibrium dialysis but much simpler to carry out." Arch. Biochem. Biophys. **187**: 132.

Svensson, H. (1946). Ark. Kemi Mineral. Geol. **22A**: 10.

Takeo, K. and S. Nakamura (1972). "Dissociation constants of glucan phosphorylase of rabbit tissues studied by polyacrylamide gel disc electrophoresis." Arch. Biochem. Biophys. **153**: 1.

Van Holde, K. E. and R. L. Baldwin (1958). "Rapid attainment of sedimentation equilibrium." J. Phys. Chem. **62**: 734.

Velick, S. F., J. E. Hayes and J. Hartling (1953). "The binding of diphosphopyridine nucleotide by glyceraldehyde-3-phosphate dehydrogenase." J. Biol. Chem. **203**: 527.

Winzor, D. J. and W. H. Sawyer (1995). Quantitative Characterization of Ligand Binding. New York, John Wiley and Sons, Inc.

Yang, Y., H. Wang and D. A. Erie (2003). "Quantitative characterization of biomolecular assemblies and interactions using atomic force microscopy." Methods **29**(2): 175.

CHAPTER 3:

CHARATERIZATION OF NUCLEOTIDE – TRANSCRIPTION ELONGATION COMPLEX INTERACTIONS

3.1 NTP-TEC Binding and Regulation in Transcription Elongation

The regulation of transcription is dependant on the interactions between RNAP and NTPs; however, the mechanism for NTP incorporation is not fully understood. Biochemical studies have suggested that more than one type of interaction between NTPs and RNAP effect the kinetics of transcription (Slepneva *et al.*, 1978; Nierman *et al.*, 1980; Slepneva, 1980; Darst, 2000; Foster *et al.*, 2001; Holmes *et al.*, 2003; Burton *et al.*, 2005). Non-catalytic allosteric NTP binding has been shown to shift transcription onto the activated synthesis pathway (Foster, Holmes *et al.*, 2001; Holmes and Erie, 2003), possibly by driving translocation (Burton *et al.*, 2005). Other work has suggested that more than two NTPs regulate transcription *via* interactions with RNAP and the downstream DNA during elongation (Burton *et al.*, 2005).

In addition to secondary channel access to the catalytic site, one model depicts an second possible route for NTP entry. Based on their results, Kennedy and Erie (2007) suggest that a NTP putatively bound to fork loop 2 can be shuttled past the bridge helix into the active site for incorporation via the main channel. Additionally, binding to fork loop 2 may trigger a cascade of conformational changes that have a "gate keeper" effect on NTP access to the active site via the secondary channel. The cartoon in Figure 3.1 is a representation of a transcription elongation complex (TEC) in the post translocated state

(Kennedy *et al.*, 2008). The catalytic site and the putative location of the allosteric site (fork loop 2) are identified, but are shown unoccupied by NTPs. Highlighted in Figure 3.1 is the close proximity of fork loop 2 to the downstream DNA position i+2. On the other side of the bridge helix and the mobile trigger loop is the catalytic site in register with the i+1 nucleotide (the product terminus postion (i) is not labeled).

The models showing simultaneous nucleotide occupancy fit well with the biochemical data; however, direct evidence does not exist that proves that multiple NTPs can bind tightly to TECs at once. We sought to determine the number of tight binding sites that exist on TECs; in doing so, we aimed to ascertain the non-templated NTP occupancies of those sites. In addition, we were interested in determining the passive (non-competitive) off rates for NTPs bound to TECs, as well as investigating possible active (competitive) displaced mechanisms for NTP dissociation. Pooling these data with the current doctrine in nucleotide incorporation will aid in generating mechanistic models for RNA synthesis by RNAP.

Here we present a purification method specific to transcription that facilitates the characterization of NTP-TEC binding and dynamics. We estimate the total NTP-TEC binding stoichiometry to be 2. We find however, that each non-catalytic NTP exhibits unique binding behavior that may be closely related to the sequence context of the template DNA.

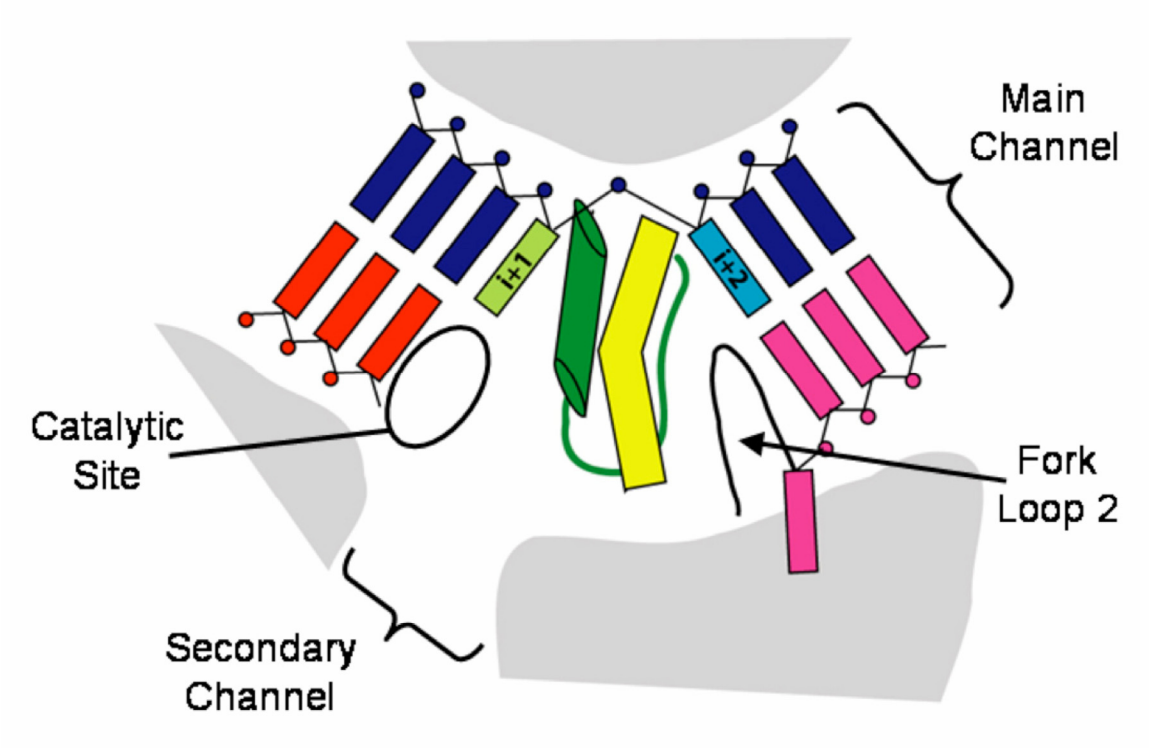

Figure 3.1 A Cartoon Model Showing Multiple Template Dependant NTP Binding Locations. Fork loop 2 (βD loop I), the bridge helix (F-helix) and the trigger loop are shown in black, yellow and green, respectively. The template strand of the DNA is shown in dark blue, with the exception of the i+1 and i+2 downstream bases, displayed in light green and light blue, respectively. The non-template DNA strand (pink) is shown leaving the main channel near the fork loop. The nascent RNA strand is displayed in red. The RND-DNA hybrid is displayed in the post-translocated state here. Figure courtesy of Kennedy and Erie (2008) (Kennedy *et al.*, 2008).

3.1.1 Previous NTP-SEC Ratio Assays

Synthesis and purification of stalled elongating complexes (SECs) in our laboratory is traditionally facilitated by irreversibly binding biotinalated template DNA (bound to the SEC) to streptavidin coated, magnetic solid support beads (Holmes *et al.*, 2003). By placing the reaction tube next to a magnet, the solution of radioactive NTPs used in synthesis can be washed away. TLC analysis of the radiolabeled NTPs and transcript bound to DNA was inhibited by the large background effects of non-specifically adsorbed NTPs on the magnetic beads. Attempts to the scavenge NTPs from the solution with an apyrase reaction were not sufficient to decrease the background radioactivity with of the low concentration restraints of purified SECs (Holmes, 2002). Efforts were also made to cleave the SECs from the beads using an EcoRI endonuclease site on the template DNA; however, the EcoRI protocol tended to slough more non-specially adsorbed NTPs from the beads than the complexes it liberated (Holmes, 2002).

Monomeric avidin coated bead matrices have recently become commercially available (Pierce, Rockford, IL). Unlike, irreversible biotin-streptavidin interactions, biotin-monomeric avidin binding is reversible *via* competition with biotin. We have developed a detailed protocol using monomeric avidin technology to synthesize and purify transcription complexes. Most important, during the SEC-support matrix separation, the protocol does not induce the release of non-specifically absorbed NTPs from the matrix. We have termed the protocol Reversible Matrix Assisted Phase Partitioning (RevMAPP).

3.2 Methods

3.2.1 RevMAPP Method: SEC Synthesis and Purification

Monomeric avidin coated UltraLink matrix beads were prepared in accord with the supplied supporting literature (Pierce, Rockford, IL). To bind the template DNA to the matrix, biotinalated DNA (200 nM) was incubated in 20 μL of monomeric avidin coated UltraLink matrix slurry [1.0 mM phosphate buffer (pH 7.2)] for 20 min at room temperature. The phosphate buffer was exchanged for 1X transcription buffer [30 mM HEPES-NaOH (pH 8.0), 10 mM Mg^{+2} glutamate, 200 mM K^{+} glutamate, 1 $mg \cdot mL^{-1}$ BSA, and 1 mM DTT] via a series of three 200 μL washes, each subsequent to 20 sec spinning at 5000 RPM (200 x G) in a Nanofuge bench top centrifuge (Hoefer Scientific Instruments, San Francisco, CA). Open Promoter Complexes (OPCs) were formed by adding 100nM RNAP at 37°C for 10 min a final suspension volume of 40 μL. To synthesize stalled elongation complexes, 20 μM ATP, 20 μM GTP and 15 μM UTP were added to a final volume of 60 μL. In each experiment, one or more [α-^{32}P]- or [γ-^{32}P]-labeled NTP was used; a record was kept of the radioisotope specific activities for the subsequent determination of the transcript free nucleotide concentration.

The addition of all NTPs minus CTP stalled transcription during elongation at position 24 as per the DE13 sequence:

5'-pppAUGUA GUAAG GAGGU UGUAU GGAA**C** AACGC AUAAC CCUGA-3'

where "**C**" was the first CMP templated for incorporation. In some experiments, only [γ-^{32}P]-labeled nucleotides were used during SEC synthesis. When [γ-^{32}P]-ATP was used, the only source of radioactive signal from the nascent transcript was the 5' γ-phosphate. Alternatively, SEC syntheses with NTPs labeled on the α phosphate was used; in which case

the radioactively of the transcript was proportional to the number of the type of NTP in the DE13 sequence. For example, comparing free [α-^{32}P]-UTP to a stoichiometric equivalent of transcript from SECs made using [α-^{32}P]-UTP, the transcript is 7 times more radioactive.

The fundamental post-synthesis steps in the RevMAPP protocol are pictorially diagramed in Figure 3.2. The RNA synthesis described above was allowed to occur for 60s before 200 µL of cold transcription buffer was added. The suspension was phase partitioned by centrifugation at 200xG for 5 - 10 sec and the supernatant was removed. Special care was taken to not disturb the loose ~20 µL matrix pellet. The complexes were resuspended and centrifuged repeatedly until the supernatant was free of detectable by a Geiger counter. To prevent the release of non-specifically adsorbed NTPs from test tube walls during further reactions or quenching procedures, the complexes attached to monomeric avidin beads were transferred to a new tube prior to bead-SEC separation.

SECs were removed from the monoavidin beads by incubating the matrix in 10-25 µL 1 mM biotin solution for 4-5 min. The solution was centrifuged at 3000 x G for 1 min and the supernatant was removed. To remove any beads still suspended in solution, the supernatant was passed through a 0.22 µm, 10 µL capacity syringe filter (Fisher Scientific, Pittsburg, PA). Before PAGE analysis, the samples were boiled at 90°C for 30 sec in formamide and loading dye (bromothymol blue and xylene cyanol). All samples were run analyzed by 8 M urea-20 % polyacrylamide gel electrophoresis. For analysis of NTP and SEC quantities, the samples were run at 55 W for 4 hours. For detailed analysis of the transcript length distribution, the sample was electrophoresed at 55 W for 8 hrs.

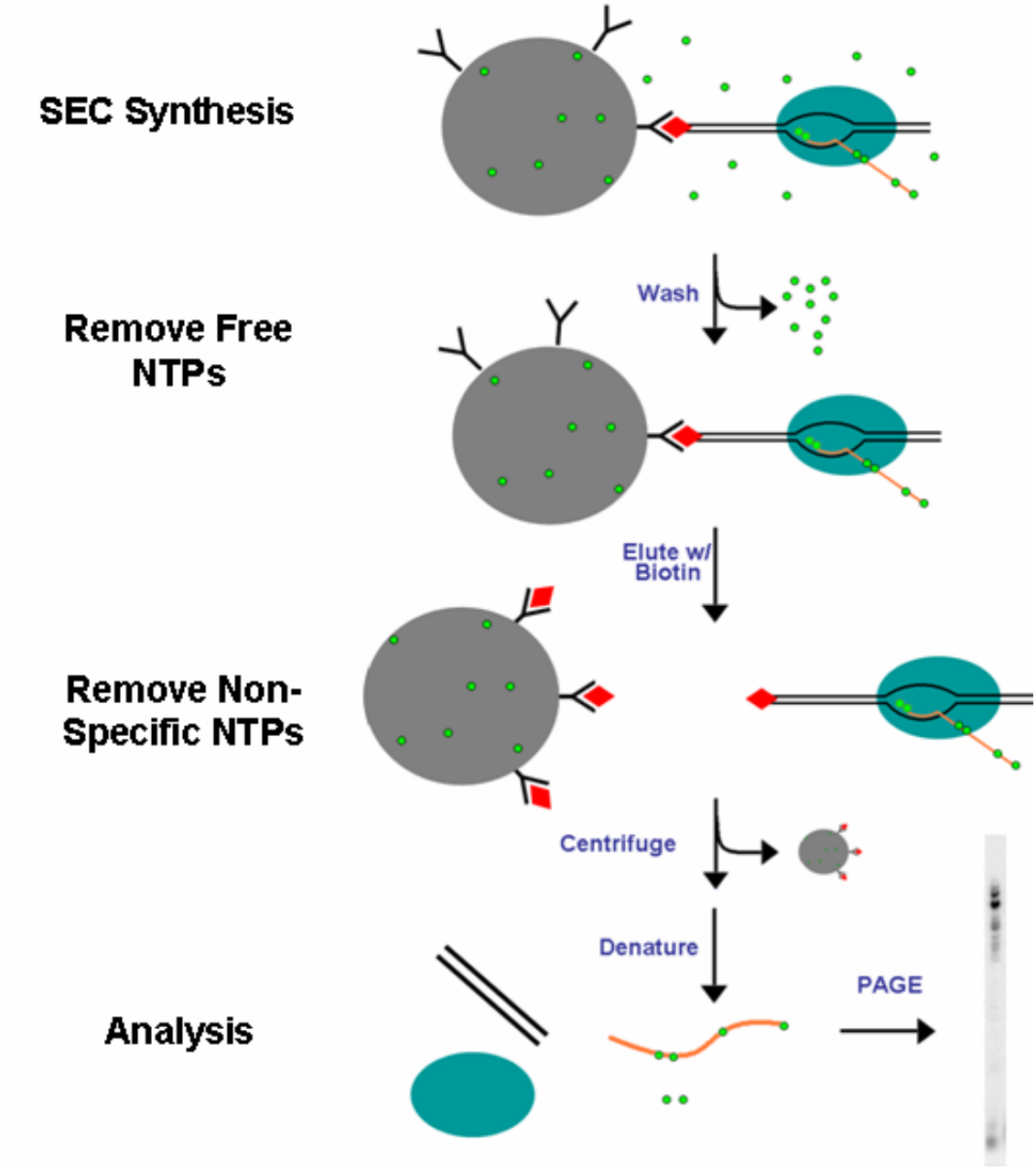

Figure 3.2 The Fundamental Steps of the RevMAPP Protocol. The green dots represent ^{32}P radiolabeled nucleotides. The grey sphere is an UltraLink monomeric avidin coated bead, the red diamonds are biotin. The DNA, RNA and RNAP are shown in black, tan and teal, respectively. The 20% PAGE gel image in the lower right shows an example of how the radiolabeled transcript lengths (top of gel) and NTPs (bottom of gel) migrate. Subsequent to RevMAPP, only the NTPs initially bound to RNAP appear on the gel.

3.2.2 Determination of the Minimum Required Washes

To determine the minimum number of washes needed to effectively remove the nonspecific background with the RevMAPP protocol, the value of the NTP-SEC ratio was monitored after each wash, up to 16. After each re-suspension step (wash), an aliquot of the matrix was removed; the complexes from the aliquot was eluted from the matrix with biotin and analyzed by PAGE (see figure 3.2). The NTP-SEC ratio was quantified by analyzing the radioactivity in the NTP and transcript bands on the PAGE gels using the Image Quant software (version 5.2). For each NTP-SEC ratio determination, the transcript radioactivity was divided by the number of bases in the sequence for the corresponding NTP. Each type of NTP-SEC wash control was performed 3 times (N=3).

3.2.3 Determination of NTP-SEC Stoichiometries

The RevMAPP protocol was followed for the determination of the ATP-SEC, GTP-SEC and UTP-SEC ratios. Each experiment was validated by a number of crucial controls, as outlined in Appendix B: RevMAPP Controls. Briefly, all experiments reported here were validated by RNAP- (negative) controls to identify sources of non-specific absorption of NTPs. Additionally, the transcript lengths synthesized by RNAP were monitored to ensure that the vast majority of complexes contained the same sequence context (template postion)

3.2.4 Determination of NTP-SEC Dissociation Rates

Figure 3.3 schematically explains the off rate analysis in buffer and in the presence of 1 mM unlaced competitor. SECs were prepared with [α-^{32}P]-GTP and the free NTPs were removed as described above. The ~20 µL of SECs attached to the matrix were diluted 10X

with transcription buffer and split into several aliquots. The aliquots were then washed an additional 3X from 5 to 180 min. Any GTP that had dissociated from the SECs between the time of the initial synthesis and the time of the final wash was removed from solution. Each aliquot was eluted and the GTP-SEC ratio was measured. A second batch of SEC was made with labeled GTP and split into aliquots. Instead of diluting the complexes in buffer alone, the SECs were diluted in a solution of 1 mM unlabeled GTP, and the time course was followed as explained above. Both competitive and non-competitive experiments were completed using [α-^{32}P]-ATP as well. All GTP and ATP experiments were completed in duplicate (N=2). A preliminary study of the UTP rate of dissociation in the absence of competitor was also preformed.

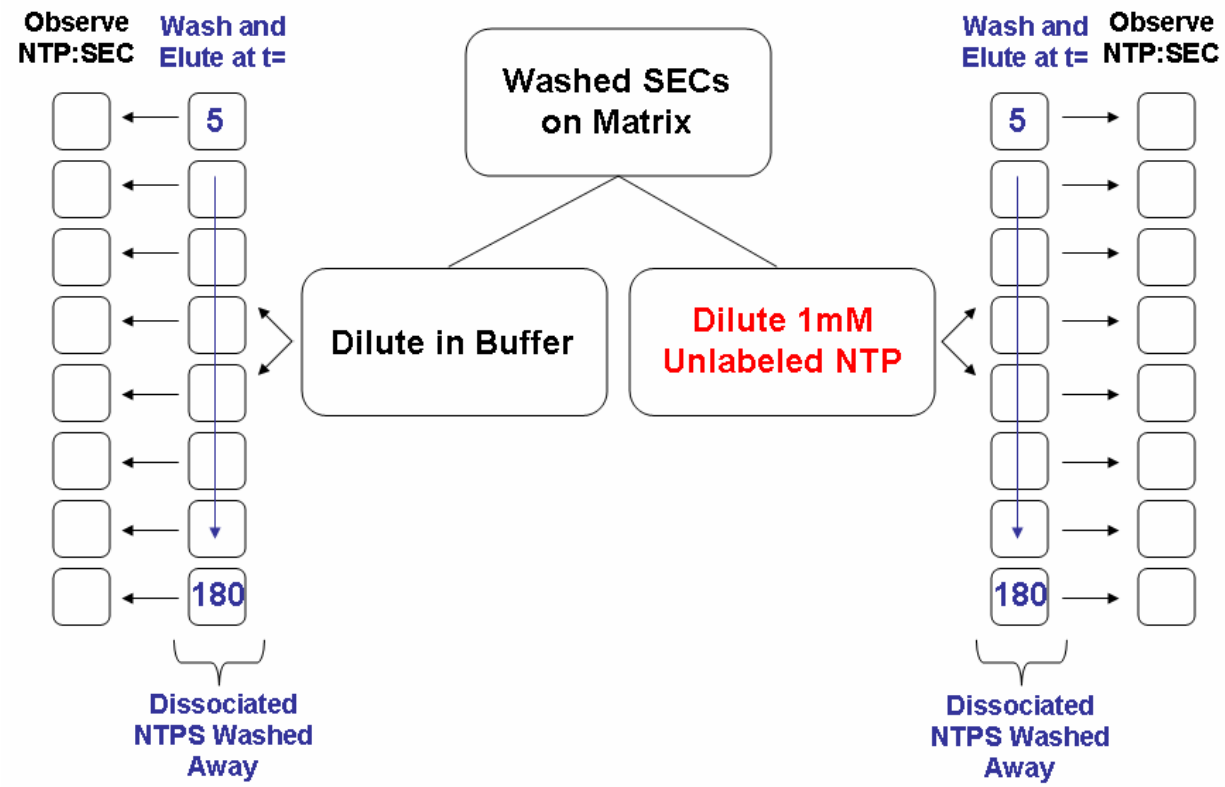

Figure 3.3 Diagram of NTP-SEC Dissociation Rate Experiments. The NTP-SEC ratios were analyzed as a function of time both in the presence and absence of unlabeled competitor. Time (t) is in min. The time a NTP-SEC aliquot is allowed to dissociate begins at the first purification wash after synthesis, and ends at the last wash during the time course. GTP and ATP analyses were completed.

3.2.5 Competition Assays Using dNTPs

To investigate the displacement of NTPs by dATP and dCTP, SECs were synthesized with [α-^{32}P]-ATP, -GTP or –UTP, and the free NTPs were washed away. Each batch of SECs were split into three fractions: one that was washed an additional 3 times, one that was incubated in 100 μM dCTP for 5 minutes before 3 additional washes, and another that was incubated in 100 μM dATP for 5 min before 3 additional washes. The complexes were eluted from the matrix and the GTP-SEC ratios were observed. The assay was also followed using 100 μM dATP as the competitor. Each was repeated at least 3 times (N=3). Figure 3.4 is a diagram for the dNTP competitive assay.

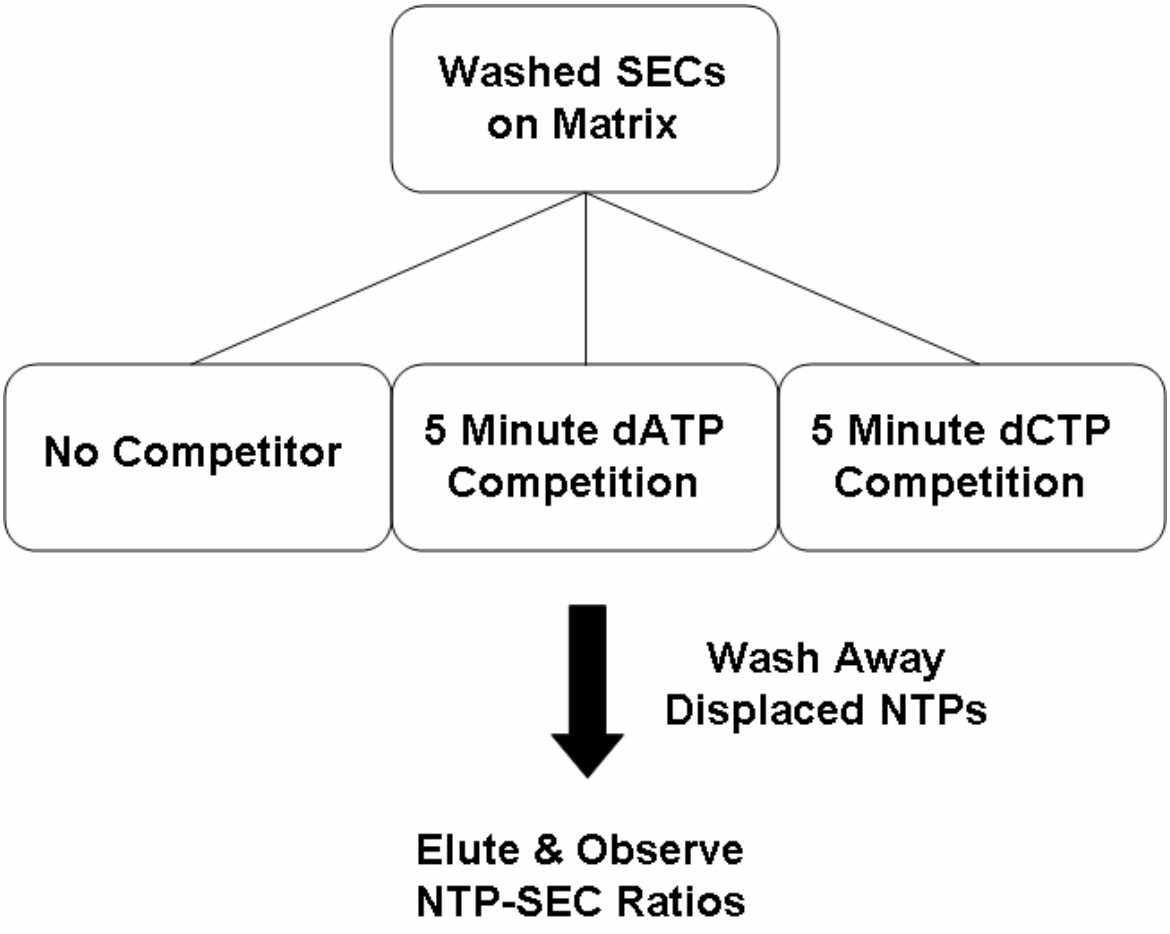

Figure 3.4 Diagram of the dNTP competitive Assay. The dATP and dCTP competitive assays were completed to study the displacement of GTP, UTP and ATP from SECs.

3.2.6 Detection of NTP Displacement Related to Catalysis

To probe the effects of catalysis on the NTP-SEC occupancies, SECs were synthesized on the UltraLink matrix using [α-^{32}P]-UTP and were split into two fractions: one that was incubated in a 30 μM CTP solution, and one that was left unaltered (control). After one min, both the control fraction and CTP reaction were washed 3X with transcription buffer and eluted for UTP-SEC ratio analysis. Figure 3.5 is a diagram of the procedure followed for the CTP catalysis assay. Radiolabeled ATP and GTP were also used in the NTP-SEC catalysis assays. All catalysis assays were performed a minimum of 3 times (N=3).

To observe the effects of catalysis on ATP and GTP simultaneously, [α-^{32}P]-ATP and [γ-^{32}P]-GTP were used to synthesize one batch of SECs, and the catalysis assay was followed as shown in figure 3.5. Equal specific activities of the radionucleotides were used in the synthesis. [γ-^{32}P]-GTP does not radiolabel the transcript since the radioactive PP_i is released. In the simultaneous ATP-GTP-SEC catalysis assay, the only source of transcript radioactivity was from [α-^{32}P]-ATP incorporation.

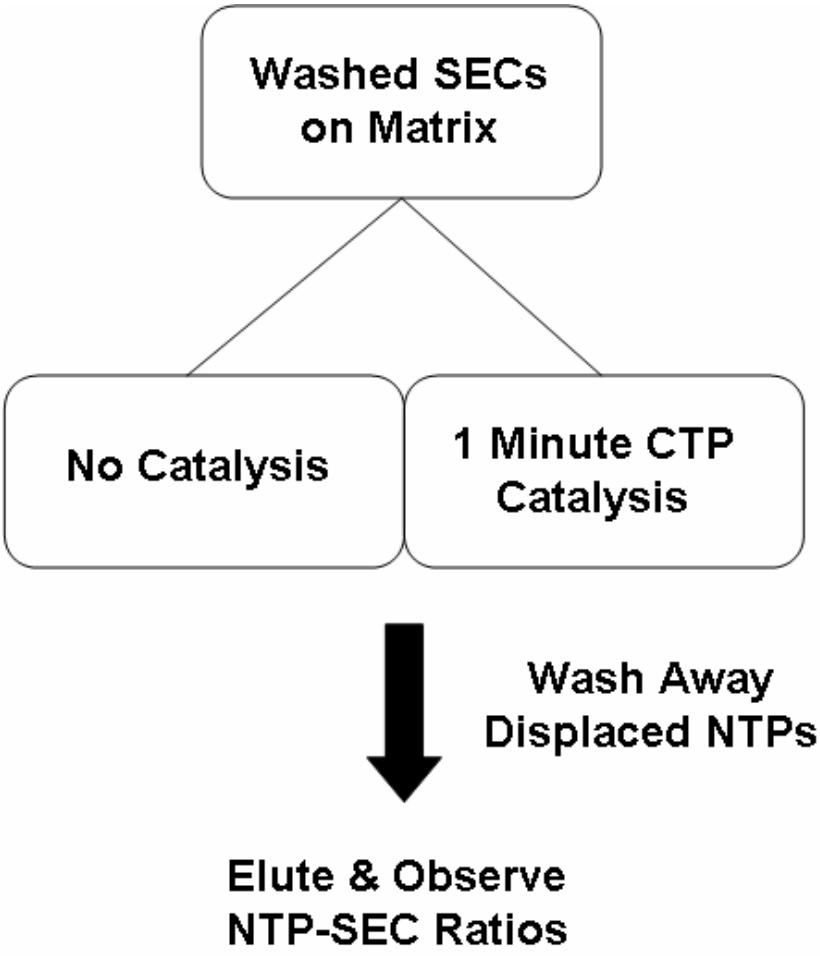

Figure 3.5 Diagram of CTP Catalysis Assay for NTP Displacement. The catalysis assays were completed for ATP, UTP and GTP.

3.2.7 GTP Binding Affinity Assay

Figure 3.6 is a diagram of the procedure followed for the GTP binding affinity assay. SECs we synthesized using [α-^{32}P]-ATP and the free NTPs were washed away (see figure 3.2). The SECs were fractionated, diluted in transcription buffer and placed on ice for at least 2 hours to allow the bound GTP to completely dissociate (see table 3.2). [α-^{32}P]-GTP was then titrated into fractions, ranging from 0.63 μM to 150 μM. To increase the sensitivity of the lower concentrations, we increased the specific activity of [α-^{32}P]-GTP. The final GTP-SEC stoichiometries were normalized per the specific activity of each concentration. The solution was allowed to incubate for 1 min. Each titration was washed ~7 times before being transferred into a new tube, washed 2 more times, eluted with biotin, and analyzed by 8 M urea 20% PAGE. The GTP-SEC titration was completed in duplicate (N=2).

To determine whether the binding between the titrated GTP and the RNAP was at equilibrium, a cold (unlabeled) competition was performed (Winzor *et al.*, 1995). SECs were prepared as above and labeled 30 μM GTP was divided into two fractions. To one of the fractions, 1 mM cold GTP was added in and the solution was allowed to incubate for an additional 60 sec before washing and analysis. See Appendix B: RevMAPP Controls.

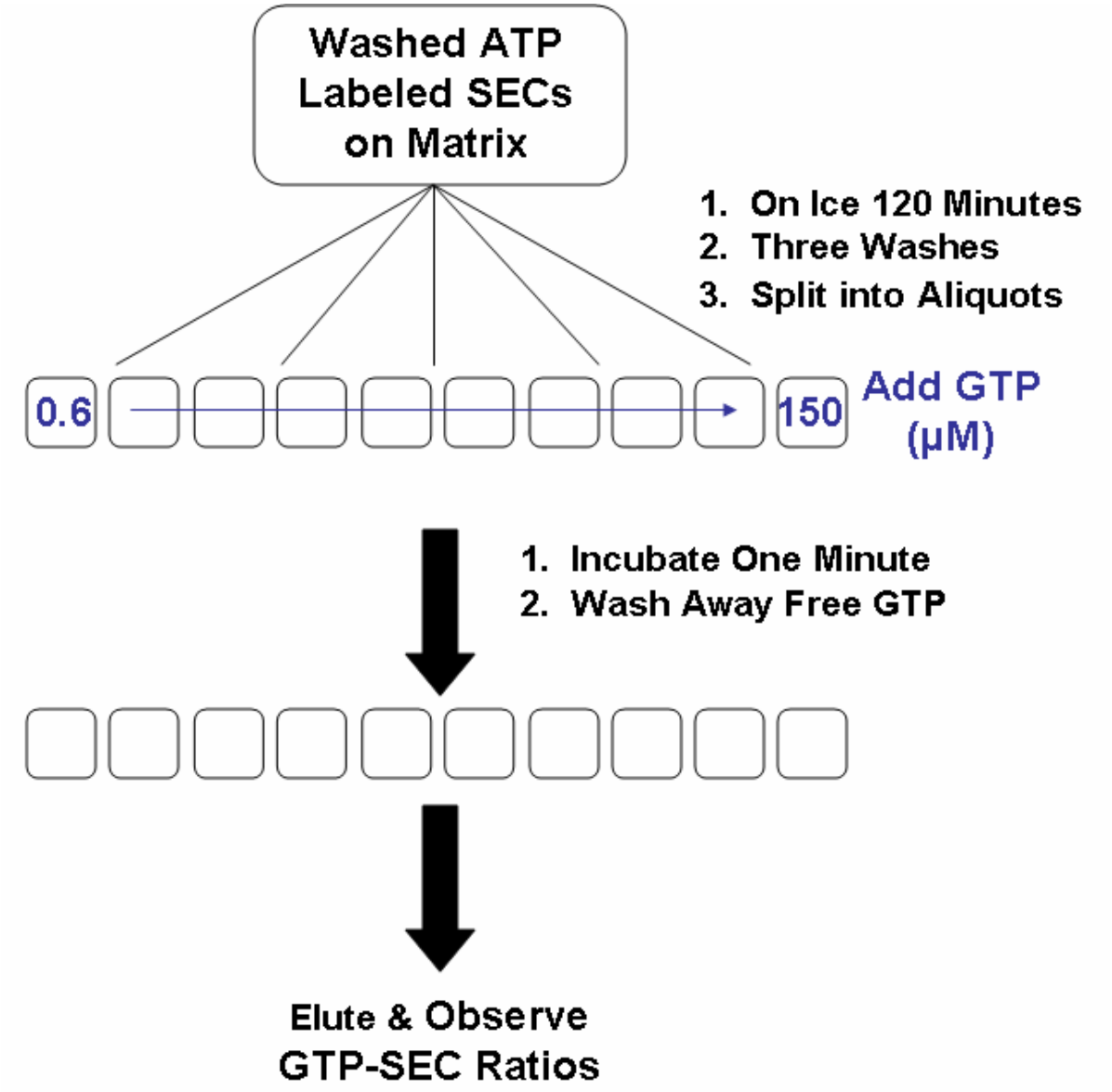

Figure 3.6 Diagram of the GTP-SEC Binding Affinity Assay.

3.3 Results

3.3.1 Approximately 7-10 Washes are Required to Remove Non-Specific Background

Example data from the minimum wash control experiments are shown in Figure 3.7. In this experiment, we observed the UTP-SEC ratio decrease over the first 6 washes before a minimum value of 0.83 was reached; ~80 % of SECs have a UTP bound. The data show that the UTP-SEC value remained at 0.83 ± 0.06 for washes 7 -16. We were able to complete wash number 7 within five min of SEC synthesis. The last wash (16) was completed around 10 minutes after SEC synthesis. In Figure 3.7, the observed UDP band was an artifact of over-boiling (see Appendix B: RevMAPP Controls). We determined that the minimum NTP-SEC values were reached in 7-10 washes for ATP-SEC and GTP-SEC wash controls as well.

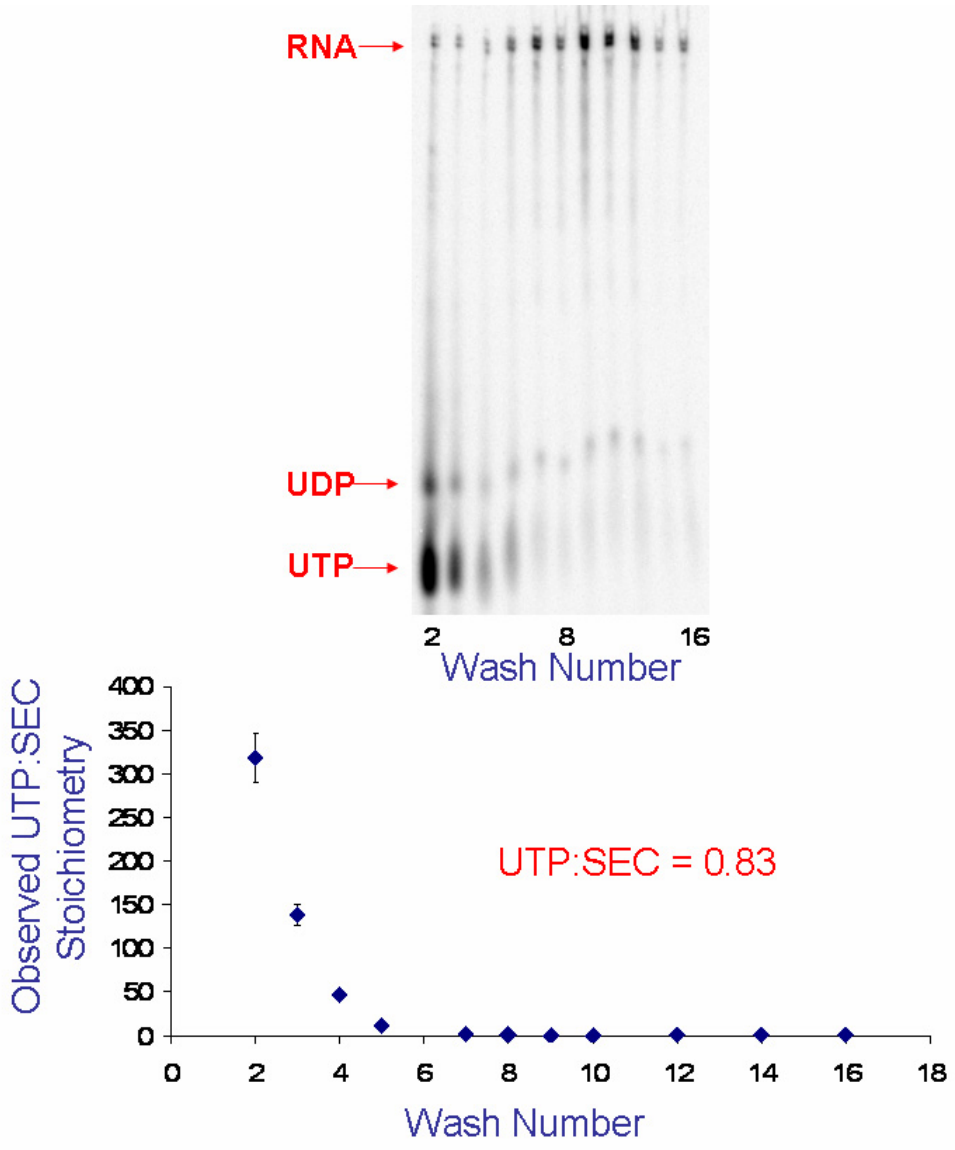

Figure 3.7 RevMAPP Removes Non-Specific Background in about 7 Washes. In this UTP-SEC wash control example, the PAGE gel was quantified with ImageQuant (version 5.2). The transcript radioactivity was divided by 7 and compared to the UTP + UDP bands; some of the UTP was thermally degraded due to over-boiling (see Appendix B: RevMAPP Controls). The observed that the UTP-SEC stoichiometry reached a minimum of 0.83 ± 0.06 in as little as 7 washes in less than five minutes, as seen in the graph of the data.

3.3.2 The Tight NTP-SEC Stoichiometry is Roughly 2.

Figure 3.8 shows some of the data collected that lead us to decipher the individual nucleotide occupancies on SECs and compile the total NTP-SEC stoichiometry. Table 3.1 shows that individual and total NTP-SEC occupancies that we observed. For the NTP-SEC calculations, we normalized the transcript radioactivity proportionally to the number of labeled nucleotides in the transcript (as explained above). The various transcript lengths contained different numbers of incorporated NMPs depending on the DE13 template DNA sequence. The radioactivity of each band was quantified and dived by the number of labeled nucleotides in the corresponding transcript length. For [α-^{32}P]-GTP and [α-^{32}P]-UTP occupancy determinations, the transcript was body-labeled on the corresponding α-phosphates throughout the transcript (Figures 3.8a and 3.8b). Shown in Figure 3.8c is the determination of the ATP-SEC ratio where [γ-^{32}P]-ATP was used to synthesize the SECs. When [γ-^{32}P]-ATP was used, on the γ-phosphate of the transcript was the only source of RNA radioactivity. We observed that using [α-^{32}P]-ATP for ATP-SEC analysis revealed the identical occupancy of ATP. Every experiment reported in this section pass a number of RevMAPP controls (Appendix B: RevMAPP Controls)

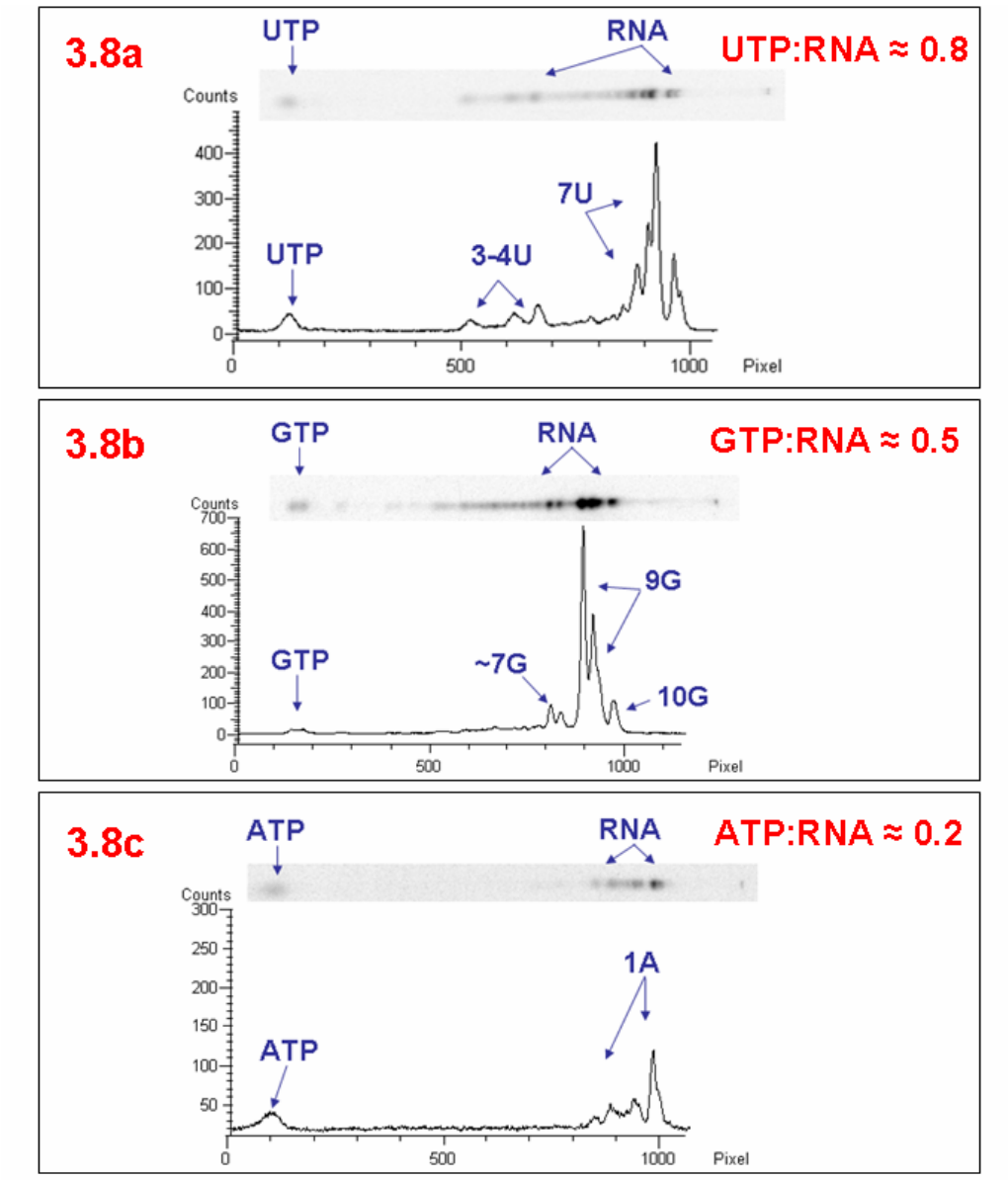

Figure 3.8 Direct Calculation of All Non-Templated NTP-SEC Stoichiometries. The DE13 DNA template is displayed at the bottom of this figure for reference. The numbers of radionucleotides in each RNA band are identified in each of the gels. The UTP- and GTP-SEC ratios were determined using α-phosphate labeled NTPs (Figures 3.8a and 3.8B) and the ATP-SEC ratio was determined using γ-phosphate labeled ATP for this example (Figure 3.8C). The DE13 DNA template sequence is shown at the bottom for reference.

Nucleotide	ATP	GTP	UTP	Total
NTP:SEC Stoichiometry	0.22 ± 0.09	0.53 ± 0.09	0.84 ± 0.12	**1.62 ± 0.30**
Iterations (N)	6	5	4	——

Table 3.1 NTP:SEC Stoichiometry Consensus. We report here the individual and total NTP occupancies on SECs purified using the RevMAPP purification protocol. We compiled these data from a number of iterations (N) that passed a myriad of RevMAPP validation controls (see Appendix B: RevMAPP Controls).

3.3.3 The NTP-SEC Rates of Dissociation are Slow

Figure 3.9 is a plot of the GTP-SEC ratio decay in the presence and absence of 1mM unlabeled GTP competitor. We report the passive (no competitor) and active (with competitor) rates of GTP-SEC dissociation are shown in Table 3.2. We determined that rate of GTP dissociation is not affected by 1 mM unlabeled GTP competition. We assayed the active and passive rates of ATP-SEC ratio decay from the data shown in Figure 3.10. As the data show in Table 3.2, ATP is dissociated from SECs very slowly in the absence of competitor. In the presence of unlabeled 1 mM ATP however, we observe a 10-fold increase in the rate of dissociation.

Our preliminary studies of the UTP-SEC passive off rate in the absence of cold competitor appears be very slow; similar to the k_{off} of ATP. We could not perform a 1 mM unlabeled UTP competition because UTP will quickly misincorporate for CTP under moderate (mid-micromolar) UTP concentrations (Erie *et al.*, 1993; Cunningham, 2008).

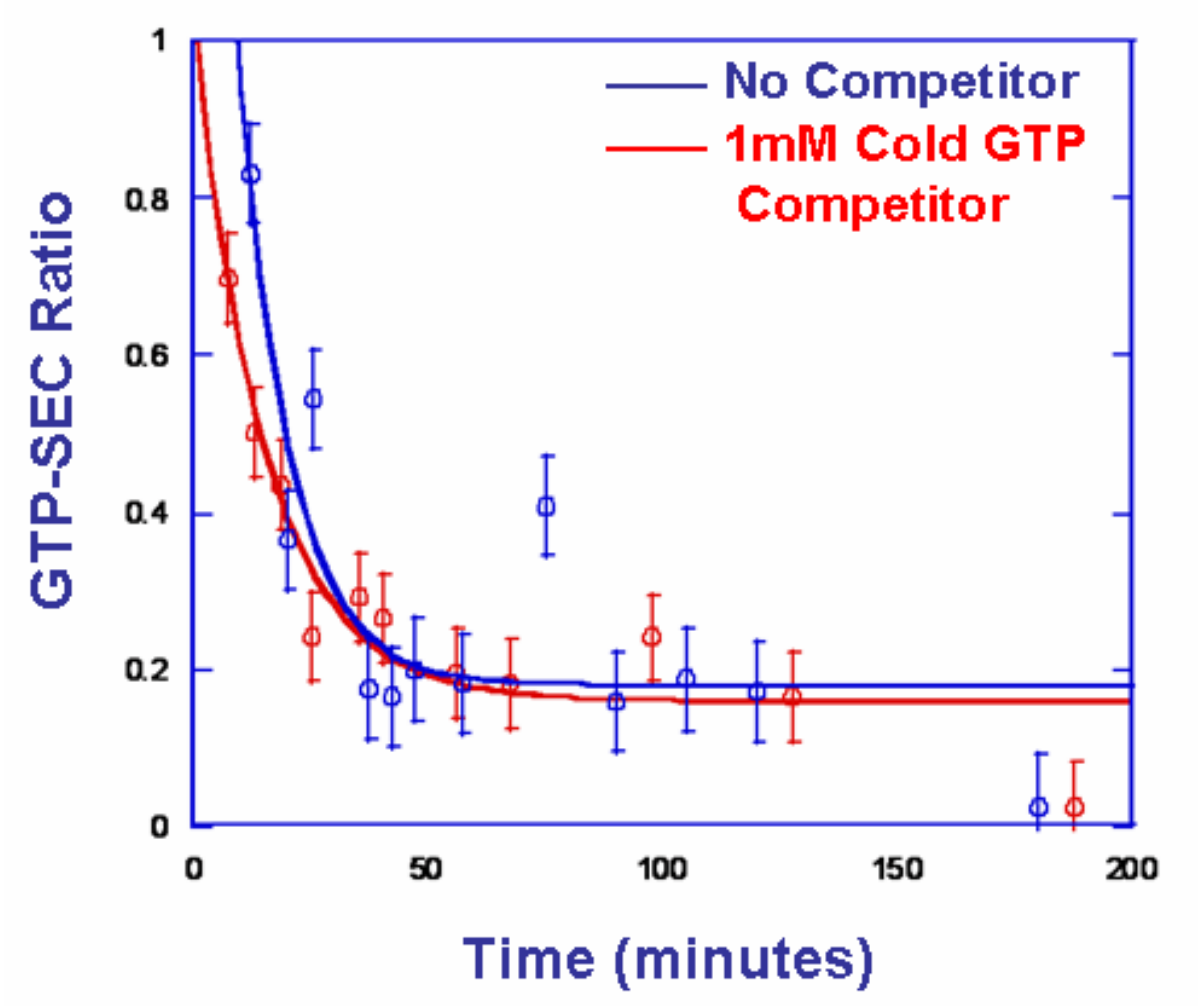

Figure 3.9 GTP-SEC Ratio Decay is Unaffected by a Cold Competitor. The GTP-SEC occupancies plotted as a function of time in the presence and absence of unlabeled GTP. These data were fit to a single exponential decay expression.

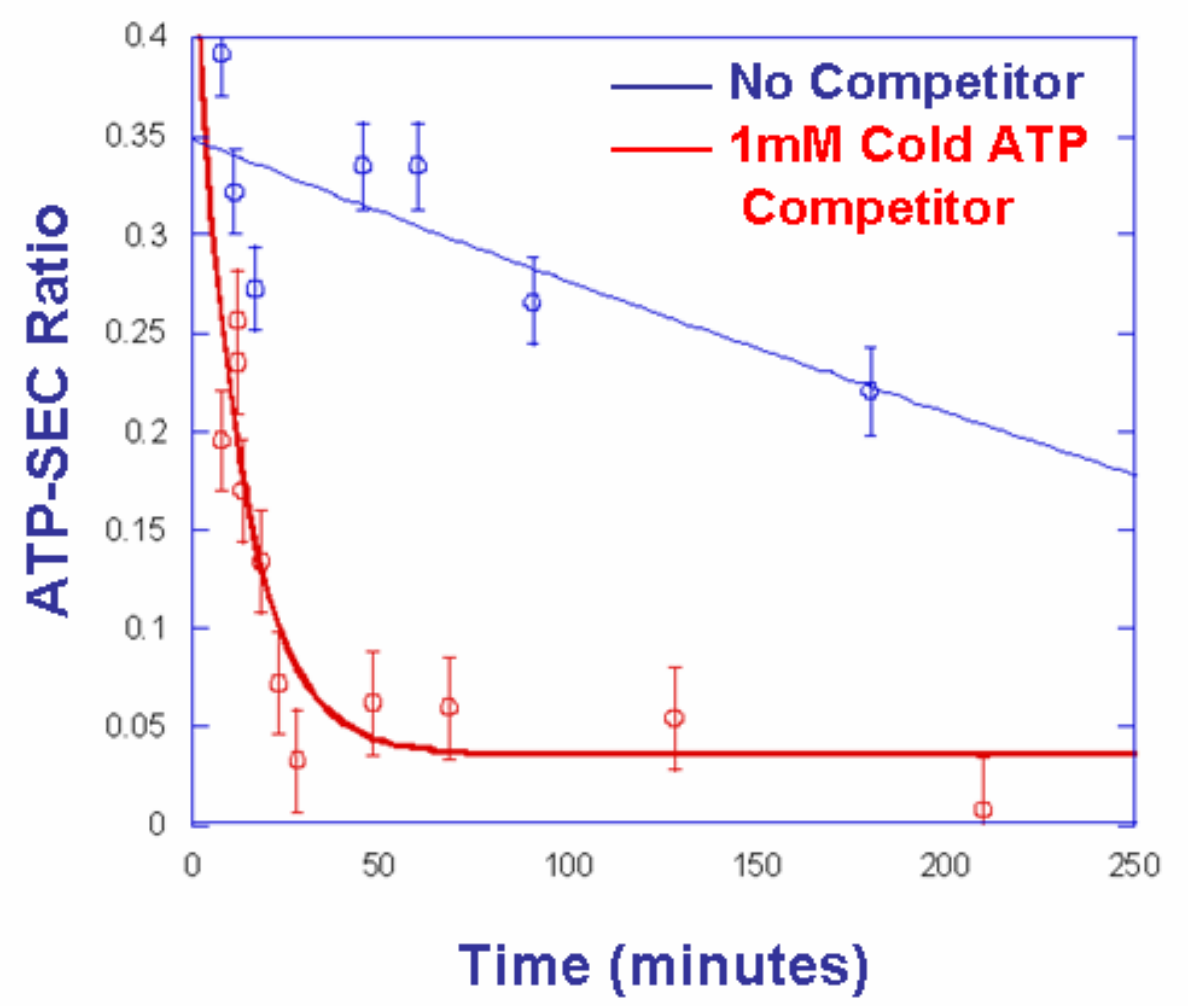

Figure 3.10 ATP-SEC Ratio Decay is Affected by the Presence of Cold Competitor. The ATP-SEC occupancy was monitored in the presence and absence of 1mM unlabeled ATP and plotted as a function of time. The passive off rate of ATP in the absence of competitor is very slow. The presence of 1mM cold ATP actively accelerates the dissociation of the ATP-SEC complexes 10 fold.

Nucleotide	Cold Competitor	Decay (k_{off})	N
GTP	none	$0.091 \pm 0.038 min^{-1}$	2
GTP	1 mM GTP	$0.065 \pm 0.018 min^{-1}$	2
ATP	none	$7.0e^{-4} \pm 2.7e^{-6}$ min-^{1}	2
ATP	1 mM ATP	$0.080 \pm 0.003 min^{-1}$	2
UTP	none	$1.1e^{-3}$ min^{-1}	1

Table 3.2 The Passive and Active Dissociation Rate of NTP-SEC Complexes. We report the passive off rates for ATP, GTP and preliminary results for UTP. We show the data for the active rate of dissociation for GTP-SEC and ATP-SEC complexes as well.

3.3.3 ATP, GTP and UTP are Displaced Differently by dATP and dCTP

We present in Figure 3.11 an example of a dNTP competition assay. The data in Figure 3.11 show that 100 μM dCTP displaced GTP from the SEC. Our experiments revealed that dCTP displaced GTP and UTP, but not ATP. We found that 100 μM dATP completely displaced GTP within 5 minutes, but not UTP or ATP. Table 3.3 shows the comprehensive results of the dNTP competition study.

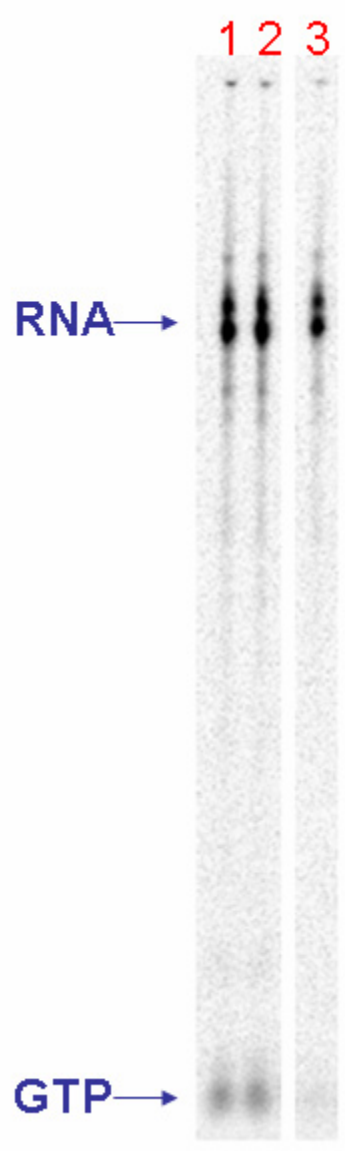

Figure 3.11 An Example of a dNTP Competitive Assay: GTP is Displaced by dCTP. In Lane 1, the GTP occupancy of purified GTP labeled SECs were analyzed; the GTP-SEC ratio was ~0.5. In lane 2, a fraction of the complexes were allowed to incubate for 5 min in buffer. Lane 3 shows the effect of a 5 min, 100 μM dCTP incubation. The GTP was completely removed by dCTP.

	Displaced 100% GTP	Displaced 100% UTP	Displaced 100% ATP
100 μM dCTP	YES	YES	NO
100 μM dATP	YES	NO	NO

Table 3.3 Competition dNTPs Selectively Displace NTPs from SECs. This table reports whether or not we observed complete displacement of NTPs by incubating the complexes in 100 μM dNTPs.

3.3.4 Catalysis Completely Displaces UTP and ATP, but not GTP, from Purified SECs

Shown in Figure 3.12 are the results of catalysis experiments with GTP and UTP where, in both cases, we observe 100 % elongation past all C-stall template positions. See Appendix B: RevMAPP Controls, for a discussion for the relevance of the transcript distribution. Subsequent to 100 % catalysis with 30 μM CTP, the data show (Figure 3.12a) that nearly 100% of the UTP bound to the SECs was removed. In Figure 3.12b, however, we show that only about 25 % of the GTP bound to SECs was displaced as a result of complete catalysis.

We observed that the extent of catalysis by 30μM CTP varied between experiments. For example In the ATP-SEC catalysis assay shown in figure 3.13, we noted that the ATP-SEC ratio was reduced by half when approximately 50% of the complexes were walked past the C-stalls with 30 μM CTP (See Appendix B for a discussion on the simultaneous NTP occupancy and distribution transcript analysis).

In the simultaneous ATG-GTP-SEC catalysis assay, we observed 100 % catalysis; 100% of the ATP was removed in this experiment and only 40% of the GTP was displaced as a result of catalysis (Figure 3.14). Our analysis of the data in Figure 3.14 shows that the GTP-SEC ratio was reduced from 0.49 to 0.29 subsequent to catalysis.

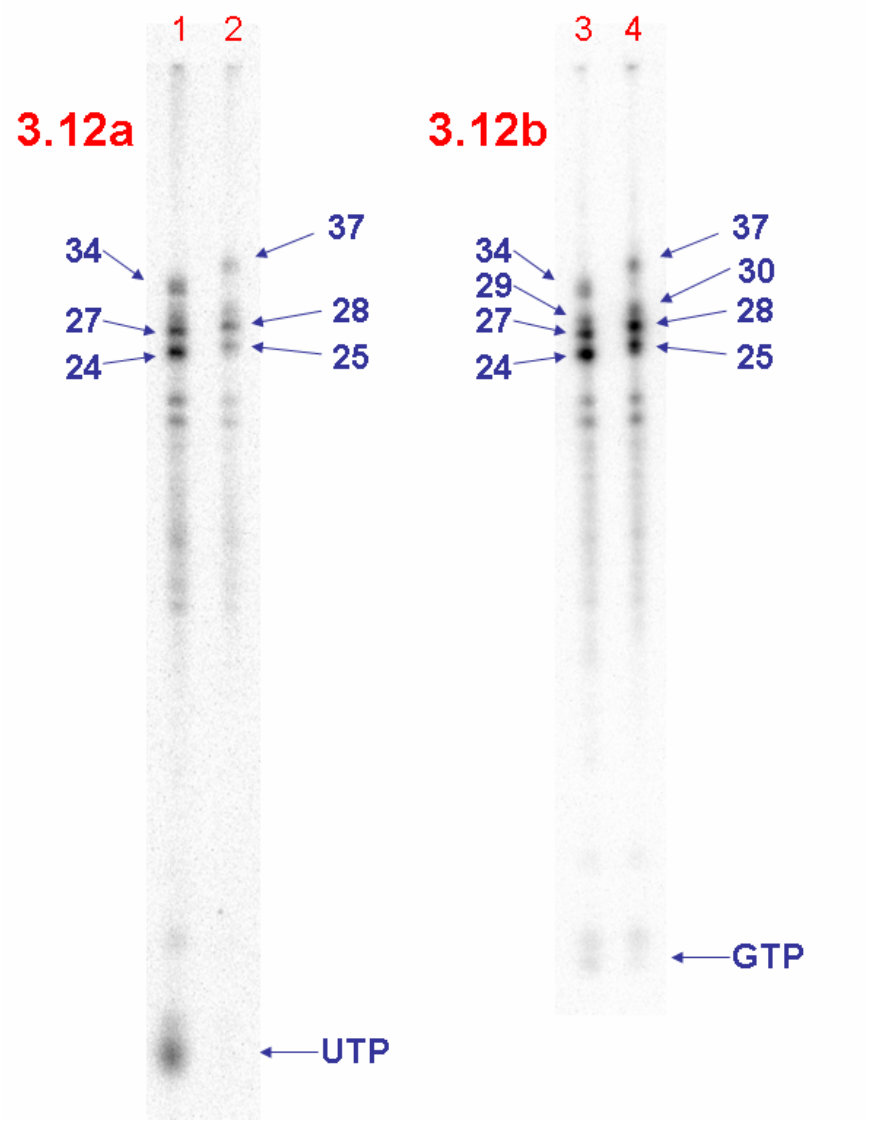

Figure 3.12 UTP is Displaced Due to a Single Nucleotide Incorporation Event; GTP is only Partially Displaced. The transcript length positions are labeled for reference (see Appendix B). In Figure 3.12a, lane 1 shows a the analysis of the UTP-SEC ratio in a sample of complexes made with radiolabeled UTP. In Lane 2, 30 μM CTP was added to walk the C-stalls 100% (see Appendix B); the UTP is completely displaced from the SECs. In the GTP-SEC catalysis assay in Figure 3.12b, lane 3 is the unaltered GTP-SEC ratio analysis and lane 4 was incubated with CTP. Only 40% of the GTP was removed as a result of catalysis.

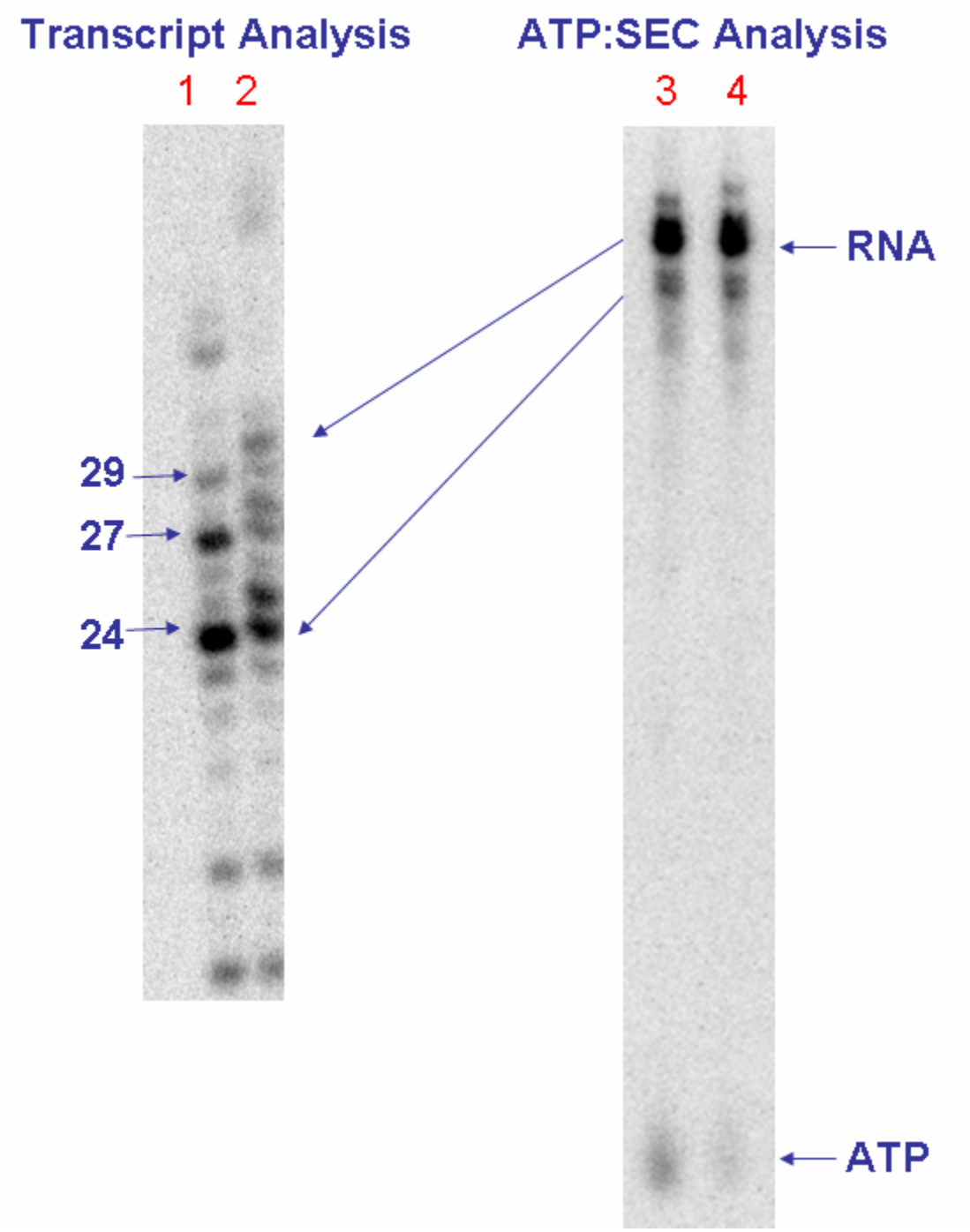

Figure 3.13 Partial Catalysis Equivalently Displaces ATP from SECs. On the left, the unreacted and CTP walked samples (lanes 1 and 2, respectively) were analyzed for transcript postion, revealing 50% catalysis. On the right, the data show that ATP-SEC ratio was reduced from 0.22 to 0.12 (lanes 3 and 4 respectively) due to catalysis.

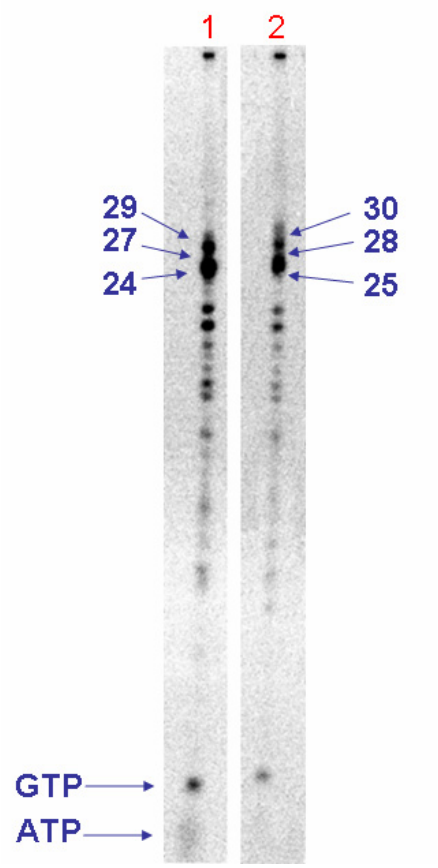

Figure 3.14 ATP Completely Dissociates from SECs during Catalysis and GTP Does Not. The transcript lengths are identified for reference (Appendix B). In lane 1, the unaltered GTP-SEC ratio was 0.49, and the ATP-SEC occupancy was 0.23. As a result of complete catalysis, 100% of the ATP was displaced and 40% of the GTP was removed; the data show that the GTP-SEC occupancy after catalysis was 0.29.

3.3.4 GTP Binds to Purified SECs at Equilibrium with an Affinity of 26μM

We fit the GTP binding data to a rectangular hyperbolic expression, and determined that GTP binds to SEC with a K_D of 25.6 μM ± 3.5. We noted that the saturated stoichiometry of GTP on purified SECs was 1.25 ± 0.06.

Additionally, we observed that the ATP-SEC ratio did not significantly change over the course of the ~3 hr experiment. Even the higher concentrations of GTP (150 μM) did not displace ATP. We noted that the ATP-SEC stoichiometry in the GTP titration remained above 0.20.

We found that the results of the cold ligand competition experiment showed that GTP binding to the purified SEC was doing so under equilibrium conditions (Appendix B) (Winzor *et al.*, 1995).

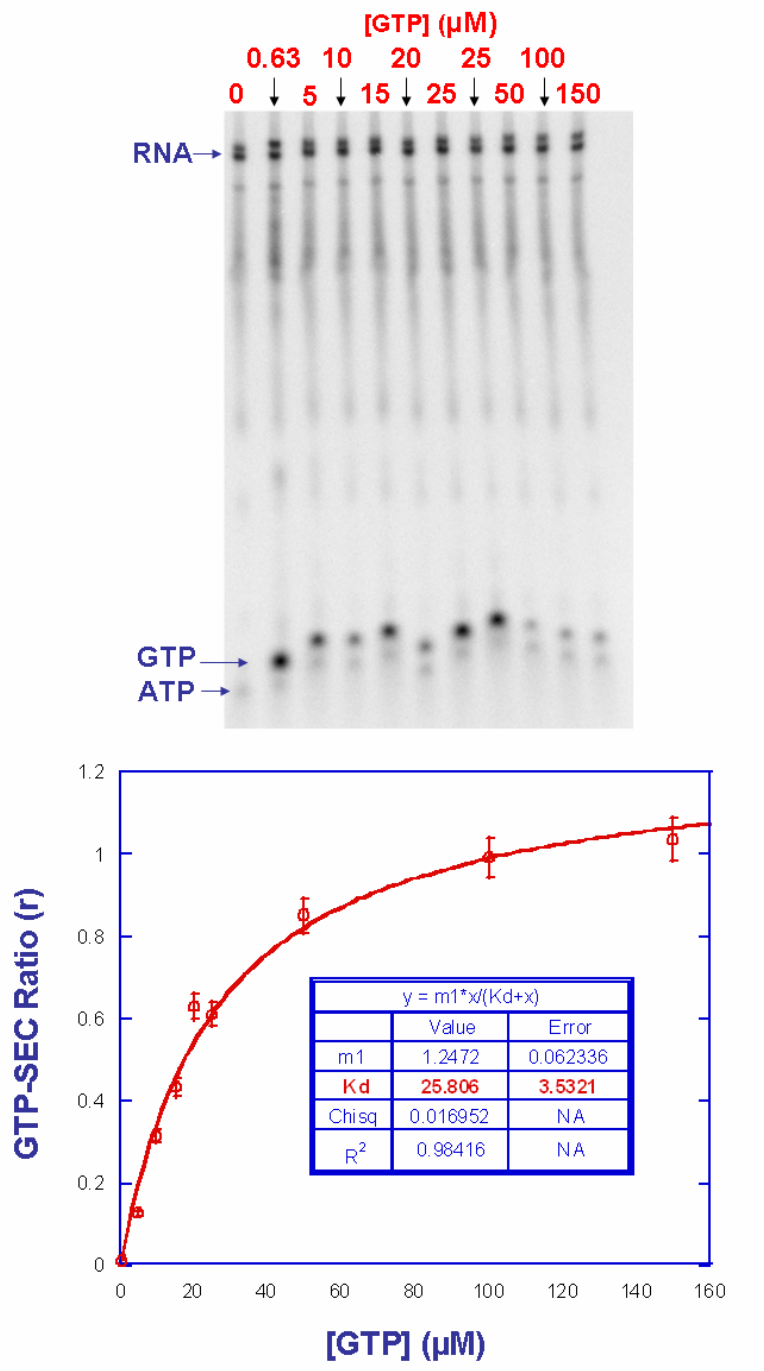

Figure 3.15 The GTP-SEC Dissociation Constant is 26µM. The PAGE gel (top) for the GTP titration to purified SECs is shown. Fitting the titration data to a rectangular hyperbolic expression reveals that GTP binds to purified SECs with a dissociation constant (K_D) of 25.8 ± 3.5 µM and a saturated stoichiometry of 1.25 ± 0.06.

3.4 Discussion of NTP Interactions with Stalled Elongation Complexes

We were able to avoid the adverse affects of background interference in NTP-SEC binding analysis by developing the RevMAPP purification protocol. RevMAPP facilitated our observation of tightly bound NTPs on SECs. Our data show that a 2:1 NTP:SEC stoichiometry exists, which is in agreement with the presence of a second NTP binding site on RNA polymerase (Table 3.1). We observe that 84% of SECs bound a UTP tightly, about 53% of complexes bound GTP tightly, and roughly 22% of complexes tightly bound an ATP. We have learned that the dissociation rates of NTPs bound to SECs are very slow, however ATP is actively displaced in the presence of 1mM unlabeled ATP at a rate 10-fold faster than the passive ATP off rate (Table 3.2). We conducted a number competition studies using the non-specific ligands dATP and dCTP (Table 3.3). We additionally related the total displacement of UTP and ATP to a single nucleotide incorporation event. Conversely, GTP was only partially displaced from the enzyme due to catalysis. We determined that GTP could be titrated into a solution of purified SECs, and the equilibrium binding affinity is ~26 μM at a saturated occupancy of ~1.25 (Figure 3.15). Although the passive dissociation rate we report for the GTP bound to enzyme stalled at position +24 is slow, a cold ligand competition experiment proved that the titrated GTP was binding under equilibrium conditions (Appendix B).

3.4.1 The RevMAPP Protocol is a Major Addition to the Transcription Analysis Toolbox

We have identified a method that for the first time allows us to directly quantify the amount of a tightly bound NTP on transcription elongation complexes. Our previous models of nucleotide incorporation were based on the assumption that both the catalytic and

allosteric sites were unoccupied subsequent to washing the SECs (Figures 1.7 and 1.8) (Foster, Holmes *et al.*, 2001; Holmes and Erie, 2003). The binding data that we captured using the RevMAPP protocol can now be combined with previous biochemical information to help us re-think how transcription elongation resumes off of a stall, and possibly how the transitions between unactivated and activated synthesis pathways are regulated by NTP binding. Specifically, we re-examine the mechanism for NTP misincorporation by RNA polymerase.

The means to remove non-specifically adsorbed NTPs from a solution of stalled elongation complexes was crucial in eliminating the background interference that previously prevented the determination of NTP-SEC stoichiometries. Previous work in our lab found that agarose support beads used in the purification of SECs were a detrimental source of non-specifically adsorbed background ligands (Holmes, 2002). The employment of a monomeric avidin coated UltraLink^{TM} support matrix allowed us to seamlessly combine our existing elongation complex synthesis protocols with a reversible means of SEC immobilization. The reversibility of the SEC immobilization facilitated the isolation of SECs in an environment that was totally free of background interference at any level preventing the observation of NTP-SEC binding events.

Appendix B is partially dedicated to the necessary controls for binding analysis when using the RevMAPP protocol. The most crucial topic of Appendix B is the RNAP- (acceptor negative) control that was used frequently to identify sources of non-specific background. We found that contribution of non-specific background NTPs on bead matrices, test tube walls, and pipette tips were only some of the issues that need to be dealt with on an experiment to experiment basis.

Taken together, the RevMAPP protocol has allowed us to embark on investigations that were previously impossible, and our results radically change some of the aspects concerning how we picture the stalled elongation complex at the start of biochemical investigation, such as a kinetic assay. More importantly, we have barely come to realize the potential of our new technique; we certainly now have many more questions concerning NTP-SEC binding than we have answered. Along with crystal structures, kinetics experiments and mutagenesis techniques, the development of the RevMAPP purification protocol will bring new understanding to the complicated regulation of transcription elongation by nucleotide binding.

3.4.2 UTP is Locked into the Catalytic Site in the Absence of CTP

RNAP has a propensity to misincorporate certain NTPs at specific DNA template positions. For example UTP will misincorporate for CTP at position +24 of the DE13 DNA template (Erie *et al.*, 1992; Erie, 2002; Cunningham, 2008). The studies by Erie and Cunningham *et al*. suggest that misincorporation only takes place on the activated synthesis pathway, and that unactivated conformations leads to a trapped states that can only be rescued by the correct NTP. The model put forth by Cunningham *et al.* (2007) for activated pathway misincorporation suggests that in the absence of the correct NTP, UTP acts allosterically on both the RNAP and the DNA. The conformation shift of RNAP by UTP binding to fork loop 2 facilitates proper alignment of the DNA i+1 template base with the catalytic site, although the model suggests that the template alignment takes place much more slowly than with the correct NTP. A second UTP can then enter the catalytic site through the secondary channel. Figure 3.16 is a recent crystal structure showing the restricted access

through the secondary channel where binding to the active site closes the trigger loop over the NTP, locking it into place (Toulokhonov *et al.*, 2007; Vassylyev *et al.*, 2007). From here, UTP can be incorporated if the base becomes aligned with the DNA template, the RNAP active site and the RNA product terminus. Figure 3.17 is the model proposed activated pathway misincorporation (Cunningham, 2007). The model also suggests that if the UTP enters into the catalytic site prior to the slow allosteric conformational changes, the NTP can bind non-productively to the catalytic site such that the base is not properly aligned with the i+1 DNA template position. Cunningham and Erie suggested that the incorrect NTP might fray the DNA such that the i+1 base align with fork loop 2. With the trigger loop holding the UTP in the catalytic site and the i+2 DNA template position interacting with the allosteric site, the UTP is prevented from leaving the catalytic site via the secondary channel, and misincorporation cannot occur without proper DNA alignment.

Our NTP-SEC occupancy data (Table 3.1) argues that nearly all of the purified elongation complexes contain a bound UTP that dissociates extraordinarily slowly (Table 3.2). We propose a few minor changes to the model put forth for activated misincorporation and unproductive trapping of UTP to the active site (Cunningham, 2008). Our results show that 100% of the UTP bound to the enzyme is displaced during catalysis using 30 μM CTP, suggesting that the UTP was bound somewhere relevant to nucleotide incorporation. Additionally, dNTPs have been shown to misincorporate at low levels with SECs, and dNTP base selection is template dependant (Svetlov *et al.*, 2004). Our data show that dCTP displaces UTP quickly while dATP does not, possibly indicating a specific dCTP/UTP competition for interactions with the i+1 template position. Previous results using transient state kinetics suggested that the incorporation of CTP takes place primarily in the unactivated

state when coming off of the stall, implying that the allosteric site is not necessarily used during the addition of a only the CTP substrate (Foster *et al.*, 2001; Kennedy, 2007).

We posit that UTP is bound to the catalytic site; the trigger loop is in locked (closed) position and the ternary complex conformation is incapable of NTP incorporation. Our preliminary data showing a very slow passive off rate for UTP, and the specific CTP and dCTP displacements of UTP are in agreement with the locking mechanism suggested and rescue data presented previously (Cunningham, 2008). With UTP unproductively locked into the active site, misincorporation can eventually occur upon the addition of more UTP (Erie *et al.*, 1992; Cunningham, 2008) by binding to the allosteric site and dislodging the template DNA fray from fork loop 2. As with the previous model, we suggest that slow translocation occurs due to the weak DNA template interactions with the UTP bound to the fork loop, a mechanism that serves as a fidelity check since UTP is the wrong base. The slow conformational change allows the UTP bound to the catalytic site to align with DNA as the i+1 template position enters the active center. The UTP may remain trapped by the trigger loop long enough for proper alignment and catalysis. We speculate that the population of complexes observed on the unproductive pathway might be the result of translocation and release of the UTP bound to the catalytic site *via* the secondary channel; through a series of conformational checks for binding compatibility, base discrimination by the i+1 DNA template position may be sufficient to prevent misincorporation (Batada *et al.*, 2004; Kettenberger *et al.*, 2004; Westover *et al.*, 2004). The concentration dependant extents of misincorporation observed previously (Cunningham, 2008) may simply be a result of UTP's affinity for the allosteric site (reported K_M = 6 μM).

Figure 3.18 shows a new possible mechanism that explains both the misincorporation rate and extent dependence on UTP concentration in the presence of SECs. With UTP trapped in the catalytic site subsequent to the stall, a second UTP binding to the allosteric site may shift the ternary complex conformation into a state capable of misincorporation of the bound NTP, or releasing it. The open catalytic site may rebind an NTP, or allosteric NTP may further dissociate from the SEC. NTP re-binding to the allosteric and catalytic site is slow for the incorrect NTP, providing kinetic trap that limits the extent of misincorporation and controls the fidelity of transcription elongation.

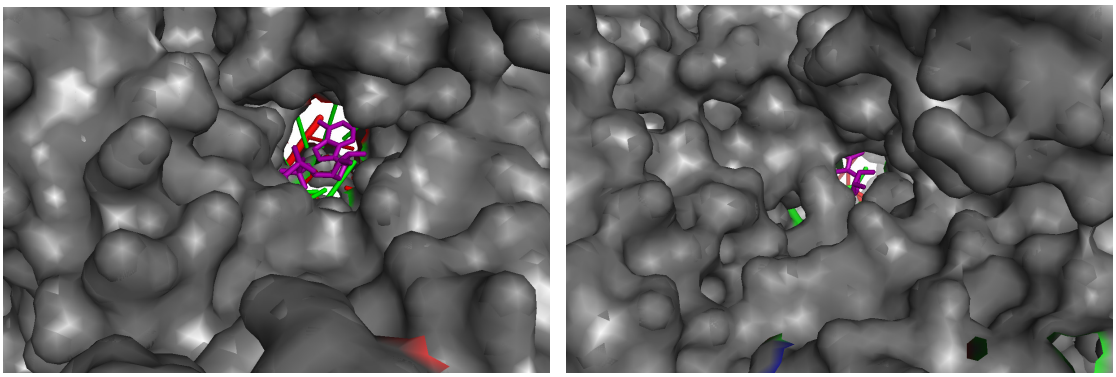

Figure 3.16 Access to the Secondary Channel is Regulated by the Trigger Loop. On the left, the secondary channel opened (A, PDB 2PPB) which allows access of an NTP (purple) to the catalytic site. When the trigger loop is closed (B, PDB 2O5J), the secondary channel access is restricted (Kennedy *et al.*, 2008).

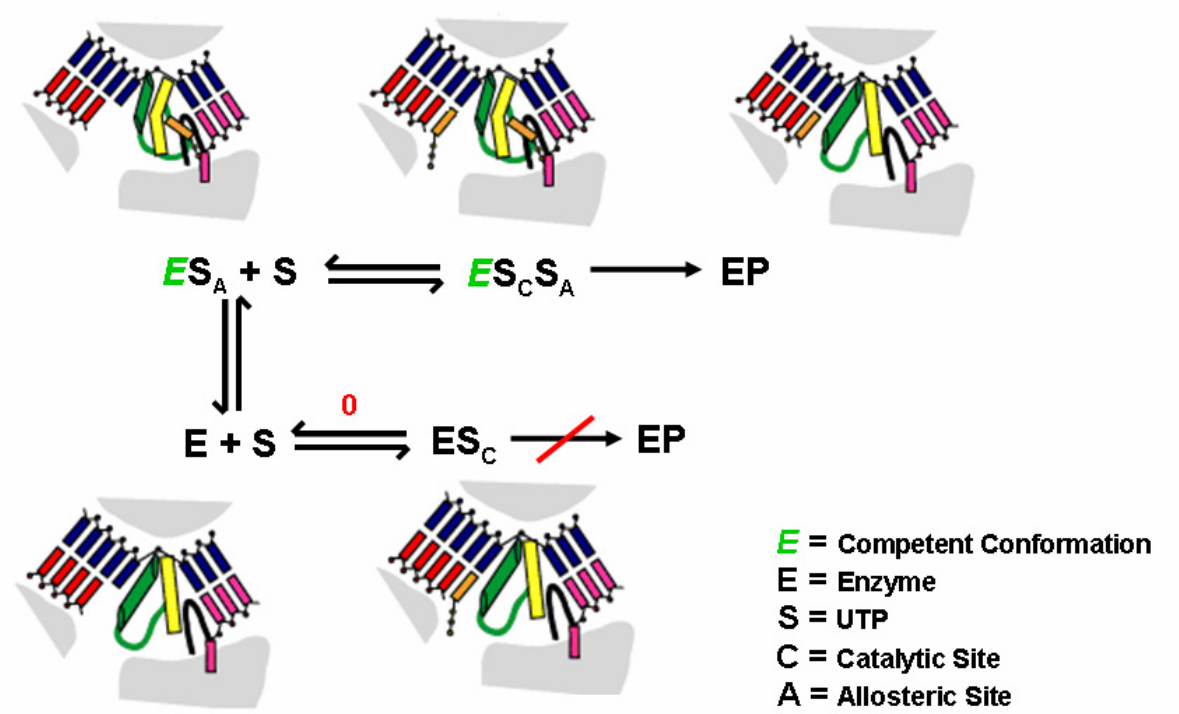

Figure 3.17 A Previously Proposed Model for Activated State Misincorporation. The DNA template and non-template strands are shown in blue and pink, respectively. The RNA chain and the incorrect NTP are displayed in red and orange. Fork loop 2 pictured in black and the bridge helix (F-helix) is in yellow. The mobile trigger loop is shown in green (borrowed from Cunningham and Erie (2008)).

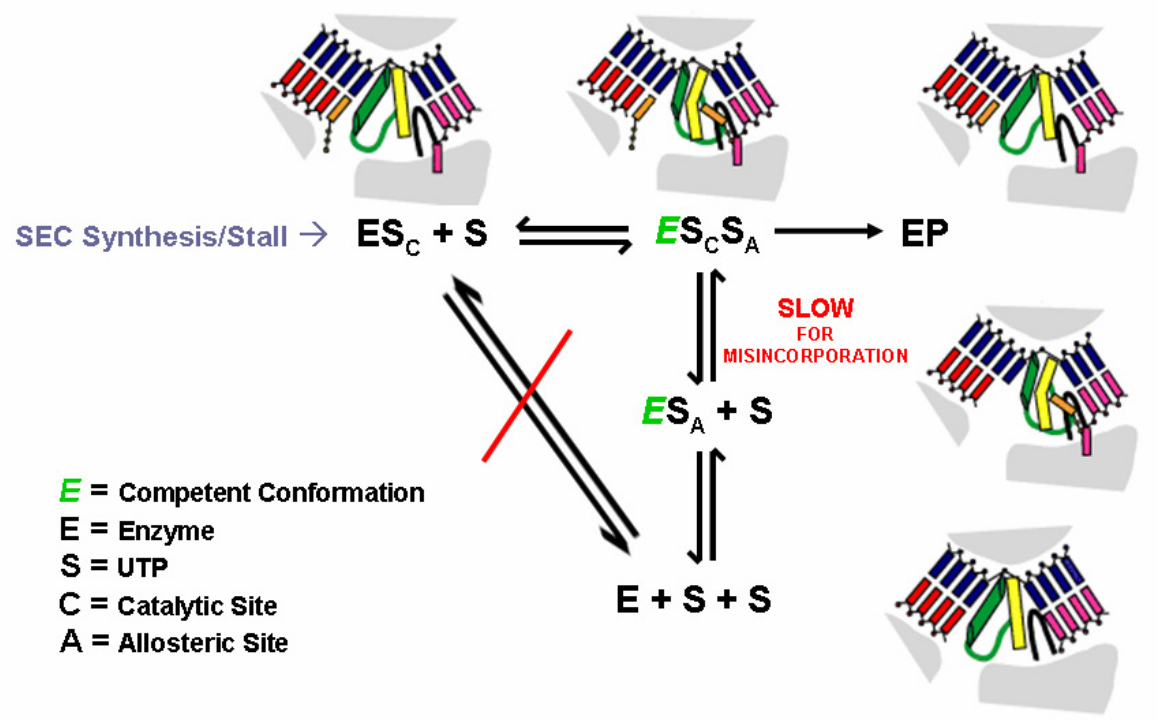

Figure 3.18 A New Proposed Mechanism for NTP Misincorporation. With UTP trapped in the catalytic site subsequent to the stall, the mechanism for UTP misincorporation changes. Allosteric UTP binding either induces a conformation change that allows for limited misincorporation, or permits dissociation of the bound UTP. Re-binding of UTP to the allosteric and catalytic sites may be slow, which may be a fidelity check during transcription elongation.

3.4.3 ATP May Occupy the Catalytic Site of SECs not binding UTP

One possible explanation for the 20 % occupancy of the ATP on SECs is that ATP is trapped in the catalytic site on the SEC that do not bind UTP subsequent to the stall. The catalytic assays, ATP, and dATP competition studies show suggest that ATP is bound to a catalytically relevant position. The combination of UTP and ATP occupancies account for a stoichiometry of one NTP bound to the catalytic site of SECs.

Alternatively, previous work in our laboratory shows that the i+2 nucleotide plays a very important role in the equilibrium between unactivated and activated synthesis pathways (Foster *et al.*, 2001; Holmes, 2002; Kennedy, 2007). ATP likely has a high affinity for the putative allosteric site when stalled at a C-A (i+1, i+2) DNA template position. The kinetics of single nucleotide incorporation are biphasic. Kennedy *et. al.* (2008) showed that pre-incubation with ATP (the i+2 NTP) shifts the enzyme into the active pathway, theoretically by binding to fork loop 2 and aligning the i+2 template position, thereby assisting in the proper alignment of the i+1 position with the active site. In the absence of pre-incubation, SECs prepared with the DE13 DNA template undergo approximately 20% activated catalysis, the remainder of the nucleotide incorporations take place on the unactivated pathway.

We observed that about 20% of SECs are occupied by ATP, within error. These results are consistent with notion allosteric binding of ATP drive translocation and open the catalytic site for activated synthesis. Roughly 80% of the SECs are bound by UTP, within error. ATP possibly drives translocation to unlock the trigger loop, and release an equivalent portion of UTP trapped in the catalytic site.

Translocation of the DNA template and alignment of the i+1 position may explain the slow off passive rate of the ATP bound after the stall (Table 3.2). We show that dNTPs (Table 3.3) and GTP (Figure 3.15) have no effect on the displacement of ATP; probably because the ATP is base paired with the i+2 template DNA aligned with the fork loop. We observed that 1 mM ATP will actively displace the bound ATP 10-fold faster than the passive dissociation (Figure 3.10), but the displacement is still quite slow (Table 3.2) and does not occur to a full extent. These results are consistent with previous competitive studies carried out by Kennedy and Erie (2008) that show that ATP can be sequestered in the main channel and shuttled into the catalytic site for incorporation.

Although tight ATP binding to fork loop 2 is consistent with the biphasic kinetics of nucleotide incorporation and 80 % UTP occupancy, it is highly unlikely that 20% of SECs bind ATP irreversibly to the conformationally dynamic allosteric site for extended (hours) periods of time.

3.4.4 GTP Binding May Be Magic

If our reasoning is correct, SECs that have ATP bound (~20%) are completely driven into the post-translocated state, and the catalytic site is unoccupied, allowing binding and incorporation of CTP to occur on the activated pathway (Foster *et al.*, 2001; Holmes, 2002; Kennedy *et al.*, 2008). The remaining ~80% of SEC are occupied by UTP at the catalytic site; the only possibility is that the 0.5 GTP:SEC occupancy (Table 3.1) is related to binding to the allosteric site when ATP is not. Translocation may not be completely driven by GTP binding to the fork loop because the weak (unpaired) interactions with the DNA template are not sufficient. Unlike ATP binding to the allosteric site, 1 mM dCTP or dATP will displace

the GTP, supporting the notion that fewer interactions are being made with the RNAP and DNA. We find, however, that GTP is not always displaced from the enzyme when catalysis is carried out (Figures 3.12 and 3.14). In our catalytic studies, we commonly observed a small population of stalled complexes that were not active around the +13 to +20 region of the DE13 sequence. The "dead-end" complexes are in a region of the template rich with U and G. GTP may be bound to these complexes in a manner similar to the "trapped" UTP in the SECs stalled at position 24. One possibility is that CTP somehow squeezes into the catalytic site directly through the partially closed of secondary channel and displaces UTP, leaving some of the GTP bound to the fork loop.

The GTP bound to the enzyme during a stall also dissociates slowly, and the addition of 1 mM GTP to the SEC does not significantly increase the rate of dissociation by active displacement (Table 3.2). In our titration of GTP to SECs, the complexes were incubating in buffer ice for >2 hours to allow any reversibly bound NTP to dissociate. Although the passive off rate of GTP bound during a stall is slow, we found that equilibrium binding was achievable during the titration. Our results showed that the binding affinity was ~26μM and that the GTP-SEC stoichiometry at saturation was ~1.25. Possibly, the partial dissociation of UTP (most of the ATP remained bound to the enzyme through out the titration of GTP, see Figure 3.15) and perhaps a conformational shift of some nature opened sites on the RNAP that did not bind GTP in the same orientation or location. The high stoichiometry suggests that the more than one site on RNAP is at least partially filled by the titrated GTP. Additionally, the SEC synthesis GTP concentration was 20 μM. Our GTP binding study (Figure 3.15) shows that at 20μM GTP, the occupancy is about 0.25; only half the occupancy we observe during the stall and in the presence of UTP and ATP. Compared to the GTP

bound to SECs during the stall, the titrated GTP is binding to the SECs in different places and with different affinities and rates.

We speculate that GTP may be binding to one or more position that have been implicated in binding the regulatory nucleotide ppGpp (guanosine tetraphosphate *and* guanosine pentaphosphate), or "magic spot" (Artsimovitch *et al.*, 2004; Vrentas *et al.*, 2008).

Magic spot is a rare regulatory nucleotide involved in stringent control - transcription inhibition during times of NTP starvation. Earlier work suggested that magic spot binding was located near the catalytic site (Artsimovitch *et al.*, 2004); two orientations of ppGpp were co-crystallized with *T. thermophilus*. While recent studies with mutant of RNAPs from *E. coli* have refuted the regulatory effect of the previously defined ppGpp binding location (Vrentas *et al.*, 2008), the ability of ppGpp to bind to the identified location still stands. The recent work by Vrentas *et. al.* (2008) shows that magic spot may bind in more locations than originally thought. The specificity of the guanosine tetra- and pentaphosphate binding studies are enough to at least raise suspicion that GTP might bind to these site on RNAP.

3.5 Future Direction with NTP-SEC Binding Dynamics

Our development of the RevMAPP protocol has allowed us to ask questions directly probing the interactions of NTPs with transcription elongation complexes that have never been possible before. As a result, we have only begun to scratch the surface of the experiments that need to be done to comprehensively characterize NTP-SEC binding dynamics. As short list of experiments certainly include the following:

More Competitive Assays: In this work, a handful of intrinsic competitions, dNTP competitions and catalytic assays were performed to begin the compilation of the large NTP dynamics picture. We now have the ability to assay NTP-SEC occupancies under almost any conditions. Competitions with other NTPs, antibiotics, obscure nucleotides (such as magic spot) should be carried out. The active displacement (off rate) experiments should also be done for every combination of ligand competition. Fast dissociation kinetics can be assayed on a fast flow device (quench flow). The equilibrium binding of GTP raises several questions. One possible answer might be the binding of GTP to other guanosine specific sites, such as the magic spot positions. GTP Competitive assays with ppGpp are in order.

Different Sequence Contexts: The work we present here is done with the original DE13 template. Position i+1 through i+4 are CAAC. Our lab has made several mutations to this template *via* site directed mutagenesis, producing sequence contexts such as CGAC, CAGC, CA_5C, and others. Changing the i+2 templated nucleotide (and beyond) may reveal the intricacies commanding NTP-SEC occupancy. Changing the i+1 position is another important task, one that has not even been addressed in the multitude of standard nucleotide incorporation kinetics experiments performed in our lab.

Mutant RNAP Studies: Our lab has knocked out allostery in transcription by deletion of crucial NTP binding amino acids in fork loop 2. Obtaining NTP-SEC occupancies for the Δ-loop mutant in *E. coli* RNAP may also tell us more about where NTPs are binding.

BIBLIOGRAPHY

Artsimovitch, I., V. Patlan, S.-i. Sekine, M. N. Vassylyeva, T. Hosaka, K. Ochi, *et al.* (2004). "Structural Basis for Transcription Regulation by Alarmone ppGpp." Cell **117**(3): 299.

Batada, N. N., K. D. Westover, D. A. Bushnell, M. Levitt and R. D. Kornberg (2004). "Diffusion of Nucleoside Triphosphates and Role of the Entry Site to the RNA Polymerase II Active Center." Proc Natl Acad Sci U S A **101**(50): 17361.

Burton, Z. F., M. Feig, X. Q. Gong, C. Zhang, Y. A. Nedialkov and Y. Xiong (2005). "NTP-Driven Translocation and Regulation of Downstream Template Opening by Multi-Subunit RNA Polymerases." Biochem Cell Biol **83**: 486.

Cunningham, C. (2008). Insight into the Fidelity of Escherichia coli RNA Polymerase: Investigation of Misincorporation During Transcription Elongation Utilizing Transient State Kinetics. Chemistry. Chapel Hill, University of North Carolina at Chapel Hill. **Ph.D.:** 150.

Darst, S. A. (2000). "Unpublished results."

Erie, D. A. (2002). "The Many Conformational States Of RNA Polymerase Elongation Complexes And Their Roles In The Regulation Of Transcription." Biochimica et Biophysica Acta **1577**(2): 224.

Erie, D. A., O. Hajiseyedjavadi, M. C. Young and P. H. v. Hippel (1993). "Multiple RNA Polymerase Conformations and GreA: Control of the Fidelity of Transcription." Science **262**(5135): 867.

Erie, D. A., T. D. Yager and P. H. von Hippel (1992). "The single-nucleotide addition cycle in transcription: a biophysical and biochemical perspective. [Review] [156 refs]." Annu Rev Biophys Biomol Struct **21**: 379.

Foster, J. E., S. F. Holmes and D. A. Erie (2001). "Allosteric Binding of Nucleoside Triphosphates to RNA Polymerase Regulates Transcription Elongation." Cell **106**: 243.

Holmes, S. (2002). Downstream DNA Sequence Effects on Transcription Elongation: NTP Binding Induces Translocation Via A Ratchet Motion. Chemistry. Chapel Hill, University of North Carolina at Chapel Hill. **Ph.D.**

Holmes, S. F. and D. A. Erie (2003). "Downstream DNA Sequence Effects on Transcription Elongation: Allosteric Binding of Nucleoside Triphosphates Facilitates Translocation Via a Ratchet Motion." J Biol Chem. **278**(37): 35597.

Holmes, S. F., J. E. Foster and D. A. Erie (2003). "Kinetics of multisubunit RNA polymerases: experimental methods and data analysis." Methods Enzymol **371**: 71.

Kennedy, S. R. (2007). Modulation of Transcription Elongation via the Main Channel in Eschericia coli RNA Polymernase. Chemistry. Chapel Hill, NC, University of North Carolina at Chapel Hill. **Ph.D.:** 162.

Kennedy, S. R. and D. A. Erie (2008). "A Non-catalytic Nucleoside Triphosphate Binding Site on RNA Polymerase Regulates Transcription." submitted to Cell March, 2008: 32.

Kettenberger, H., K.-J. Armache and P. Cramer (2004). "Complete RNA Polymerase II Elongation Complex Structure and Its Interactions with NTP and TFIIS." Mol Cell **16**(6): 955.

Nierman, W. C. and M. J. Chamberlin (1980). "The effect of low substrate concentrations on the extent of productive RNA chain initiation from T7 promoters A1 and A2 by Escherichia coli RNA polymerase." J Biol Chem **255**(10): 4495.

Slepneva, I. A. (1980). "Detection of nucleoside triphosphate binding sites of two types in Escherichia coli RNA-polymerase by affinity labeling." Mol Biol Rep **6**(1): 31.

Slepneva, I. A., N. V. Zakharova and J. M. Backer (1978). "Kinetic evidence for multiple binding sites of nucleoside triphosphates in Escherichia coli RNA polymerase." FEBS Lett **87**(2): 273.

Svetlov, V., D. G. Vassylyev and I. Artsimovitch (2004). "Discrimination Against Deoxyribonucleotide Substrates by Bacterial RNA Polymerase." J Biol Chem. **279**(37): 38087.

Toulokhonov, I., J. Zhang, M. Palangat and R. Landick (2007). "A Central Role of the RNA Polymerase Trigger Loop in Active-Site Rearrangement during Transcriptional Pausing." Cell **227**(3): 406.

Vassylyev, D. G., M. N. Vassylyeva, J. Zhang, M. Palangat, I. Artsimovitch and R. Landick (2007). "Structural Basis for Substrate Loading in Bacterial RNA Polymerase." Nature **448**(7150): 163.

Vrentas, C. E., T. Gaal, M. B. Berkmen, S. T. Rutherford, S. P. Haugen, W. Ross*, et al.* (2008). "Still Looking for the Magic Spot: The Crystallographically Defined Binding Site for ppGpp on RNA Polymerase Is Unlikely to Be Responsible for rRNA Transcription Regulation." J. Mol. Biol.(article in press): 14.

Westover, K. D., D. A. Bushnell and R. D. Kornberg (2004). "Structural Basis of Transcription: Nucleotide Selection by Rotation in the RNA Polymerase II Active Center." Cell **119**(4): 481.

Winzor, D. J. and W. H. Sawyer (1995). Quantitative Characterization of Ligand Binding. New York, John Wiley and Sons, Inc.

CHAPTER 4:

DEVELOPMENT OF NOVEL HIGH EFFICIENCY PHASE SEPARATIONS FOR LIGAND BINDING STUDIES

4.1 The Development of Novel Phase Separations

In Chapter 2, we summarized the myriad of phase separations that that facilitate ligand binding analyses (Winzor *et al.*, 1995). At low concentrations of acceptor, a phase separation's ability to reduce non-specific free ligand adsorption is a major performance limiting factor. In Chapter Three, we presented the development of the RevMAPP protocol which allowed us to directly probe nucleotide binding to low nanomolar concentrations of RNAP during transcription elongation. However, we designed the RevMAPP protocol specifically for transcription, and its application may be limited to the analyses of ligand-acceptor pairs compatible with biotin affinity purification. In addition to RevMAPP, we pursued the invention of several novel phase separation procedures to remove nucleotides (a charged ligand) from a solution containing acceptor. Our methods were designed to maximize the speed of NTP removal and reduce non-specific ligand adsorption while capturing protein acceptors for binding analysis. To develop new, versatile, high performance separations for ligand acceptor analyses, we modified or combined the concepts of existing dialysis (Svensson, 1946; Colowick *et al.*, 1969; Ford *et al.*, 1984), filter binding (Harris *et al.*, 1988) and electrophoresis techniques (Takeo *et al.*, 1972; Garner *et al.*, 1981).

4.1.1 Small Volume Electrodialysis

The speed of dialysis techniques are limited by the mass transport of ligands to a semi permeable membrane. In traditional dialysis, stirring is used to eliminate solution concentration gradients and increase mass transport of ligands to the dialysis membrane. Since NTPs are charged ligands, we were curious to see if a negative voltage would drive nucleotides to the membrane faster than diffusion alone. By decreasing the sample solution volume (α-phase), we hoped to reduce the time require for the phase separation by reducing the distance molecules needed to travel. The idea of a small sample volume was also attractive to for the purposed of material (acceptor protein) conservation. Here we present the development and performance of small volume electrodialysis (SVED).

4.1.2 Reverse Microfiber Dialysis

Microfibers have been used as a versatile sample collection tool for drug-protein binding analyses and the detection of neurotransmitters and amino acids both *in vivo* and *in vitro* (Oravcová *et al.*, 1996; Liu *et al.*, 1999; Zhou *et al.*, 2004). Microfiber use for traditional equilibrium dialysis has been quantitatively compared to filter binding for pharmacological studies (Herrera *et al.*, 1990). However, microdialysis is typically used for sample collection. Microfiber sample collection has been used in-line with analysis by HPLC (Wang *et al.*, 1997) and capillary electrophoresis (Hogan *et al.*, 1994). Recently, microfibers were used to de-salt samples in-line with nanoelectrospray ionization-mass spectrometry; the authors infused the analyte into the fiber, rather than using the microfiber as a sample collection vehicle (Jakubowski *et al.*, 2005). We wanted to examine the possibility of purifying ligand-protein mixtures with microfibers by infusing the fiber with the sample

solution instead of collecting free ligand from the exterior of the microfiber. Rather than capture a sample of the free ligand, in our case the perfusate of the microfiber would contain only the bound complex and free acceptor, assuming the system was allowed to reach dialysis equilibrium with a large surrounding β-phase. In dialysis, sources of non-specific NTP adsorption include any experimental equipment that confine the dialysis α-phase solution. We postulated that sources of non-specific adsorption could be reduced by using microfibers made from regenerated cellulose. The microfiber membrane would completely house the dialysis solution, reducing NTP solution contact with experimental materials. Plus, microfibers have a very high membrane area to volume ratio. Compared to conventional dialysis apparatuses, the geometry of microfibers would greatly decrease diffusion limited dialysis equilibration time. We felt that the very small inner volume (5 μL) of microfibers would also aid in the conservation of protein acceptor.

Microfibers have been previously used as filtering vehicles. One study using hollow microdialysis fibers to purify the contents of a PCR reaction for analysis by esi-mass spectrometry reported that Mg^{+2} was readily removed from the interior of a hollow microdialysis fiber (MWCO = 13,000) at a sample infusion flow rate of $2\mu L \cdot min^{-1}$ (Hannis *et al.*, 1999). However, only 20 to 30 % of dNTPs were removed from solution. The authors attribute dNTP retention to the "large solvation sphere associated with the triphosphate groups," and also cite "base stacking of monophosphate nucleotides." They claim the large solvation sphere and the base stacking increased the "apparent molecular weight" of dNTPs. We were not at all convinced that dNTP solvent dynamics or base stacking would make a small nucleotide (MW < 1000 Da) act as if it were larger than 13,000 Daltons. Non-specific adsorption of dNTP to the regenerated cellulose walls may have partially caused the retention

of nucleotide. It is also possible, but unlikely, that the solution did not fully reach dialysis equilibrium due to Gibbs-Donnan effects. A third possibility is that the complex PCR mixture containing DNA polymerase, primers, PCR products, etc, simply clogged the pores of the fiber. The findings by Hannis *et. al.* did not discourage us from pursuing reverse microfiber dialysis.

4.1.3 Short Travel Gel Electrophoresis

A variety of agarose and polyacrylamide electrophoretic techniques are commonly used to separate biological molecules with very low background, especially when using radiochemical methods. Electrophoresis has been used for nearly 30 years to ascertain binding parameters for DNA-protein interactions (Garner *et al.*, 1981). However, the utility of using an electrophoresis gel as a simple filter for ligand-acceptor mixtures has never been investigated. The electrophoresis of NTPs through gel materials is considerably faster than the migration of large proteins. We theorized that application of a voltage to a short plug of agarose or polyacrylamide might quickly pass NTPs and in the time required to for proteins to enter the gel matrix. Our invention of short travel gel electrophoresis (STaGE) for equilibrium binding assays is described below.

4.2 Materials and Methods

In this section, we present the basic design, dimensions and materials used in the construction of the small volume electrodialysis (SVED), microfiber dialysis, and short travel gel electrophoresis (STaGE) apparatuses.

4.2.1 SVED Design

The basic design of SVED (Figure 4.1) consisted of small plastic well mounted on top of a semi-permeable regenerated cellulose dialysis membrane (MWCO = 13,000 Da; thickness = 20μm). The well base was sealed with silicone. The well diameter was 4mm and its depth was ~3mm. The well held a maximum of ~100 μL α-phase (solution to be dialyzed). We noted that a 20 μL droplet of aqueous α-phase barely spread to cover the bottom of the well which minimized the solution contact with well walls, and maximized the solution interaction with the membrane surface. We calculated the area to volume ratio of 20 μL α-phase in the 4mm diameter to be $0.628 mm^2 \cdot \mu L^{-1}$. A platinum wire ring electrode (negative lead) was mounted to make contact the very top of the α-phase droplet. The positive lead was placed in a 1mL flow cell that made contact with other side of the cellulose membrane (β phase). The flow cell was deployed to displace ligand from the β-phase-membrane boundary by eliminating concentration gradient and preventing back diffusion through the filter. The β-phase was flowed into a collection 500 mL receptacle containing 300 mL of H_2O at *t=0*. We tested a variety of other synthetic hydrophobic membrane materials, including polytetraflouroethelene (PTFE), polyethersulfone (PES), polyester (PET), and other proprietary thin layer membranes generously supplied by Sterlitech (Kent, WA).

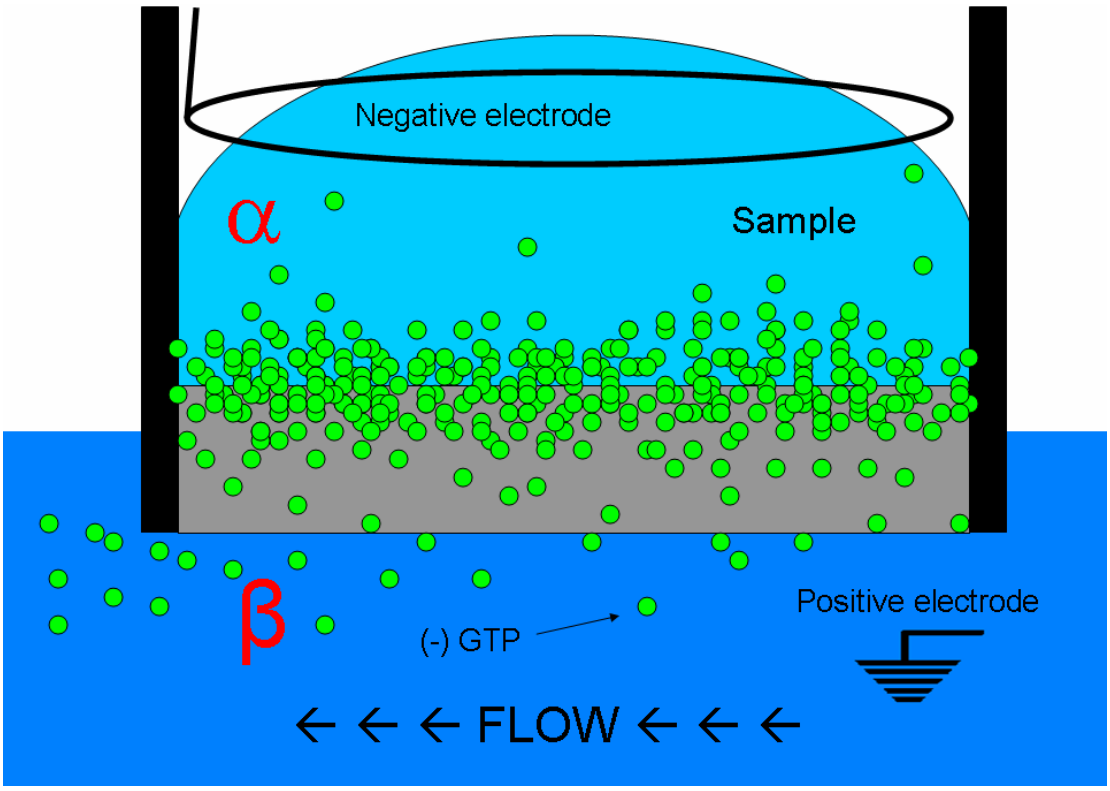

Figure 4.1 Small Volume Electrodialysis Design. In this schematic, 20 µL of sample to be dialyzed (α-phase) is pipetted into the upper reservoir well. The α-phase contains 1X TAE buffer and radioactive GTP (green dots). A negative electrode is mounted on the top of the droplet. The semi permeable membrane is shown in grey. The β-phase (1X TAE) is washed through the lower 1 mL flow cell, which contains the positive electrode (ground). The distribution of green dots probably represents the location of GTP molecules a few seconds after the voltage is switched on. Note: The ground electrode is located near the exit of the flow cell in the actual design, and the collection receptacle for the β-phase effluent is not shown in this schematic.

4.2.2 Reverse Microfiber Dialysis Design

A schematic of our basic reverse microfiber dialysis design is shown if Figure 4.2. Hollow microdialysis fibers (MWCO = 13,000) were obtained from Spectrum Labs (Rancho Dominguez, CA). The regenerated cellulose fibers have an inner diameter of 200 μm, a wall thickness of 8 μm, a length of 6 inches (15.24 cm) and hold a maximum volume of 5 μL. The area to volume ratio of a 15.24 cm fiber is 19.14 $mm^2 \cdot \mu L^{-1}$. We spliced the fiber to plastic tubing via removable couplings sealed with silicone. The detachable design allowed us to rapidly load an aqueous α-phase sample, reconnect the fiber, and infuse the sample *via* air pressure created by a syringe-controlled hydraulic force. For dialysis purification, the fiber was placed into a 250 mL, room temperature buffer bath containing aqueous β-phase for dialysis purification. The β-phase was stirred to prevent concentration gradients around the microdialysis fiber. The other end of the fiber could be suspended above a collection receptacle or connected to an addition coupling with plastic tubing for controlled sample handling or re-infusion.

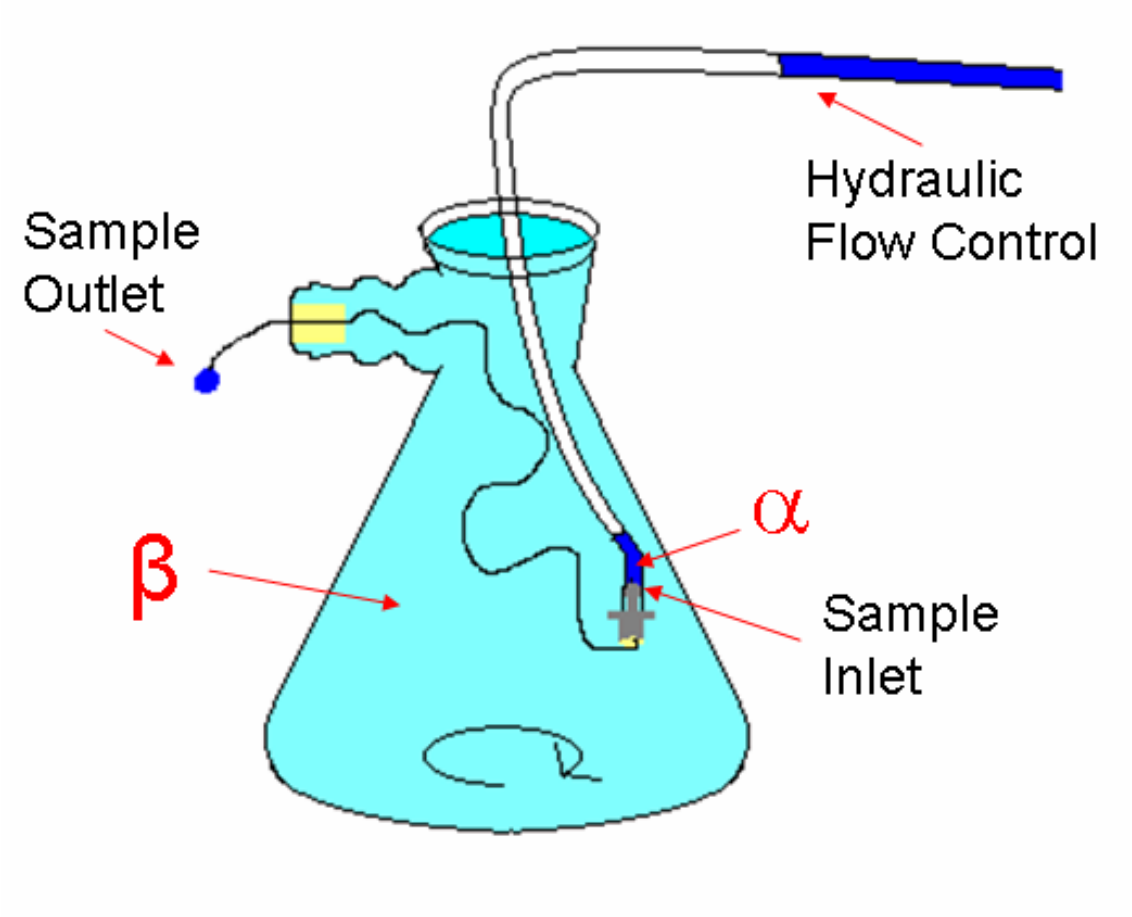

Figure 4.2 The Reverse Microfiber Dialysis Apparatus. In this schematic, the α-phase is shown at the inlet and outlet of the microdialysis fiber, which is shown as a thin black strand submersed in the β-phase. The α-phase contains the ligand-acceptor mixture. Both the α- and the stirred β-phase consists of 1X TAE buffer. α-phase infusion and perfusion is controlled by forced air from a hydraulic flow control syringe.

4.2.3 STaGE Design

The design of short travel gel electrophoresis is schematically represented in Figure 4.3. We constructed a plastic mold which allowed us to form agarose or polyacrylamide structures that housed a 7.5 mL negative electrode reservoir located over a cylindrical sample loading well 4mm in diameter and 5 mm deep. The distance from the bottom of the sample well into a 125 mL positive electrode buffer below was 5 mm. The 125 mL lower reservoir also served to capture free ligands electrophoresed through the plug. The 125 mL positive electrode buffer is stirred to homogenize the liberated ligand concentration to allow precise analysis of nucleotide "filtering".

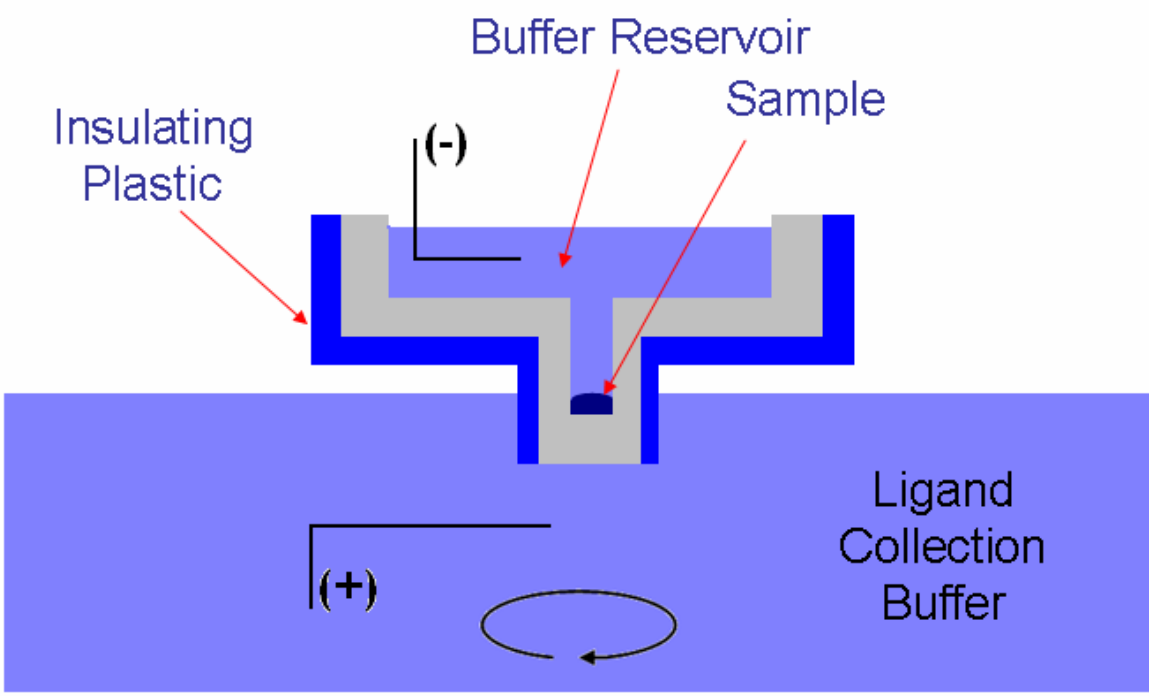

Figure 4.3 The Short Travel Gel Electrophoresis Design. A plug molded from agarose (1-2%) or polyacrylamide (7-15%) is formed (grey) to house a single sample well. The mold is shielded on all surfaces except for those directly underneath the separation plug. The total distance from the sample (shown in navy) to the ligand collection buffer is 5 mm.

4.3 Novel Method Characterizations

Each new phase separation presented here was characterized for the speed and extent to which the method was capable of removing NTPs from a buffer solution. We also investigated some of the techniques' ability to capture a protein from solution, purify NTPs from a protein solution, and/or aid in deciphering ligand acceptor dissociation constants.

4.3.1 SVED Experimental and Results

Experimental: To test SVED's ability to remove free nucleotide from the α-phase efficiently, we loaded 20 μL of 20 μM [α-^{32}P]-GTP (10 Ci·mmol^{-1}) in TAE buffer [40 mM Tris-base, 1 % (w/v) Acetic Acid, 1 mM EDTA, 5 mM Magnesium Acetate, pH 7.8]. The β-phase consisted of TAE buffer, and was flowed at 2 mL·min^{-1}. The α-phase droplet was deposited directly though the ring electrode onto the surface of the membrane, and the negative voltage (-100V$_{max}$) was turned on immediately. The voltage varied slightly as the solution warmed; the power was held at 2 W. To characterize the speed that SVED was able to remove GTP from the α-phase, we recorded the appearance of radioactively in the β-phase collection receptacle with and without the negative voltage applied to the α-phase. We calculated the total radioactivity of the β-phase by scintillation counting 250 μL aliquots of the liquid in the collection receptacle and factoring in the total liquid volume at the time of aliquot removal. The results of this experiment is shown if Figure 4.4. The extent of GTP removal was assayed after several minutes of electrodialysis. We recovered and analyzed the α-phase by scintillation counting, and compared the sample to the pre-SVED radioactivity.

Results: The appearance of nucleotide in the β-phase with no voltage applied to the unstirred 20 μL droplet of 20 μM [α-^{32}P]-GTP in TAE is shown in Figure 4.4a. Based on a

linear fit to these data, we estimated the dialysis equilibration time to be no less than one hour. Figure 4.4b shows the time dependence on ligand arrival in the β-phase with -30 to -70 volts applied (2 W) to the α-phase. The maximum removal of GTP from the α-phase was reached in roughly 7.5 min. The initial rate (first 2-3 min) of GTP appearance in the β-phase was similar to that of the non-voltage control. After 20 min of SVED, the α-phase was carefully removed an analyzed for presence GTP by scintillation counting. We repeatedly observed the GTP concentration in the SVED purified α-phase to be 50-200 nM, indicating a reduction of GTP concentration of 2-3 orders of magnitude. The 20 μM GTP purification was repeated several times (N=5). We also conducted experiments with starting GTP concentrations of 2 μM, 100 μM and 500 μM (N≥2). We found that the same purification time was needed for each concentration (~7 to 8 minutes), and that the extent of purifications was near 3 orders of magnitude for each concentration.

We observe similar rates of GTP appearance in the β-phase with and without a voltage in the first few minutes of dialysis, indicating that the migration of GTP through the membrane is not changed by the applied voltage. The current efficiency of conventional electrodialysis is such that only small ions can be electrophoresed through dialysis membranes efficiently (Shaffer *et al.*, 1980). We tested the power limits of SVED and our findings were consistent with the low current efficiency of other electrodialysis methods. We found that anything above 3 W required more than 100 V using TAE buffer and regenerated cellulose. Higher voltages induced electro-osmosis, and usually flooded the α-phase quickly. At slightly higher voltages, enough to produce ~2.5 W, we saw no evidence to indicate faster SVED purification times.

Several synthetic hydrophobic membrane filters were tested for their SVED performance and ability to resist non-specific GTP absorption. PTFE, PES and PET were not capable of purifying the α-phase more quickly, or to a fuller extent.

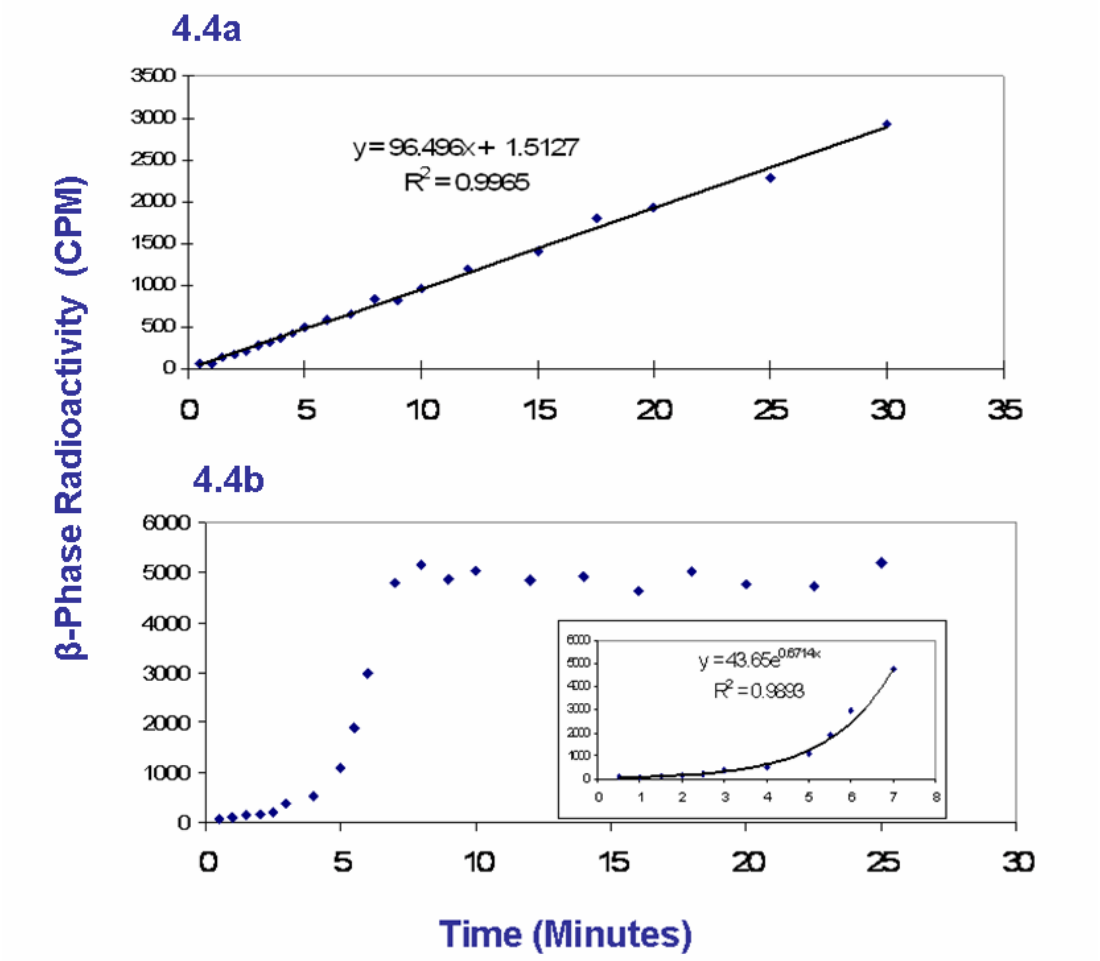

Figure 4.4 Electrical Current Aids in the Mass Transport of Nucleotides to the Surface of a Semi-permeable Membrane. The dialysis of GTP is observable by the appearance of in the radioactivity in the β-phase. In 4.4a, no voltage is applied to the SVED well. In 4.4b, a negative voltage is applied to produce 2W.

4.3.2 Reverse Microfiber Dialysis Experimental and Results

Experimental: As with the SVED technique, we wished to assay the reverse microfiber dialysis design for its ability to remove GTP from solution. Both α- and β-phases were comprised of TAE buffer (pH 7.8) and the α-phase contained 20 μM [α-^{32}P]-GTP (10 Ci·mmol^{-1}) solutions. We prepared the fiber for sample infusion by rinsing the interior with 20 – 30 μL ethanol, 20 – 30 μL ddI H_2O, and then 20 - 30μL TAE buffer. We submersed the fiber in TAE bath for at least 5 minutes prior sample injection. When we were ready to inject the sample (α-phase), we removed the fiber from the TAE and ejected any remaining buffer from the fiber volume. Since the maximum inner fiber volume is 5 μL, we limited out injects to 3 – 4 μL to ensure 100 % sample contact with the inner membrane surface. We submersed the fiber into the β-phase and removed small 250 μL aliquots from the β-phase over time to assay the appearance of GTP. To test the re-usability of a single fiber, consecutive 4 and 2 μL injections were made while monitoring the appearance of radioactive GTP in the β-phase. The perfusate was collected after dialysis purification and analyzed by scintillation counting for GTP content. Moderate pH changes (pH 6.0 –pH 9.0), temperature changes (10-35°C) and cation buffer composition (5 to 50 mM Mg^{+2} or Na^{+}) were tested for major influence on microfiber dialysis performance. In addition to the 20 μM GTP experiments (N=5), a 100 μM GTP assay was performed.

We characterized reverse microfiber dialysis purification for its efficacy in "washing" transcription stalled elongation complexes free of unbound NTPs. As a control, biotinalated SECs were prepared and purified using streptavidin coated magnetic beads (10 washes) as previously described using radioactive GTP (Holmes *et al.*, 2003; Cunningham, 2007; Kennedy *et al.*, 2008). We also synthesized SECs without beads (~35 nM), and infused 4 μl

of the solution into the reverse microfiber dialysis apparatus. The relative efficacies of the magnetic-bead versus microdialysis purifications were compared by separating the solutions' nucleic acids (radioactive RNA and NTPs) by 8 M urea-20 % PAGE.

Results: Within four to five min for reverse microfiber dialysis, we observe maximum appearance of GTP into the β-phase (*e.g.* Figure 4.5a). Scintillation count analysis of the dialyzed α-phase indicated a reduction of the 20μM GTP to 0.6 – 20 nM, reproducibly (N=6). In the 100 μM GTP trial, we observed a proportional reduction of GTP concentration to 45 nM. We found that moderate changes of pH and temperature and minor changes to cation compositions in the α- and β-phases had little effect on dialysis performance, although lower than 5 mM Mg^{+2} slightly lengthened the time need for maximum dialysis. In the consecutive injection experiment shown in Figure 4.4b, the 4 and 2 μL, 20 μM GTP samples were dialyzed in to completion in 4 to 5 min. As the data show, the entry of GTP into the β-phase was proportional to the volumes injected. We observed no reduction in purification performance with the second injection; both samples were reduced to ~500 pM after reverse microfiber dialysis.

The comparison between reverse microfiber dialysis and affinity-bead purification of SECs is shown in Figure 4.6. Analysis of the GTP-SEC ratios (see Chapter 3) revealed a major reduction in free NTP background with microfiber purification. The GTP-SEC ratio calculated after the microdialysis purification was ~10, indicating much more recovered free NTPs relative to the recovered SEC. The lengths of RNA transcript were identical in both affinity bead and microfiber purifications.

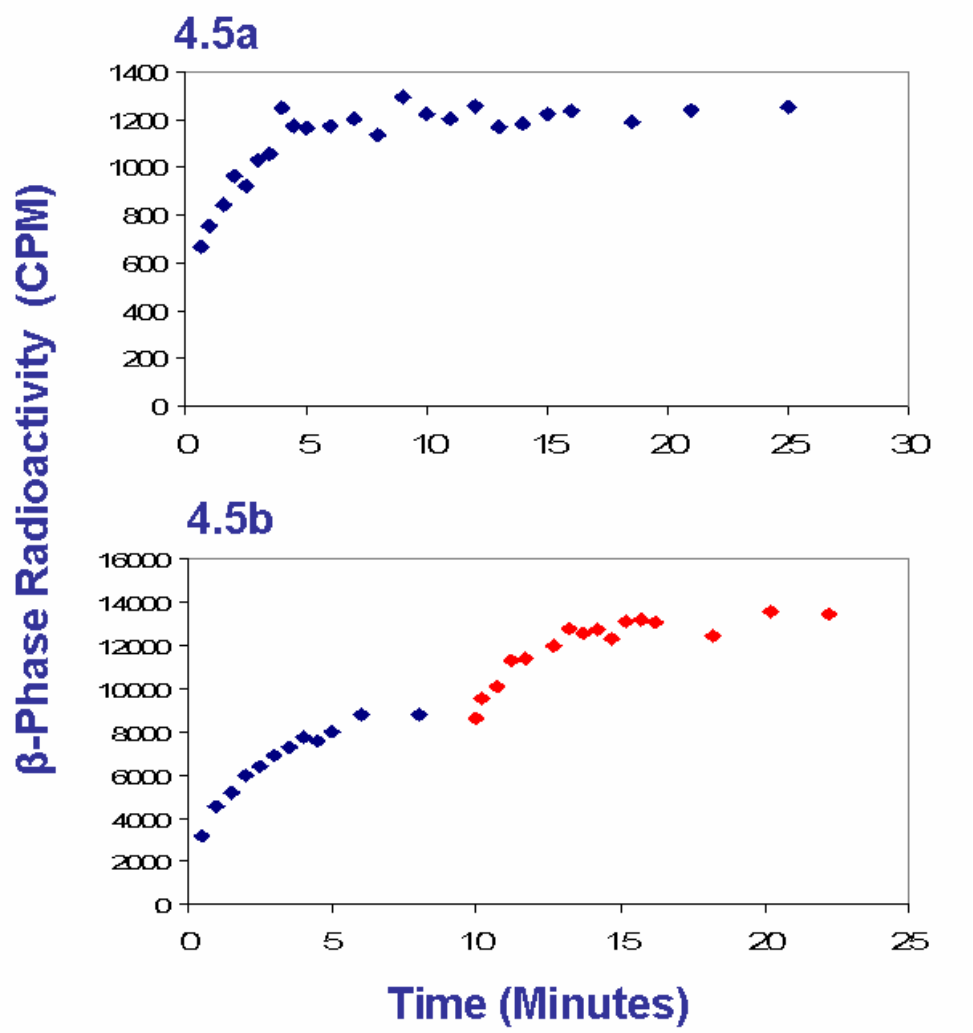

Figure 4.5 Reverse Microfiber Dialysis Repeatably Purifies a Nucleotide Diluate Solution in just 4 to 5 Minutes. In the top graph (Figure 4.5a), the data are from an experiment that assayed of the appearance of GTP in the β-phase assayed over a 25 min using reverse microfiber dialysis. In the bottom plot (Figure 4.5b), the appearance of β-phase GTP for two consecutive injections was assayed. In blue is the radioactively observed from a 4μL injection, and shown in red is the second 2μL injection.

Figure 4.6 Microfiber Dialysis Purification of SECs is More Effective than Magnetic Affinity Beads. Radioactive RNA and GTP are separated by PAGE. On the left are the separated contents from a SEC solution purified by magnetic affinity beads, showing a very large amount of recovered GTP background relative to the transcript. Shown on the right is the PAGE analysis of RNA and GTP recovered using reverse microfiber dialysis.

4.3.3 STaGE Experimental and Results

Experimental: As with SVED and reverse microfiber dialysis, we needed to characterize STaGE for its ability to quickly and completely remove micromolar concentrations of NTPs from a few microliters of sample. Using our customized STaGE gel mold, an agarose or polyacrylamide gel was poured. The upper and lower electrode buffer reservoirs of the STaGE apparatus were filled with TAE buffer [40 mM Tris-base, 1 % (w/v) Acetic Acid, 1 mM EDTA, 5 mM Magnesium Acetate, pH 7.8]. Under a low loading voltage (-15 V, 1-2 W), a 10 μL [α-^{32}P]-GTP (20 μM, 10 Ci·mmol^{-1}) sample in 10 % glycerol/bromothymol blue was carefully loaded into the bottom of the STaGE. Immediately after loading, the power was increased to 5 W (60 -100 V). The liberation of GTP from the STaGE plug was monitored over time by scintillation counting of 250 μL aliquots of the stirred positive electrode buffer. A range of agarose and polyacrylamide gel compositions were characterized for free nucleotide migration times, practical tensile strength and thermal stability. The STaGE phase separation was characterized for non-specific adsorption of free ligand by segmenting the plugs and scintillation counting various structures.

To test the reproducibility of protein capture using STaGE gels, we loaded 10 μL bovine serum albumin (BSA) (0.1 mg·mL^{-1}) in 2 % agarose and 10 % polyacrylamide gels. The agarose and polyacrylamide gels were run at 5 W for 5 and 7 min, respectively. We visually tracked BSA migration by segmenting the STaGE gels and individually staining the sections with Coomassie.

We characterized the STaGE phase separation for its efficacy as an equilibrium binding assay. We chose ATP binding with MutS from *Thermus aquaticus* (*Taq*) as a test system since the binding parameters have been previously described (Antony *et al.*, 2004).

We incubated 100 nM *Taq*-MutS in nucleotide binding buffer (50 mM Hepes, 5 mM $MgCl_2$, 150 mM KCl, 10% glycerol, pH 7.8) and bromothymol blue for 3 minutes with 0.53 to 200μM [α-^{32}P]-ATP (25Ci·mmol^{-1}). After each titration incubation (equilibration) period, we loaded the sample onto a 10% polyacrylamide STaGE mold under -10 V (~1 W). The power was immediately increased to 5 W for electrophoresis for 5 min. Each gel was segmented and the plug sections of the STaGE mold were scintillation counted to detect bound MutS.

Results: Figure 4.7 shows the GTP appearance in the free ligand collection buffer using 2 % agarose (Figure 4.7a) and 10 % polyacrylamide (Figure 4.7b) STaGE gels run at 5 W. In the agarose gel, GTP begins to appear in collection buffer within the first 30 sec of electrophoresis, and we observe maximum ligand removal from the gel 3.5 min (N=12). In the polyacrylamide STaGE gel, nucleotides appear in the collection buffer at 1.75 min, and the purification reached full extent by 4.25 min (N=9). We noted that while 2 % agarose removed NTPs from the sample in less total time, we removed NTPs from the 10 % polyacrylamide STaGE in a shorter band.

The dissection and non-specific absorption analysis of both agarose and polyacrylamide STaGE gels revealed that no detectable amounts of radioactivity were observable anywhere in the gel structure or negative electrode reservoir. In some instances however, sloppy loading technique was found to be responsible for radioactive GTP diffusion into the negative electrode reservoir and reservoir walls. We rarely detected the presence of ligand captured in the plug section of the STaGE gels.

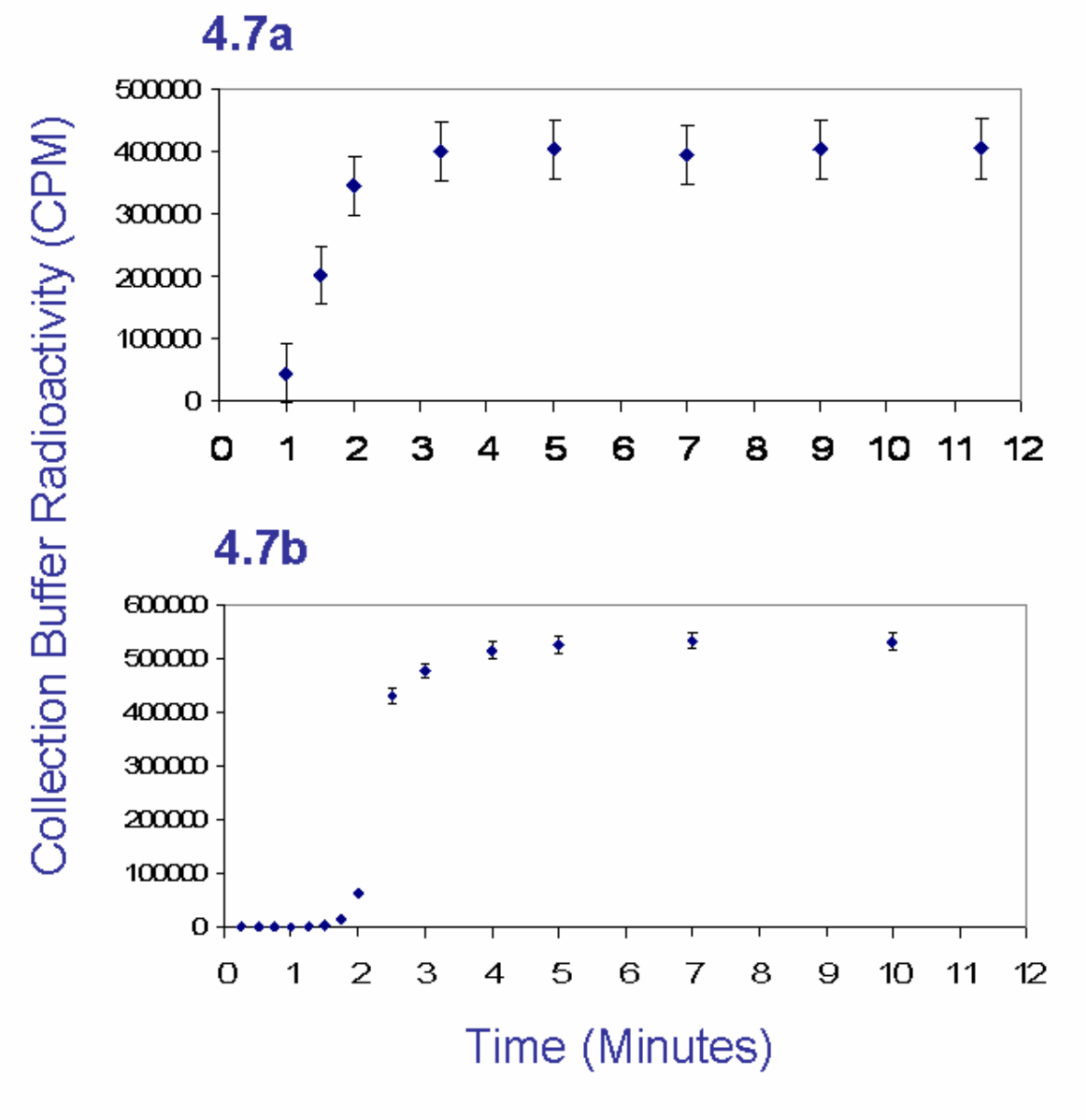

Figure 4.7 Electrophoretic Filtering by Agarose and Polyacrylamide STaGE Gels. In Figure 4.7a, the appearance of GTP is assayed by observation of radioactivity in the ligand collection buffer using an agarose STaGE gel. Polyacrylamide STaGE was characterized for GTP filtering in Figure 4.7b.

Upon Coomassie staining the electrophoresed STaGE gels loaded with BSA, we observed that 2% agarose STaGE gels did not trap the protein band tightly. We found protein throughout the travel plug, the sample well walls, and even into reservoir basin. With polyacrylamide STaGE however, we observed the majority of the BSA captured in a thin band on the short 5mm travel path, mostly near the bottom of the well.

We found similar protein migration behavior with polyacrylamide when imagining the segments of a STaGE gel that was used to filter free radioactive ATP from ATP-MutS complexes (Figure 4.8a). The highest concentration of radioactivity is observed near the top of the travel plug, as captured by a phosphorimaging storage screen (Eastman Kodak, Rochester, NY) and analyzed on a Typhoon 9410 phosphorimaging scanner (Amersham Biosciences Corp. Piscataway, NJ).

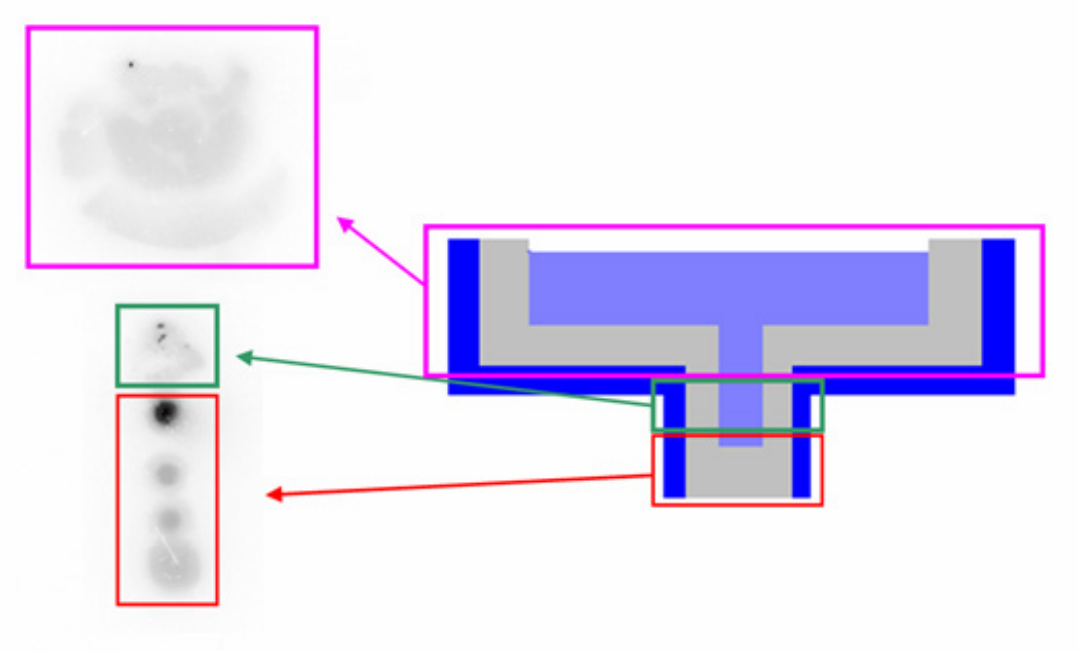

Figure 4.8 Polyacrylamide STaGE Captures ATP bound to *Taq*MutS. Separation of free ATP from an equilibrated of solution of 100 nM *Taq*MutS and 100 μM [α-32P]-ATP (25 $Ci \cdot mmol^{-1}$) leaves a tight band of radio-ligand bound to acceptor near the top of the short travel separation plug (outlined in red). The electrode reservoir and reservoir walls (outlined in magenta) and the sections of the sample well walls (green) did not capture ATP-MutS complexes.

The results of the ATP-*Taq*MutS titration are shown in Figure 4.9 (N=2). We fit the data to a rectangular hyperbolic function. We observe one molecule of ATP binding to MutS with a $K_D = 9.4 \pm 1.9$ μM. The free ATP concentration was calculated by subtracting the concentration of bound complexes observed from the titration concentration of ATP.

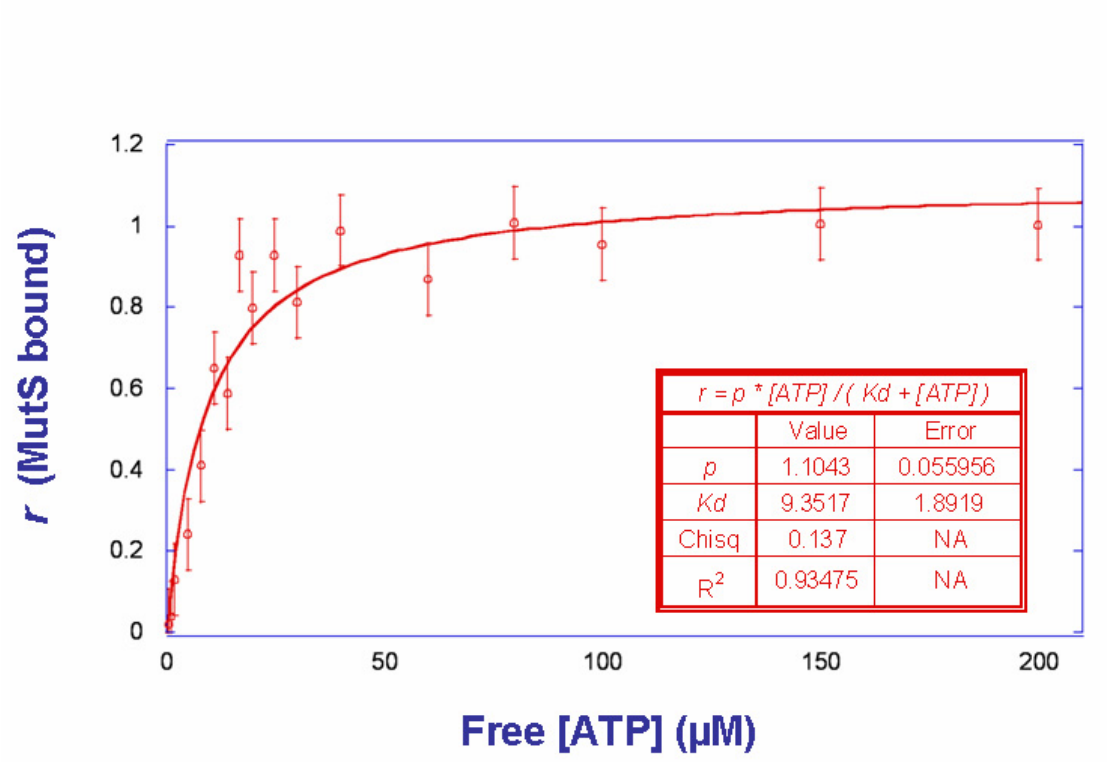

Figure 4.9 ATP-*Taq*MutS Binding Analysis Determined by STaGE Purification. The data were fit to a rectangular hyperbolic expression to reveal a binding stoichiometry of 1 and a binding affinity of 9.4 μM.

4.4 Novel Phase Separation Discussion

We developed an arsenal of new phase separation techniques aimed at quickly separating solutions of nucleotide ligands and protein acceptors. Small volume electrodialysis (SVED), reverse microfiber dialysis and short travel gel electrophoresis (STaGE) have been characterized in their ability to remove free nucleotides from a buffer solution and resist non-specific adsorption. We show that microfiber dialysis and STaGE perform in at reasonable analytical proficiency, and may offer advantages for some biological assays that are constrained by limited amounts of acceptor.

4.4.1 SVED

We have demonstrated that a new phase separation, small volume electrodialysis (SVED), removed a charged ligand (GTP) from a solution faster than unstirred diffusion-limited dialysis. GTP removal was likely limited by the non-specific absorption of nucleotides to the regenerated cellulose and other materials comprising the apparatus. In the SVED phase separation experiment, we observed a sharp burst in β-phase GTP appearance around 4 min. Since electro-migration *through* the membrane is likely not occurring at only 2 W, we concluded that the negative voltage applied to the α-phase facilitated mass transport of GTP *to* the membrane and is the primary mechanism responsible for faster dialysis.

Unlike diafiltration and ultrafiltration (Winzor *et al.*, 1995), the volume of α-phase is not changed during the separation. Constant volume is a potential advantage over the other filtration techniques since the effective concentration of acceptor in solution would not change with SVED. However, the advantages of speed and constant volume do not validate the use of this apparatus for the analysis of ligand-acceptor binding in systems such as

transcription. As with all other phase separation techniques, the contribution of non-specific ligand adsorption is too high to assay mid micromolar K_D's while using only low nanomolar concentrations of acceptor.

4.4.2 Microfiber Dialysis

We found that diffusion limited dialysis using microfibers in the reverse phase (infusion of α-phase) allowed us purify away solutions of 20 μM GTP quickly. We estimated the time for GTP diffusion to the inner fiber membrane surface to be about one second, per the following comparison with the non-voltage SVED control: We calculated a 30-fold increase in the area to volume ratio of microfibers compared to the SVED well design. The cylindrical geometry of the hollow microdialysis fibers permitted a ligand in the fiber to productively diffuse toward the semi-permeable membrane in two dimensions (x-y), and in two directions (+/-), where a ligand in the SVED well could move productively in one dimension (z), and one direction toward the bottom of the well (-); therefore, the limiting diffusion time in the microfiber was decreased 3600 X [$(2 \cdot 30)^2 = 3600$] (Figure 4.9). The dialysis time with the SVED well design (no voltage) was limited by diffusion through the α-phase. We estimated the equilibration time in the non-voltage SVED well control to be around 1 hr, and by comparison, the diffusion of a GTP particle in the microfiber α-phase reached the membrane wall in around one sec.

Since maximum GTP reduction from the α-phase was reached in roughly 5 min, we estimate that the rate limiting step in reverse microfiber dialysis of was the migration of GTP through the 8μm thick membrane wall. If five min are require for GTP to pass through the 8 μm thick membrane wall, we concluded that significant interactions were being made

between the cellulose and the GTP. Therefore, we assume that the GTP interactions with the membranes surface were the performance limiting mechanism in α-phase purification with reverse microdialysis.

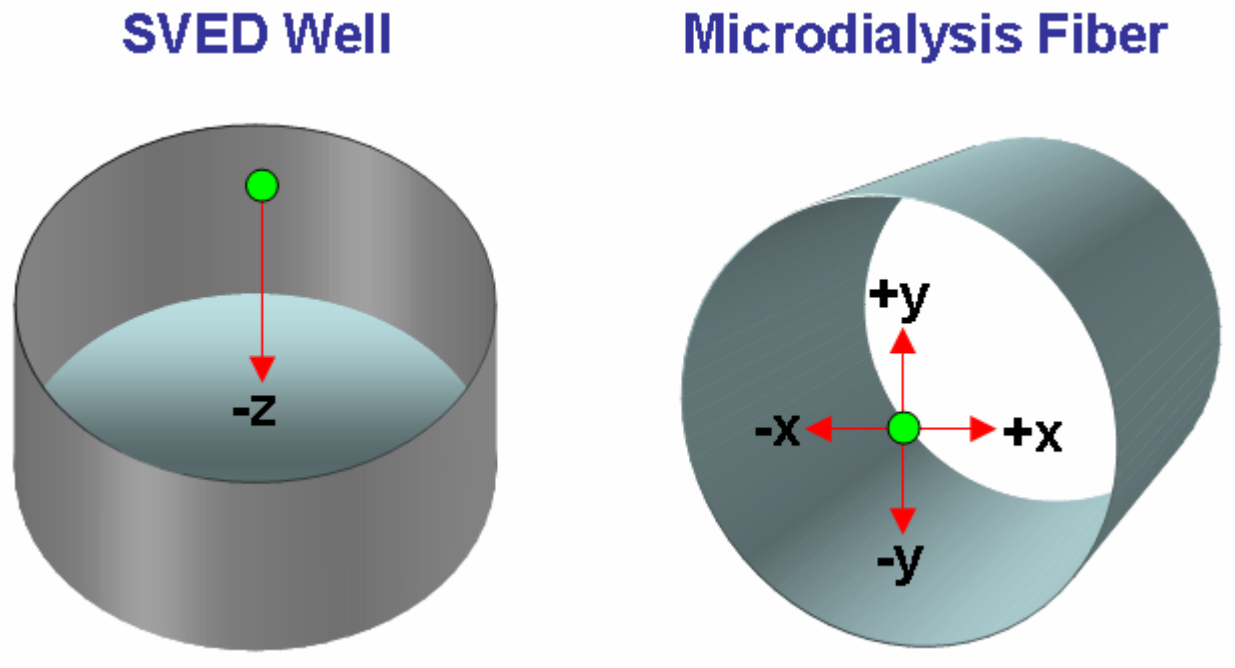

Figure 4.9 Comparison of Microfiber and Well Design Dialysis Geometries. The SVED schematic (left) shows that a GTP particle (green) may only travel to the semi-permeable membrane (blue) in one direction in the z dimension. Shown in the microfiber dialysis schematic on the right, the GTP molecule may diffuse productively to the regenerated cellulose membrane (blue) in the x and y dimensions, and in both + and – directions. Combining the microfiber geometry with the 30-fold increase in membrane area:sample over SVED, we estimated the average time for a GTP molecule to diffuse to the membrane is decreased by a factor of 3,600.

In our use of microdialysis fibers for sample purification, we consistently observed a reduction in α-phased GTP concentration by nearly 4 orders of magnitude. Several rounds of nucleotide particle adsorption and desorbtion likely took place as they passed through the membrane, possibly explaining previous reports of high dNTP recoveries using microfibers for purification (Hannis *et al.*, 1999). We conclude that the 2 $\mu L \cdot min^{-1}$ flow rate reported by Hannis *et al.* (1999) may have caused dNTPs to re-enter the inner-fiber volume between rounds of intermittent adsorption. Rather than randomly diffusing after desorption from sites near the inner-fiber surface, dNTP migration may have been biased toward the axial exit of the fiber by the sample flow, resulting in 70 % recovery of the nucleotides the authors attempted to remove.

The speed and extent of GTP dialysis in the control experiments prompted us to compare reverse microfiber dialysis with our standard laboratory methods to purify SECs using magnetic affinity beads. Microdialysis clearly has advantages over the affinity beads. Without irreversibly attaching the transcription complexes to a support particle, we were able to remove a huge majority of the free NTPs used to synthesize the complexes. The time required to purify the complexes *via* microdialysis was no longer than the time typically taken to wash the complexes attached to beads. Since NTP solutions were commonly reduced to high pm levels, an SEC concentration of 35 nM should not have been a problem to analyze. However, the nearly 10-fold overestimation of the GTP-SEC stoichiometry (see Chapter 3) indicated to us that not enough of the free ligand was removed from the α-phase. Due to the nature of the SEC synthesis, determining the exact concentration of acceptor was impossible. It is likely that far less than 35 nM SECs were generated during synthesis, in which case small amounts of non-specific absorption would be problematic.

4.4.3 STaGE

We have shown that both agarose and polyacrylamide STaGE plugs viability remove NTPs from solution with very little or no non-specific adsorption in less than 5 min. We were able to push the applied voltage limits to short plugs of agarose and polyacrylamide by fitting a large (7.5 mL) negative electrode reservoir onto of a sample well. Earlier designs did not contain the large reservoir, and melting occurred at powers of 2 W. The higher, 5 W power limit facilitated the efficient electrophoresis of NTPs in just a few minutes, while capturing the majority of protein sample (BSA and *Taq*MutS).

We feel our results in the ATP-MutS binding study were validated by the numerous acceptor negative controls performed, and the comprehensive analysis of the plug segments. Previous studies of ATP binding to *Taq*MutS report a binding affinity of 0.9 ± 0.2 μM (Antony *et al.*, 2004). Several factors may have caused the discrepancy. In our work, we used 10-fold less MutS to prove the efficacy of STaGE versus the filter binding method used by Antony *et. al.* (2004). Additionally, the data we report are the result of completing the study only two times. There is evidence of that some of our data falls outside of the hyperbolic curve fit, especially at the lower free ATP concentrations. To capture these data, only the short travel plug sections of the STaGE gel were scintillation counted (see Figure 4.8). Some gels in our work showed evidence of loading error and some uncontrolled protein migration. It is possible that the efficiency of acceptor capture is the performance limiting with STaGE.

STaGE may offer several other advantages over other phase separation techniques used for quantitative ligand binding assays (Winzor *et al.*, 1995). STaGE acts as an

electrophoretic filter. Unlike diafiltration, STaGE is very fast. Ultrafiltration is fast, but uses a semi-permeable membrane that is highly susceptible to non-specific adsorption of charged ligands, such as nucleotides. STaGE is also potentially much more versatile than other filtration based techniques. The STaGE gel composition, travel distance, and electrophoretic power are a tunable, and may accommodate a diverse range of ligand-acceptor equilibrium binding studies.

4.4.4 Future Directions in Novel Phase Separation

SVED: While SVED was able to reduce the α-phase nucleotide concentration by more than 3 orders of magnitude in less than 10 min, the contributions of non-specific ligand adsorption limit the technique. It was apparent that removal of the α-phase agitated the solution enough to desorb NTPs from the well walls and microscopic sections of membrane that aren't helping with the separation. Finding a way to stir the 20 μL α-phase may be one way to desorb the non-specifically bound ligands from the well walls and unproductive "sites" on the membrane during the separation, instead of during α-phase collection.

Reverse Microfiber Dialysis: Reverse microfiber dialysis should be tested as a rapid method to assay ligand-acceptor interactions by traditional equilibrium dialysis in systems where high nanomolar amounts of acceptor are available. The charged nature of the phosphate groups on GTP is likely the source of non-specific adsorption to membrane. Other ligands, such as various hydrophobic drug molecules may be well suited for the fast, efficient use of reverse microdialysis purification.

STaGE: There is obvious room for improvement in the realm of sample loading and acceptor capture in STaGE purification, as is evident in the above ATP-MutS study. Not

discussed here are the several attempts we made to capture ternary stalled elongation complexes (RNA-DNA-RNAP). Often, we observed that SECs resisted entry into the gel matrix. We tested the use of lower percentage gels to facilitate easier entry into the gel, however, either the tensile strength became too low or the plugs melted at 5 W. Future investigations should employ the use of a sugar cushion or gel layers. A gummy capture layer such as 0.5 % agarose residing at the bottom of the sample well might assist in loading and immobilization of large acceptors such as ternary SECs. The future may even include multiple layered gel composition gradients for the capture of multi-component mixtures, such as NTP-DNA-Protein solutions.

The throughput of our current STaGE apparatus needs to be streamlined. Currently, only one titration sample can be processed every 10 min. Future modifications to the STaGE concept should include the creation of STaGE array capable of processing several samples at once.

BIBLIOGRAPHY

Antony, E. and M. M. Hingorani (2004). "Asymmetric ATP Binding and Hydrolysis Activity of the Thermus aquaticus MutS Dimer Is Key to Modulation of Its Interactions with Mismatched DNA." Biochemistry **43**: 13115-13128.

Colowick, S. P. and F. C. Womack (1969). "Binding of diffusible molecules by macromolecules: rapid measurement by rate of dialysis." J. Biol. Chem. **244**: 774.

Cunningham, C. (2007). Insight into the Fidelity of Escherichia coli RNA Polymerase: Investigation of Misincorporation During Transcription Elongation Utilizing Transient State Kinetics. Chemistry. Chapel Hill, University of North Carolina at Chapel Hill. **Ph.D.:** 150.

Ford, C. L., D. J. Winzor, L. W. Nichol and M. J. Sculley (1984). "Effects of thermodynamic nonideality in ligand binding studies." Biophys. Chem. **18**: 1.

Garner, M. M. and A. Revzin (1981). "A gel electrophoresis method for quantifying the binding of proteins to specific DNA regions: application to components of the Escherichia coli lactose operon regulatory system." Nucleic Acids Res. **9**: 3047-3060.

Hannis, J. C. and D. C. Muddiman (1999). "Characterization of a Microdialysis Approach to Prepare Polymerase Chain Reaction Products for Electrospray Ionization Mass Spectrometry Using On-line Ultraviolet Absorbance Measurements and Inductively Coupled Plasma-Atomic Emission Spectroscopy." Rapid Commun. Mass Spectrom. **13**: 323-330.

Harris, S. J. and D. J. Winzor (1988). "Graphical Analysis of Binding Data Reflecting Competition Between Two Ligands for the Same Acceptor Sites." Anal Biochem. **169**(2): 319-27.

Herrera, A. M., D. O. Scott and L. C.E. (1990). "Microdialysis Sampling for Determination of Plasma Protein Binding of Drugs." Pharm Res(10): 1077-81.

Hogan, B. L., L. S.M., J. F. Stobaugh and C. E. Lunte (1994). "On-line Coupling of In Vivo Microdialysis Sampling with Capillary Electrophoresis." Anal Chem **66**(5): 596-602.

Holmes, S. F., J. E. Foster and D. A. Erie (2003). "Kinetics of multisubunit RNA polymerases: experimental methods and data analysis." Methods Enzymol **371**: 71-81.

Jakubowski, J. A., N. G. Hatcher and J. V. Sweedler (2005). "Online Microdialysis-Dynamic Nanoelectrospray Ionization-Mass Spectrometry for Monitoring Neuropeptide Secretion." J. Mass Spectrom **40**(3): 924-931.

Kennedy, S. R. and D. A. Erie (2008). "A Non-catalytic Nucleoside Triphosphate Binding Site on RNA Polymerase Regulates Transcription." submitted to Cell March, 2008: 32.

Liu, Z., F. Li and Y. Huang (1999). "Determination of Unbound Drug Concentration and Protein Binding in Plasma." Biomed. Chromatogr. **13**: 262-266.

Oravcová, J., B. Böhs and W. Lindner (1996). " Drug-protein binding studies New trends in Analytical and Experimental Methodology." J Chromatogr B Biomed Appl **667**(1): 1-28.

Shaffer, L. and M. Mintz (1980). "Electrodialysis" in Principles of Desalination. New York, Academic Press.

Svensson, H. (1946). Ark. Kemi Mineral. Geol. **22A**: 10.

Takeo, K. and S. Nakamura (1972). "Dissociation constants of glucan phosphorylase of rabbit tissues studied by polyacrylamide gel disc electrophoresis." Arch. Biochem. Biophys. **153**: 1.

Wang, H., H. Zou and Y. Zhang (1997). "Multi-site binding of fenoprofen to human serum albumin studied by a combined technique of microdialysis with high performance liquid chromatography." Biochemical Chromatography **12**(1): 4.

Winzor, D. J. and W. H. Sawyer (1995). Quantitative Characterization of Ligand Binding. New York, John Wiley and Sons, Inc.

Zhou, D., L. Li and F. Li (2004). "Analytical Methodology for Drug-Protein Binding Studies." Se Pu **22**(2): 116.

CHAPTER 5:

ATOMIC FORCE MICROSCOPY OF BIOLOGICAL MARCOMOLECUAR COMPLEXES DEPOSITED ONTO ULTRA SMOOTH GLASS

5.1 Addressing a Limitation of Atomic Force Microscopy

Atomic force microscopy (AFM), also called scanning force microscopy (SFM) (Binnig *et al.*, 1986) has been used to identify and characterize a host of biological interactions and structure-function relationships in multimeric protein-DNA complexes (Bustamante *et al.*, 1994; Erie *et al.*, 1994). Our laboratory has used AFM to elucidate protein-DNA and protein-protein binding constants, and determine protein stoichiometries and oligomerization (Yang *et al.*, 2003). Recently, our lab has captured AFM images that helped us identified conformational changes in the DNA mismatch repair protein, MutLα, related to adenine nucleotide binding (Sacho *et al.*, 2008). As explained in chapter two however, AFM has limitations related to probe geometry (Figure 2.4). AFM cannot resolve adjacent molecular structures of vastly differing size. More over, the identities of similar structures in AFM images often cannot be determined; for example, two different proteins with similar mass might not be distinguishable.

Combining AFM with single molecule fluorescence (SMF) imaging techniques may provide the means to enhance the information content in topographic images. Fluorescence imaging with one nanometer accuracy (FIONA) was developed recently in the Selvin lab (Yildiz *et al.*, 2003; Yildiz *et al.*, 2004). Yildez *et. al.* (2003) showed that the central location of a fluorophore can be pinpointed within 1.5 nm. Figure 5.1 outlines a strategy for using

fluorescent quantum dots as fiduciary markers for overlaying fluorescence and topographic images. The upper left cartoon in Figure 5.1 is an example of the kind of sample that we hope to further probe. The upper right cartoon is what a topographic image would look like of the sample. The individual proteins (bound to DNA) are not resolvable. Co-deposited with the protein-DNA complexes are fluorescent quantum dots; these nanocrystals are hard spheres that will act fiduciary markers between AFM and SMF images. FIONA imaging of the same topographic area reveals the exact location of the quantum dots and the fluorophore attached to protein (lower right cartoon). The images are overlaid in the bottom right depiction of Figure 5.1. The combination of topographic and fluorescence data would allow for the identification of the overall protein-DNA complex conformation and orientation. Another avenue for combined AFM-SMF may include utilizing Fluorescence Resonance Energy Transfer (FRET), where donor quantum dot nanocrystals are fixed to the AFM probe and act as a light source (Ebenstein *et al.*, 2004).

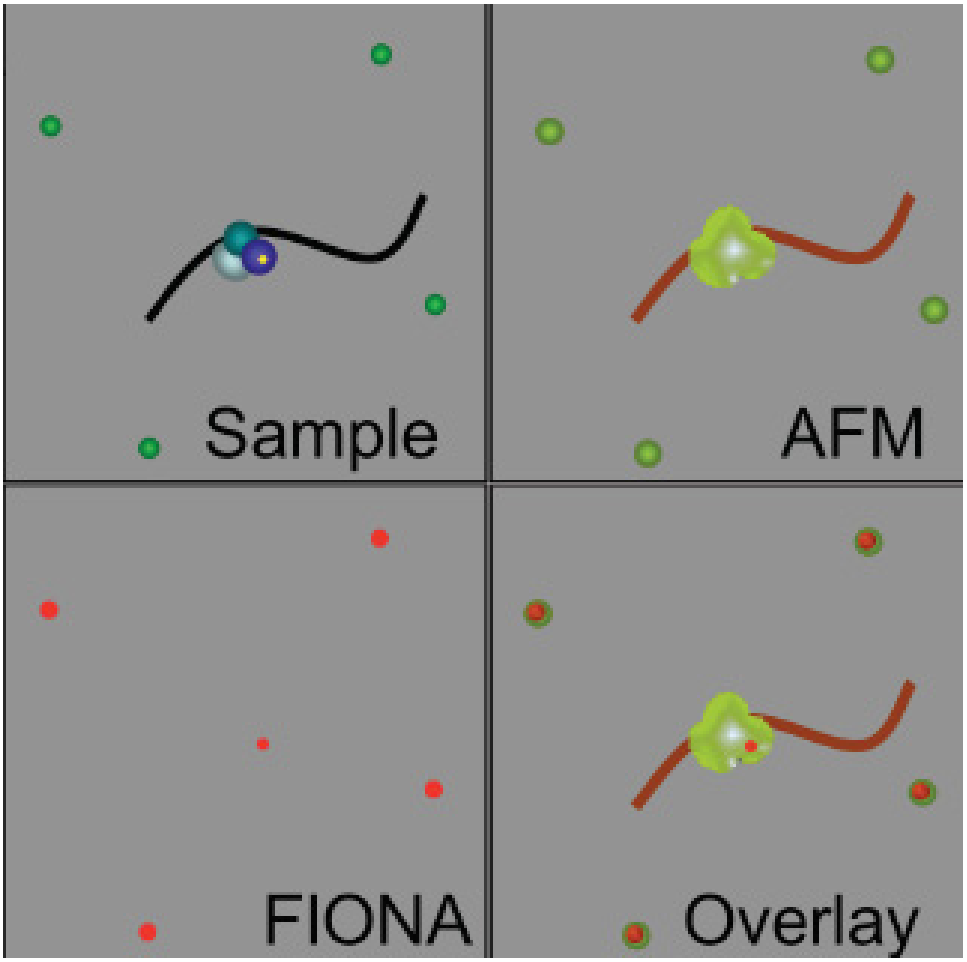

Figure 5.1 One Strategy for Combined AMF-SMF Microscopy. The upper lefty cartoon is a drawing of a multimeric protein-DNA complex (blue shaded spheres + black squiggle) deposited along with quantum dots (green spheres). The dark blue protein is fluorescently labeled prior to complex assembly and deposition. Fluorescence signal is depicted in the bottom left cartoon. The over lay of the AFM (upper right cartoon) and FIONA data would provide a picture as seen on the bottom right. The original topographic image now contains the identity of the labeled protein.

5.1.1 AFM Imaging of DNA on Mica

Freshly cleaved ruby mica is the preferred surface to deposit DNA and protein-DNA mixtures for AFM analysis for two primary reasons. First, mica is atomically flat; its root mean squared (RMS) roughness (Rq) is 0.050 nm, providing an ideal background for the imaging of proteins, DNA and other small structures by AFM. Second, mica binds DNA through a divalent cation salt bridge, effectively immobilizing DNA on the surface (Pastre *et al.*, 2003). To capture topographic information while channeling light from underside of the mica, the distance from the deposition surface to the optical microscope aperture would have to be relatively small and transparent to visible wavelengths. Thin peels of mica are flimsy, hard to prepare, and must be supported. Thin mica would be difficult to handle and the deposition surface itself might become compromised by structural failures from flexing during preparation. Also, ruby mica is red in color and may limit the spectral flexibility of potential fluorescence assays.

5.1.2 Imaging DNA with AFM on Glass

We believe there are many advantages to using thin microscope cover slips as an alternative to mica for combined AFM-SMF. Specifically, No.1 glass cover slips from Corning (Kennebunk, ME) are commonly used for the capture of single molecule fluorescence data. In this research, we describe modifications to glass cover slips that make them flat enough for topographic imaging of DNA by oscillating mode and phase mode AFM. It is known that DNA does not bind well to glass under low salt conditions (Dederich *et al.*). Biological samples deposited in physiological (high salt) buffer need to be washed with doubly deionized (ddI) water (18 $M\Omega \cdot cm^{-1}$) to prevent salt deposits that inhibit AFM

imaging. We observed that rigorous washes with ddI water aligned or rinsed away loosely bound DNA molecules on glass. In addition smoothing glass, we describe a deposition and rinse "minimal force" method that does not distort the biologically relevant molecular conformations that exist during initial complex adsorption to the imaging surface. Since all visible excitation and emission wavelengths will pass through glass efficiently, our development of glass preparations for AFM imaging may increase the flexibility of AFM-SFM.

5.1.3 Previous Work Involving AFM of DNA on Glass

Some groups have conducted AFM on glass that has been made smooth and left hydrophilic in nature to accommodate DNA binding (Wang *et al.*, 1998; Kwak *et al.*, 2002; Nakao *et al.*, 2002; Kwak *et al.*, 2003) In all of these cases, however, DNA is reported stretched or dried on glass, and is not deposited under physiological conditions. In a paper by Bensimon, a "molecular combing" method is described for the alignment of DNA onto a glass surface (Bensimon *et al.*, 1994). The controlled alignment of DNA onto a surface in all cases is conducted by balancing DNA's interaction with a surface and its propensity to follow solution flow. Taking advantage of DNA surface interactions has let researchers align and even stretch out DNA. Nakao *et al*. and Wang *et al.* suggest that combining optical techniques with AFM to image stretched DNA may be a way to conduct physical mapping of genomic DNA or clones. Images of smooth glass surfaces with stretched DNA have been produced by the application of thin polymer coatings. Work by Nakao *et al.* (2002) included the use of aromatic polymers spin coated onto glass cover slips from Matsunami Glass (Japan) that bind DNA through π- π bond interactions (π stacking). The authors report glass

RMS was decreased from Rq = 5.013 nm to 0.512 nm by using polyvinylcarbazole (PVK). Nakao *et al.* report another polymer (PPhenaz) that reduced the glass roughness to 0.312 nm, however this polymer is not commercial available.

To our knowledge, AFM images have not been published that show DNA in "natural" conformations on glass. We not only set out to flatten glass to a greater extent than found in the literature, but we also aimed to develop a method for DNA sample deposition that mimicked the irreversible binding of DNA to mica surfaces so that unaligned conformations and orientations of DNA on the surface could be observed.

5.2 Depositing DNA onto Glass

We describe a method for depositing DNA onto surface that does not wash away or align the molecules when sufficient (hydrophilic) interactions are made between the surface and the DNA. Laminar flow theory defines the fluid velocity nearest the surface to be lowest (Reynolds, 1883); we theorized that if the deposition and rinsing steps could be done under laminar flow conditions, the fluidic forces nearest the deposition surface would be lowest. Provided that sufficient interactions between the DNA and glass surface existed, the deposited DNA would not be washed away, aligned or stretched during the rinse steps.

5.2.1 The Minimal Force Deposition and Rinsing Method

We deposited 10 μL of 20 nM 550 bp DNA in physiological buffer [25 mM hepes, 10 mM sodium acetate (NaOAc), 5 mM magnesium chloride ($MgCl_2$), pH 7.8] onto glass slides that we had sonicated in 100 % ethanol (see section 5.3), and allowed the sample to incubate on the surface for 30 sec. As a control, we rinsed away one deposition droplet with 2-3 droplets of ddI H_2O three times, shaking the rinse droplet off lightly each time. After the final rinse, we dried the remaining moisture from the surface with a light stream of nitrogen. To test our hypothesis that controlled, laminar flow rinsing might reduce the forces applied to molecules on the disposition surface, we removed the deposition droplet of a second sample with a thinly cut piece of filter paper. By touching the edge of the filter paper to the droplet, we were able to controllably draw the liquid from the surfaces *via* capillary forces (see Figure 5.2). We characterized droplet removal velocity by monitoring the receding edge of droplet across the 1.0 cm cover slip. We estimated that fluid velocities were held between 0.5 and 1.0 $cm \cdot s^{-1}$ using the filter paper for liquid removal. A rinse droplet was slowly

applied by pipette and removed in the same manner as the deposition droplet. We repeated the rinse two more times, and dried the sample completely *via* a wide, very light stream of nitrogen. We kept the nitrogen flow rate low enough so that the remaining liquid on the surface was not pushed around by the drying process. It is important to note that the droplet removal was not so slow that it mimicked the results of droplet evaporation methods (Wang, Lin *et al.*, 1998), or the "molecular combing" method (a protocol that purposefully aligns DNA onto glass), which involves fluid velocities of 300 $\mu m \cdot s^{-1}$ (Bensimon *et al.*, 1994; Wang *et al.*, 1998). We show in Figure 5.2 a cartoon of a glass substrate (light blue) with DNA (squiggles) deposited in 10 μL of physiological buffer. The dark blue droplet represents either the original deposition droplet or one of three carefully applied 10 μL ddI H_2O rinses intended to prevent salt crystals. The white, uniformly thin sliced piece of filter paper (shown barely touching the droplet on the right) facilitated the controlled removal of buffer and water at velocities less than 1.0 $cm \cdot s^{-1}$. The arrows in Figure 5.2 represent the predicted fluidic velocity increase as the distance from the surface is increase. The (half) parabolic profile should also represent the lateral forces applied to objects encounter by the solution flow.

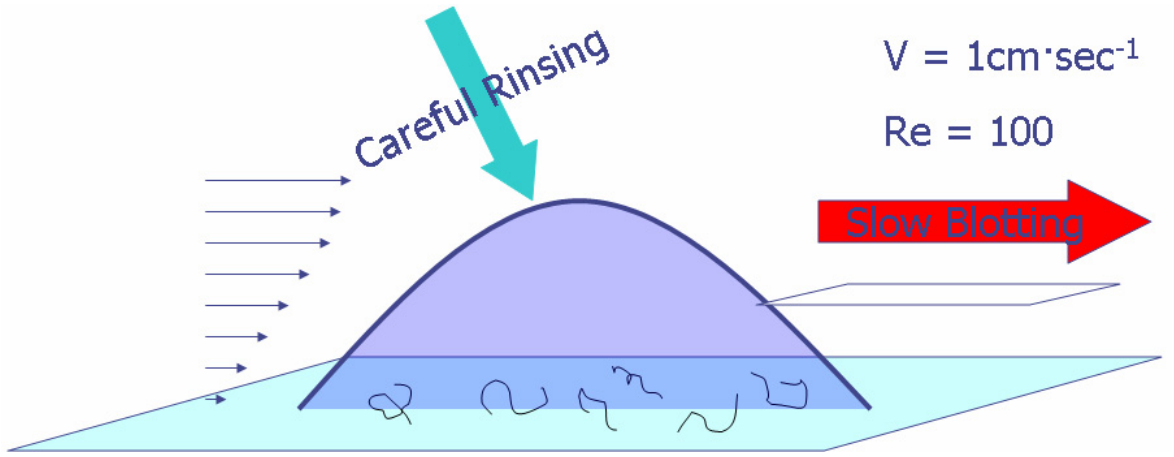

Figure 5.2 The Minimal Force Rinsing Protocol. The arrows on the left of the image qualitatively indicate the half parabolic flow profile velocity vectors at various distances from the deposition surface (flat plate model).

5.2.2 Minimal Force Method Results

Using the minimal force deposition and rinsing method, DNA bound to unmodified glass surfaces via weak electrostatic interactions was found to have a consistently greater chance of remaining bound and reproducibly unaligned as compared to vigorous rinsing and/or forceful N_2 blow drying. Figures 5.3a and 5.3b show the effects on DNA molecules deposited onto ethanol sonicated, chemically unmodified glass with and without the minimal force method, respectively. The rigorously rinsed sample image (Figure 5.3a) shows us that DNA is aligned from the upper left of the image to the lower right. We counted approximately 65 DNA molecules in the 1 μm^2 image. When we used the minimal force method to deposit and rinse the sample same amount of DNA, we observed 100+ DNA molecules in the 1 μm^2 AFM image, although the extremely high coverage of DNA prevents the identification of all the individual DNAs (Figure 5.3b). We noted that the orientations of the molecules on the surface were random. We found that the non-aligned deposition of DNA onto ethanol sonicated glass was observable in more than 90 % of the images taken when the minimal force method was used during a deposition ($N > 10$). Non-alignment of DNA was almost never observed though an imaging surface when the minimal force method was not applied.

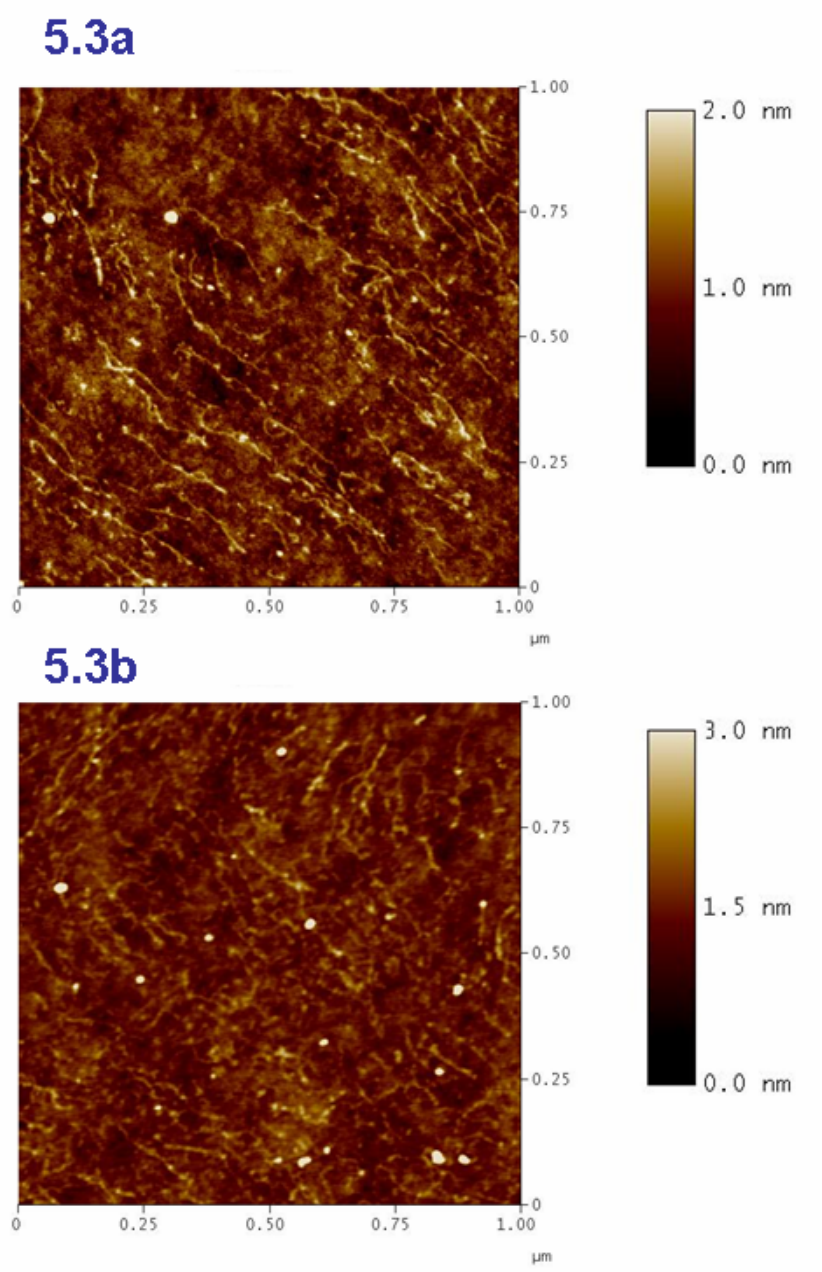

Figure 5.3 The Minimal Force Deposition Method Does Not Stretch or Align DNA on Ethanol Sonicated Glass. The AFM images shown here are 1 μm^2. The lighter colors represent taller topography. Shown above in 5.3a is ethanol sonicated glass with DNA deposited using a "traditional" deposition protocols. In Figure 5.3b, the minimal force deposition and rinse method was employed. The white spots are debris not removed during glass preparation.

5.2.3 Minimal Force Method Discussion

First, we considered the case of DNA's interaction with unmodified glass. Under low ionic strength conditions such as rinsing with doubly ddI water, DNA was not predicted to bind well to glass (Dederich *et al.*). Rigorous water rinses intended to prevent salt deposits readily aligned or washed away the loosely bound DNA molecules in our first attempts to deposit DNA onto glass. We turned our attention to the minute forces applied to the DNA during the deposition and rinsing steps. The smallest of lateral forces applied to DNA molecules bound to glass under low salt conditions would have most certainly pushed DNA around on the deposition surface. When DNA is moved from its original deposition conformation, the images are no longer representative of the two dimensional projection, or "snapshot" of the biological conformations present during the molecules' surface adhesion in physiological buffer.

To maximize our chances of depositing DNA onto surfaces that do not have an "irreversible" affinity for DNA (such as mica), we sought to reduce sources of minute lateral forces applied to the molecules on the surface during deposition and rinsing. To minimize lateral forces on DNA, we discovered that avoiding non-laminar flow conditions during droplet removal and sample blow drying was imperative. In solution mechanics, a Reynolds number (Re) is the ratio of inertial to viscous forces, and the Re calculation predicts the occurrence of laminar and turbulent flows as follows:

$$\mathrm{Re} = \frac{\rho \upsilon_s L}{\mu} \tag{5.1}$$

where *Re* is unitless, ρ is the solution viscosity (kg·[m·s]$^{-1}$), ν_s is the average fluid velocity (m·s^{-1}), L is the characteristic flow path (m), and μ is the solution density (kg·m^{-3}) (Reynolds,

1883). Fluidic velocities at all points in the liquid volume are undefined under turbulent flow conditions. However, under laminar flow conditions the solution velocity is lowest at distance nearest a flow path wall. Fluid flow mechanics across a flat plate are predicted to be laminar when Re is less than 1200 (Reynolds, 1883). Combining the fluid travel path over our deposition surface and the density and viscosity of water, we calculated the Re value to less than 100 when we limited the solution velocity to $1.0 cm \cdot s^{-1}$. Re values between the predicted laminar (< 1200) and predicted turbulent ($>\sim 10^5$) conditions are undefined, and not guaranteed to be laminar. Rigorous washing and/or blow drying certainly accelerated fluid velocities to levels that allowed Re values over 1200.

We found that our use of the minimal force method to deposit DNA, as in Figure 5.3, almost always prevented the alignment of the molecules in the images we captured. We realized that the observation of DNA coverage and alignment of may be one way to characterize the affinity of DNA on modified surfaces. Our standardized deposition protocol is referenced as facilitating such tests for surface hydrophobicity/hydrophilicity in section 5.3.

5.3 DNA on Smoothed Glass

5.3.1 Glass Modification Protocols

We lightly scored Corning No.1 glass cover slips with a diamond tipped scriber and segmented into approximately 1 cm^2 pieces. Latex gloves were worn at all times during glass handling and special care was taken not to touch the imaging surface. We characterized several preparation protocols for the purpose of glass modification including siloxane chemistry modifications, cleaning procedures, and polymer spin coating.

To test the hydrophilicity (more correctly, the DNA affinity) of the various glass surfaces, we deposited 10μL of 20nM 550bp DNA in physiological buffer [25 mM hepes, 10 mM sodium acetate (NaOAc), 5 mM magnesium chloride ($MgCl_2$), pH 7.8] using our standardized minimal force method. We noted the relative coverage of DNA on the surfaces, and the qualitative alignment of the molecules.

5.3.1.1 Sonication

For ultrasonic bath cleaning (sonication), we placed partitioned glass pieces in the bottom of a 500 mL beaker containing approximately 50 mL of absolute (100%) ethanol. The solution was covered, gently heated to 65°C and sonicated on high power for 60 min or more. Slides not immediately used were stored in the ethanol sonication bath. If not used within a few days, sonication was repeated before use. We noted which side of the glass faced up during sonication, as the bottom side was prone to microscopic scratching. Before DNA deposition, the slides were blown dry with a stream of N_2.

5.3.1.2 Chemical Modifications

We carried out several chemical modifications. First we briefly rinsed the newly cut glass to remove microscopic dust left by scoring with the diamond tipped scriber. Covalent attachment of a trimethylsilyl monolayer (TMS) via a siloxane bond was achieved by a liquid reaction with 10μL 1,1,1,3,3,3-Hexamethyldisilazane (HMDS). After 30 sec of HMDS incubation, the glass slides were turned sideways to allow the excess liquid to run off, leaving a uniform coating. We let the remaining thin layer of HMDS evaporate in air. We thoroughly rinsed away the unreacted HMDS with ethanol. We also tested mixtures of HMDS and 3-aminopropyltriethoxysilane (APTES) for surface modification characteristics. The identical reaction process was followed for depositions 100:1 HMDS:APTES (v/v).

5.3.1.3 Plasma Cleaning

We processed plasma cleaned slides with a table top Basic Plasma Cleaner (Harrick Plasma, Ithaca, NY). Prepared Corning No.1 slides were positioned on a standard microscope slide in the center of the chamber. We evacuated the chamber and introduced a small quantity of pure, reagent grade oxygen process gas. We sustained the plasma ignition at 100 watts for 10 to 60 sec. Plasma cleaned surfaces were kept as isolated from the environment as much as possible with covered Petri dishes. Any DNA depositions that took place subsequent to plasma preparation were carried out within minutes of plasma cleaning.

To find out if we could remove unreacted HMDS from TMS monolayer surfaces, we plasma cleaned the HMDS with oxygen for various times. We also deposited DNA onto the surfaces to indirectly determine the relative hydrophilicity.

5.3.1.4 PVK Polymer Coating

To find out if the reported flattening of glass with polyvinylcarbazole (PVK) (Rq=0.512nm) was limited by the choice of glass slide, we applied the PVK to Corning No.1 slides (Nakao *et al.*, 2002). As we show below, we chose a glass substrate that is nearly 20 times flatter than the slides Nakeo *et. al.* (2002) chose for their studies. We first rinsed the Corning No.1 glass slides with ethanol. We then spin coated 20 μL PVK (25 $mg \cdot mL^{-1}$) in dimethyl furan (DMF) at 4000 revolutions per minute (RPM) for 30 sec on a Cee® Benchtop Spin Coater from Brewer Science (Rolla, MO) at 25°C. No other modifications were made to the glass before sample deposition and AFM analysis.

5.3.2 Surface Characterization: Roughness and DNA Affinity

Surfaces, including mica and glass, often contain flaws such as raised areas, cracks, holes or debris observable with AFM. Glass surface areas of interest are those that are largely homogeneous in nature, and do not contain flaws.

We noted the lowest reproducible RMS roughness values observed for our variety of glass surface preparations as measured by the Nanoscope IIIa AFM image analysis software (Veeco Instruments, Santa Barbara, CA). We also qualitatively classified the surfaces in terms of their practical homogeneity. In many cases, exceptionally flat areas were identified with our preparation protocols, however only typical surface characteristics are reported. Table 5.1 is a summary of the RMS Rq measurements of our preparations and a description of their respective homogeneities.

In section 5.2, we described the minimal force deposition and rinsing method for putting DNA onto a glass surface while avoiding stretching or rinsing away of the molecules.

Here we characterize our surfaces with regard to their hydrophilicity at the molecular level. We deemed surfaces hydrophobic when they resisted DNA adherence while depositions were carried out with the minimal force method. The hydrophilic surfaces that did have an affinity for DNA were further classified as those that aligned DNA, and those that did not disturb the expected random orientations of the deposited molecules. Table 5.1 also summarizes our techniques' relative affinity for DNA deposited using the minimal force protocol.

Surface Modification	RMS Roughness (Rq)	Practical Homogeneity	DNA Coverage/ Orientation
None	0.254nm	NO	Moderate / Random
100% Ethanol Rinsing	0.251nm	YES	High / Random
100% Ethanol Ultrasonic Bath (1hour, 65°C)	0.151nm	YES	High / Random
O_2-Plasma Cleaning (20s Exposure)	0.248nm	YES	Moderate / Random
O_2-Plasma Cleaning (60s Exposure)	0.160nm	NO	High / Random
HMDS Liquid Reaction	0.201nm	YES	None / N/A
HMDS:APTES (100:1) Liquid Reaction	0.741nm	NO	N/A
Polyvinylcarbazole Spin Coating	0.543nm	NO	N/A
Combined Procedures			
HMDS/O_2-Plasma Cleaned – (20s Exposure)	0.130nm	YES	Low / Aligned
HMDS/O_2-Plasma Cleaned – (60s Exposure)	0.155nm	NO	Moderate / Random
EtOH Sonication/O_2-Plasma – (20s Exposure)	0.154nm	YES	Moderate / Random

Table 5.1 Summary of Methods that Smoothed Corning No.1 Glass Cover Slips. The surface roughness (Rq) and practical homogeneity of the respective protocols are reported. The degree of DNA coverage is reported as Low (1-2 molecules/1 μm^2), Moderate (5-20 molecules/ 1 μm^2) or High (>20 molecules/1 μm^2). The orientations of the DNA are reported as aligned or random. Each type of surface modification was repeated with a DNA deposition attempt at least 4 times (N=4). PVK and HMDS:APTES protocols were not pursued for DNA deposition characteristics.

5.3.2.1 Corning No1. Out-of-the-Box

We found that Corning No.1 glass cover slips were genuinely flat; the RMS roughness of the glass slides out-of-the-box was 0.254 nm (Figure 5.4a). Corning No.1 briefly rinsed with absolute ethanol contained isolated areas with Rq locally below 0.180 nm, although these results were not typical. We found that a series of three rinses with absolute ethanol removed a significant population of inhomogeneities, probably due to debris removal rather than structural modification. We noticed no marked improvement in Rq in comparing the homogeneous areas of the rinsed and non-rinsed out-of-the-box samples.

5.3.2.2 Sonication

We noted that sonication in absolute ethanol at 65°C for 60 min flattened glass extensively (Figure 5.4b). The Rq of the sonicated surface was improved to 0.151 nm; about 40 % smoother than the unprocessed glass.

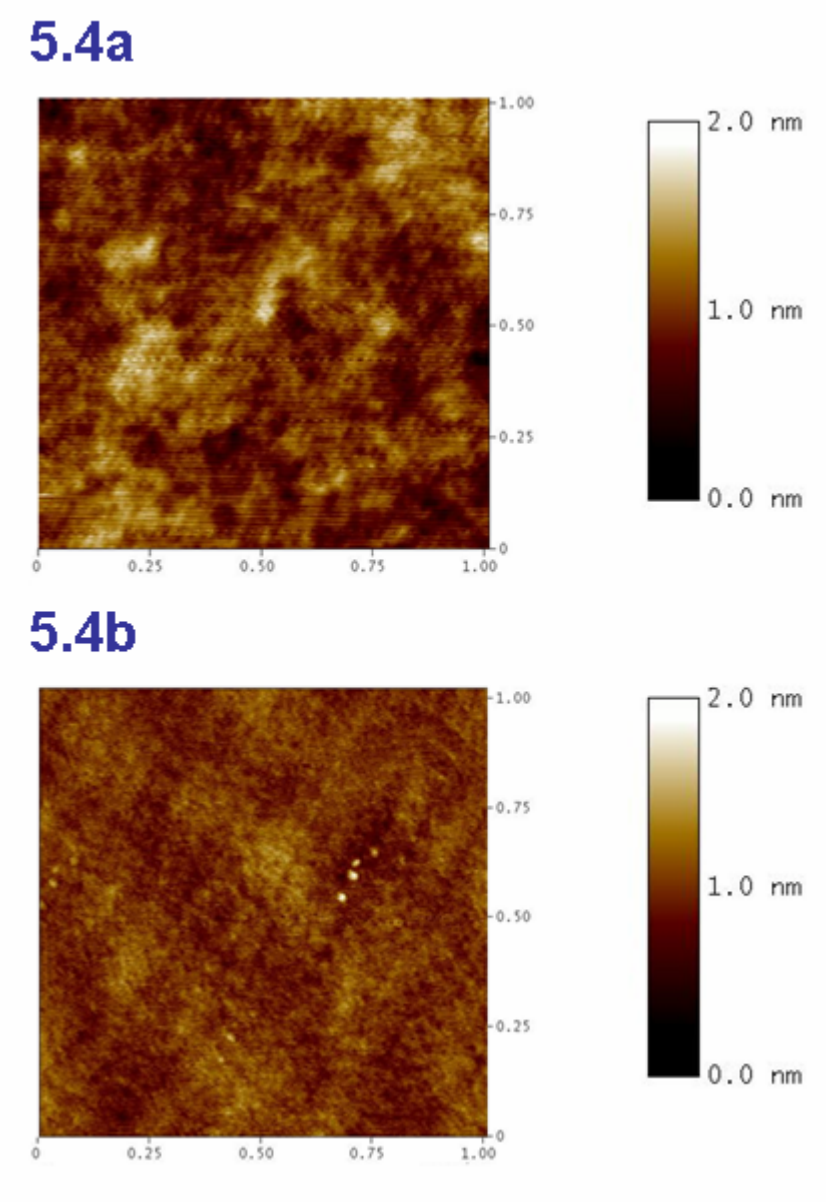

Figure 5.4. The Nanoscale Surface Effect of Sonicating Corning No.1 in Absolute Ethanol. The image in 5.4a is a 1 μm^2 AFM image of a Corning No.1 cover slip that has been briefly rinsed with absolute ethanol. Figure 5.4b a 1 μm^2 AFM image of Corning No.1 that has been sonicated in absolute ethanol for 60 min at 65°C.

5.3.2.3 Plasma Cleaning

We observed that oxygen plasma cleaning Corning No.1 for short times (circa 20 sec) at 100 W did not noticeably modify the structure of the glass surface (Figure 5.5a). The Rq value was only decreased to 0.248 nm. With extended oxygen plasma exposure, the surface contaminates were removed with about the same effectiveness as ethanol sonication, and we found Rq values locally as low as 0.160 nm. During the longer exposures, more obvious physical changes took place, as shown in Figure 5.5b. The glass was covered with tall stalagmite-like structures. The extended exposure slides were so severely damaged we could not locate homogeneous areas with low Rq. Figure 5.5c is a 3-D view of the stalagmite like structures created on glass by extended O_2-plasma exposure.

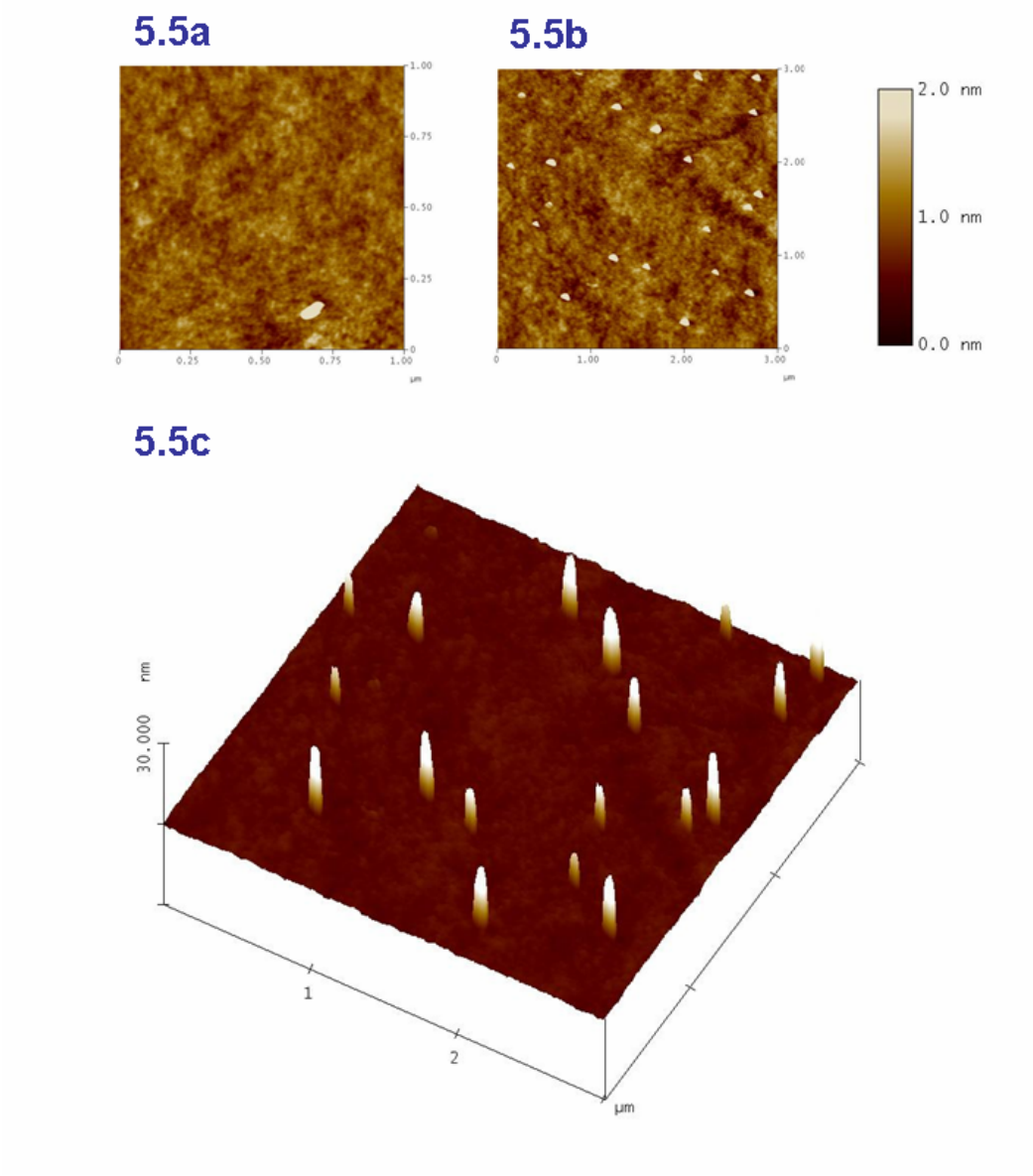

Figure 5.5 Surface Heterogeneity Appears with Longer O_2-Plasma Cleaning Exposure. In 5.5a, a piece of Corning No.1 has been rinsed with ethanol, and plasma cleaned with O_2 process gas at 100 W for 20 seconds. Figure 5.5b shows the effect of a 60 second plasma exposure. The heterogeneity in the form of stalagmite-like structures is obvious in the 60 second exposure as seen in the 3-D rendering of the data in 5.5c.

5.3.2.4 PVK Polymer Coating

We observe that spin coated Corning No.1 with PVK produced a surface Rq of 0.543 nm; nearly twice that of the unmodified glass cover slips. In PVK coated Corning No.1 we noticed several regions with large inhomogeneities in the form of holes, ranging from several nanometers to a few micrometers in diameter. Figure 5.6 is an example of the heterogeneities often found on PVK-spin coated Corning No.1 imaged by AFM.

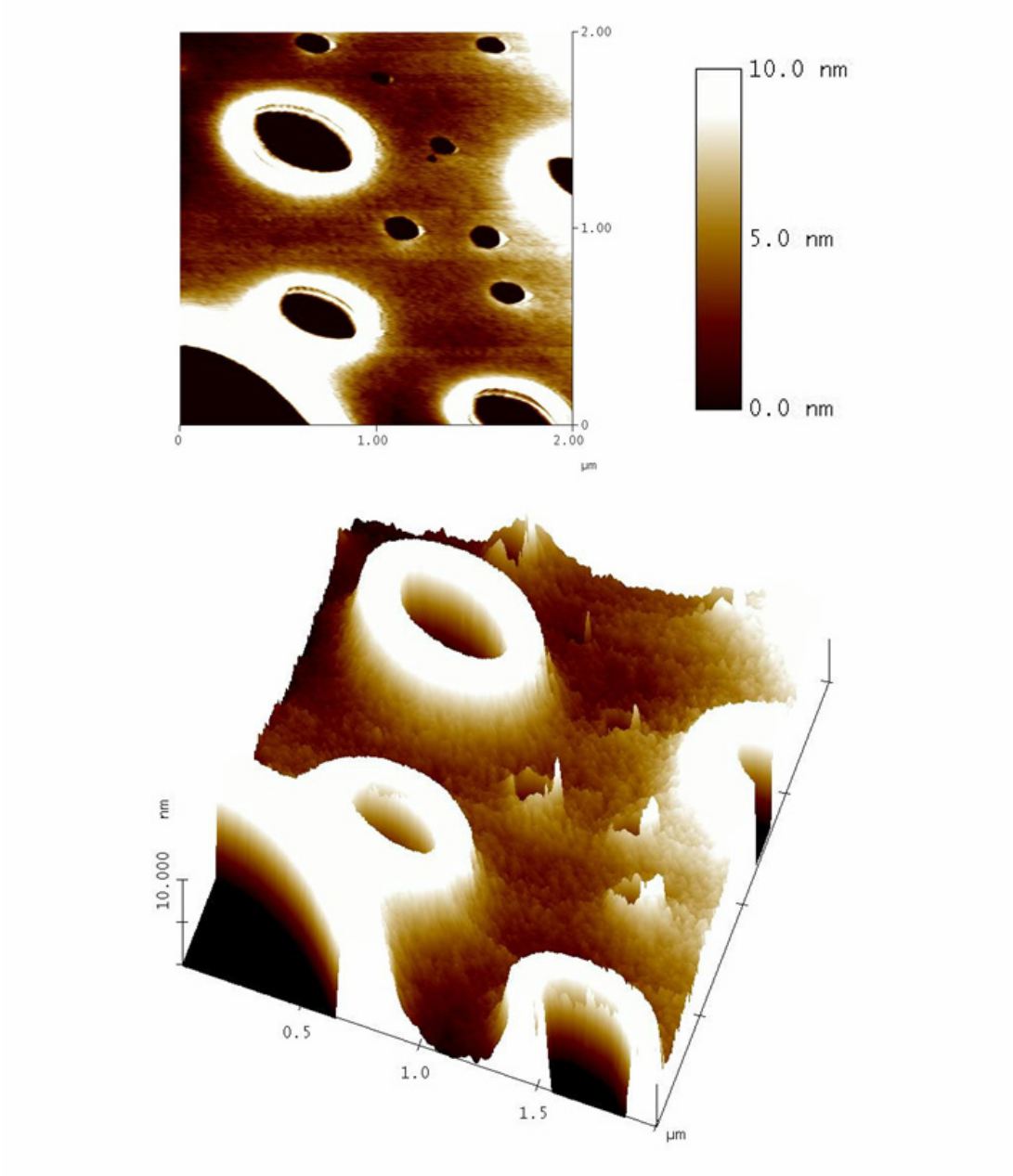

Figure 5.6 Spin Coated PVK on Corning No.1 is Very Heterogeneous on the Nano-Scale. Above is a 1 μm^2 AFM topography image of Corning No.1 that we spin coated with PVK (25 $mg \cdot mL^{-1}$) in DMF at 4000 rpm for 30 sec. The result was a surface with many heterogeneities, and Rq values of 0.541 nm; higher than that of the glass alone. The bottom image is a 3-D view of the surface accenting the geometry of the obscure heterogeneities.

5.3.2.5 Chemical Modifications

We showed that the covalent binding of a trimethylsilyl (TMS) monolayer to Corning No.1 via a liquid reaction with HMDS reduced the Rq of the surface to 0.201 nm – without prior sonication. Noticeably, glass that we modified with HMDS was almost entirely homogeneous. HMDS applied to ethanol sonicated glass possessed nearly identical surface homogeneity and Rq. However, DNA did not stick to the HMDS glass whatsoever. In the combined HMDS/APTES liquid deposition, we observe surfaces covered with aggregate islands (Figure5.7). The surfaces were not tested for DNA affinity.

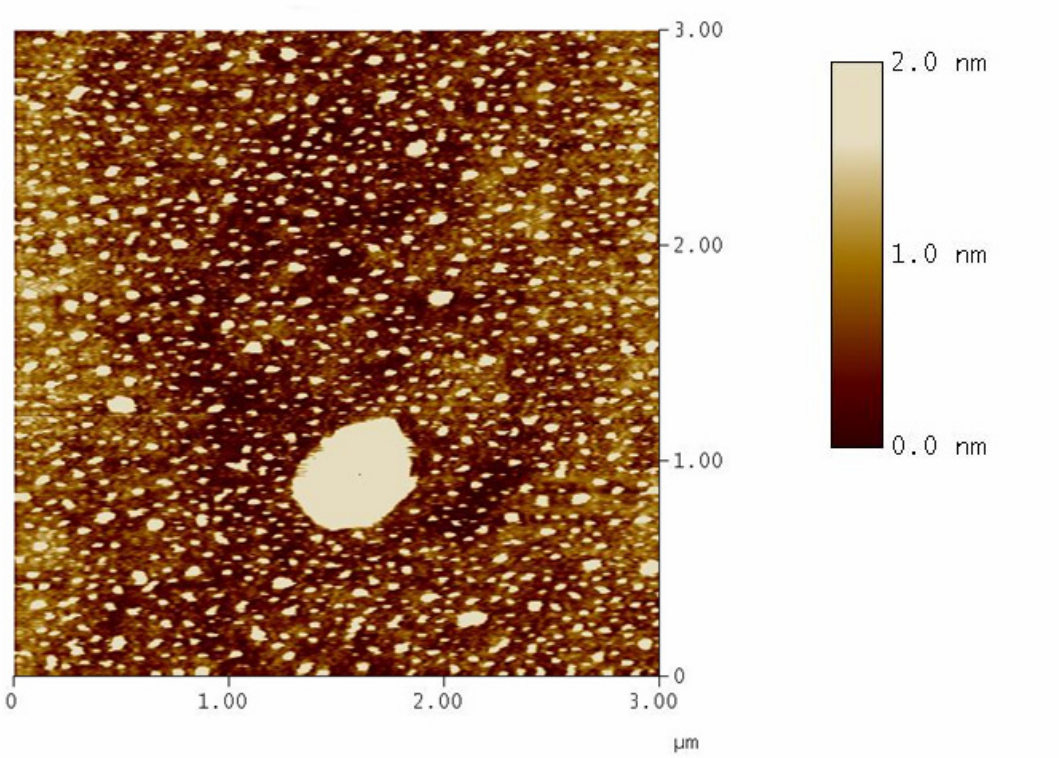

Figure 5.7 Liquid APTES and HMDS are Microscopically Insoluble. Shown here is 1 μm^2 AFM of a 100:1 HMDS:APTES liquid reaction on ethanol sonicated glass. The lighter colored are islands are taller structures, likely the effects of liquid HMDS-APTES insolubility.

5.3.2.6 O_2-Plasma Cleaned TMS Monolayers

We noted that O_2-plasma cleaning of HMDS treated glass altered the properties of the surfaces extensively. To the chemically modified glass, 20 sec of O_2-plasma exposure produced a very heterogeneous surface Rq of 0.130 nm (Figure 5.8a). We observe that DNA had an affinity for the HMDS coated surface, where as the non-plasma cleaned glass did not. The DNAs were very aligned however, and they sparsely covered the surface. We occasionally discovered examples of HMDS-O_2-plasma exposed glass that had roughness as low as 0.088 nm; nearly as flat as mica (0.050 nm).

Longer, 60 sec plasma exposures of HMDS glass (Figure 5.8b) bound DNA with much higher affinity; the surface coverage was more than doubled, and the DNAs were not aligned. The surface was heavily degraded though. We also observed some evidence of stalagmite surface heterogeneity. We observed an Rq of 0.155 nm in the rarely found heterogeneous spots in Figure 5.8b.

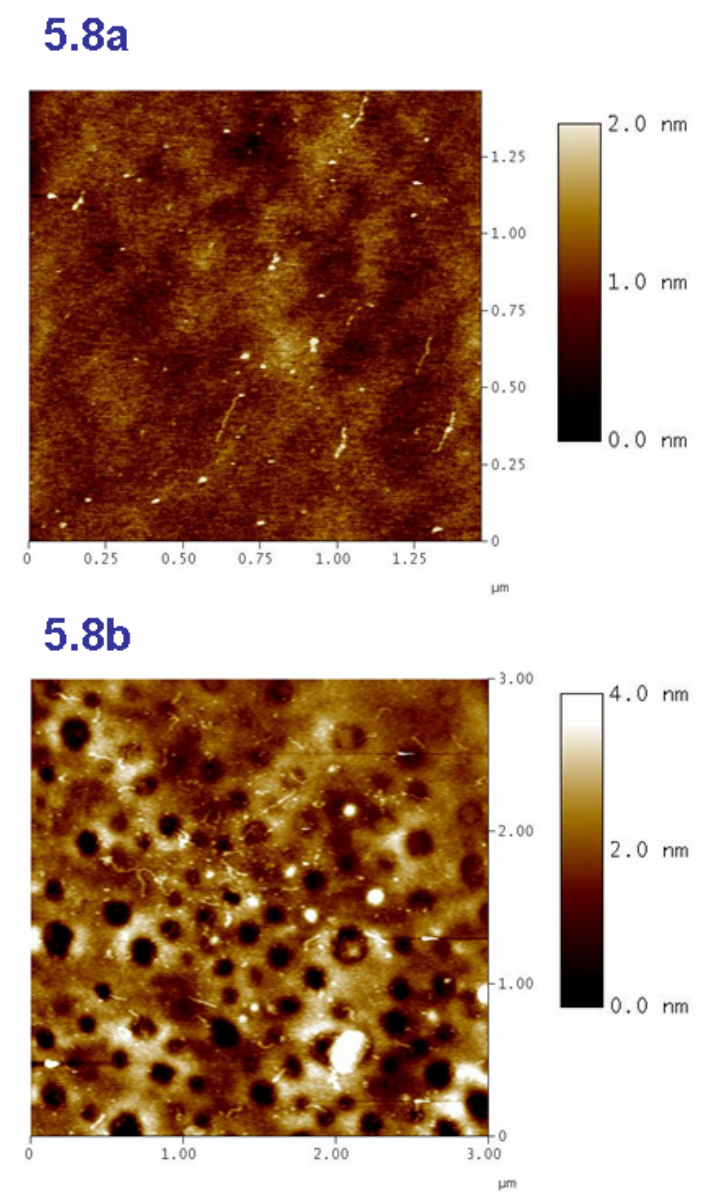

Figure 5.8 TMS Monolayers on Glass are Drastically Changed with Increasing Exposure to O_2-Plasma. Corning No.1 glass was reacted with liquid HMDS and plasma cleaned with oxygen. The image in 5.8a shows a 1.5 μm^2 area of a 20 sec plasma exposed HMDS glass sample, and 5.8b shows a 3 μm^2 area of HMDS glass that was oxygen plasma cleaned for 60 sec. The DNA bound to the short exposure glass is much more aligned than that in the longer exposure. Obvious degradation occurred during the longer exposures as well.

5.3.2.7 Combined Cleaning

We noted that ethanol sonication followed by 20 sec of O_2-plasma exposure produced surfaces comparable to those sonicated alone with an Rq value of 0.154 nm. However, a greater number of contained large homogeneous areas as compared to sonicated of plasma cleaned alone cleaning techniques.

5.3.3 Discussion of Glass Surface Preparations

There are several commercially available glass cover slips, each of them containing different physical and chemical properties depending on their production processes. For example, work has been published recently outlining several protocols for the ultrasonic bath cleaning of standard glass microscope slips from Erie Scientific (Portsmouth, NH) (Liu *et al.*, 2007). Liu *et. al.* (2007) suggest that an ultrasonic bath with 95 % methanol can remove surface impurities from the glass, and produce root mean squared (RMS) roughness (Rq) values as low as 0.46 nm. However, work from 1993 suggests that Corning No.1 glass cover slips are remarkably flat out of with box (Allen *et al.*, 1993). Allen *et al.* (1993) report that after a brief rinse with 95 % ethanol or distilled water to remove large bumps and other contaminants, the local (500 nm^2 area) roughness of Corning No.1 can be as low as 0.151 nm.

Corning No.1 glass cover slips are 0.13 to 0.16 mm thick and are made from drawn Corning No.0211 zinc titania glass. Corning No.1 is *not* of the float glass variety; due to the production method of float glass, it has different chemical compositions on each side. The optical transmission for Corning No.1 cover slips from 350 to 2500 nm is greater than 90 %, These glass slides are rigid, they can be cut, and handled with ease in comparison to mica which may fracture or break when unsupported. We selected Corning No.1 for our experiments, as it is an ideal candidate for AFM-SMF.

We found that rinsing with ethanol did not *typically* reduce the Conring No.1 Rq to the levels previously reported (Allen *et al.*, 1993). Differences may be attributed to any changes in Corning No.1 production over the last 10 years. Alternatively, it is possible that the reported area by Allen *et. al.* was a local anomaly on the glass. We did not observe

surfaces on Corning No.1 with Rq values much below .20 nm with any regularity. We did, however, find that ethanol sonication at 65°C for 60 min exposed flat surfaces similar to those reported by Allen *et. al.* Our findings suggested that while the slides were relatively flat as shipped, there were microscopic structures and/or debris particles on the glass that were removable by physical means.

Plasma cleaning with reagent grade O_2 process gas can modify objects chemically and physically. Oxygen plasma is created by evacuating a chamber (< 1 torr), introducing a low pressure of O_2 and subjecting it to a GHz frequency electric field to ionize the gas and accelerate the charged particles. Thermal electrons at around 1100 eV (electron volts) and oxygen radicals produced in the plasma field able to react with the glass and contaminate chemistry. The fast moving particles also collide with the surface to desorb loose structures via kinetic energy transfer. In our experiments, as particles were removed from the glass, the surface energy was increased which invited the DNA to stick irreversibly.

Surface temperatures of objects exposed to a plasma ignition presumably rise with exposure time; the constant bombardment may etch or alter the substrate. Our multiple observations of surface degradations were likely related to thermal events that increased with plasma exposure time.

We found that spin coating PVK onto Corning No.1 yielded approximately the same result as spin coating onto glass with 20 fold greater Rq, as reported in the literature (Nakao *et al.*, 2002). This suggested that the polymer formed a layer thick enough to cover the topography of the underlying glass, and that the imaging surface was unique to the PVK and not the glass. We were able to produce many surfaces similar to those imaged by Nakao *et al.* (2002) which showed DNA stretched onto the glass. While we found it possible to find

suitable areas for DNA imaging, the large population of inhomogeneities combined with the high Rq values produced by PVK coatings mandated that other avenues for substrate preparation for biological AFM-SMF be perused.

We discovered that a liquid deposition of HMDS flattened Conring No.1 slide extensively. It is possible that crevasses and recesses in the glass were "filled in" by the methyl groups might have laid somewhat flat on the glass surface. Alternatively, the TMS monolayer may have created a hydrophobic "tarp" over the surface, where bumps and small contaminates were smoothed over. Regardless of the mechanics of smoothing, HMDS treatment proved to be a viable method for glass modification and warranted further investigation. The slight rise in Rq over that of sonicated glass suggested unreacted HMDS might have remained networked to the surface though hydrophobic interactions. The removal of free HMDS by plasma cleaning will be discussed.

APTES has been used by previously to enhance mica's hydrophilicity for the binding of DNA (Lyubchenko *et al.*, 1993). Since the goal of this work was to not only smooth glass, but also bind DNA to the surface, a completely hydrophobic TMS monolayer would likely not do. The liquid deposition of HMDS mixed with 1% APTES to create a multi functional monolayer was investigated. As seen in Figure 5.7, it is probable that the microscopic solubility differences between the reagents inhibited the liquid deposition of a homogeneous monolayer. It is our belief that the islands observed in Figure 5.7 are actually aggregates of either HMDS or APTES. Possible solutions to this phenomenon are discussed in the future directions at the end of this chapter.

We chose O_2-plasma cleaning to remove free HMDS from TMS monolayer surfaces for several reasons. First, the low chamber pressure would allow the volatile, loosely bound

HMDS to be removed quickly. Additionally, O_2-plasma cleaning increases the surface energy of objects during contaminant removal. Since TMS monolayers are extremely hydrophobic (Ebenstein *et al.*, 2002) and completely resistant to DNA binding, we thought plasma cleaning might serve to activate the surface and increase DNA affinity. Our result was the discovery of a preparation protocol that produced flatter glass surfaces than found elsewhere in the literature. We were able to deposit some DNA onto the surface, which allowed us to conclude that the surfaces were somewhat more hydrophilic than TMS layers not exposed O_2-plasma 5.8a. The surface activation was evident in Figure 5.8b by the higher coverage of DNA and the resistance to alignment during minimal force rinsing.

5.3.4 Glass Surface Preparation Conclusions

In general, we felt that two of the methods described above for smoothing glass warranted further investigation into their DNA binding attributes: ethanol sonication, and combined liquid HMDS reactions with O_2-plasma cleaning. The simplest protocol was ethanol sonication. Not only was the preparation trivial, it presumably left the glass surface as hydrophilic as it was before the procedure. Applying a TMS monolayer via a reaction with HMDS inherently coated the surface with hydrophobic methyl moieties. We think that oxygen plasma cleaning may have helped to remove excess HMDS residue and increased the propensity for bind DNA. While we were able to remove the excess HMDS to flatten the surface, we could not activate the surface to bind DNA irreversibly before degrading the surface. Ethanol sonication was the most efficient and logical protocol we identified for preparing glass conducive to probing biological systems with AFM and SMF.

5.4 The First High Resolution AFM Images of Unstretched Protein-DNA Complexes Deposited onto Smoothed Glass under Physiological Conditions

In this chapter, we have outlined detailed, successful protocols for smoothing glass that facilitated the imaging of single biological constructs with atomic force microcopy. Our investigation of surface-DNA interactions has lead to the development of a deposition procedure that tends not to stretch or remove DNA from the glass once it has come to rest. The primary goal of this work was to enable the imaging of multimeric complexes on a surface compatible with both high resolution AFM and SMF techniques. Corning No.1 glass cover slips are commonly used for fluorescence studies and were logically chosen for this work with AFM. We wanted to obtain the first high resolution oscillating mode AFM image of protein-DNA complexes deposited under physiological conditions onto smoothed Corning No.1.

RNA Polymerase (RNAP) from *E.coli* is homologous to eukaryotic RNAP II, which is primarily responsible for the synthesis of mRNA from genomic DNA (Sweetser *et al.*, 1987). During the elongation phase of transcription, several cofactor proteins play significant roles in the regulation of RNA transcription. Characterizing the structure function relationships of multimeric transcription elongation complexes would provide much insight into one of the key steps in the central dogma of biology. A number of studies have been published that involve AFM imaging of transcription complexes (Sweetser *et al.*, 1987). Before complicated transcription processes can be studied via combined microscopy however, it was necessary to prove that RNAP-DNA complexes could be deposited onto a smooth glass surface under physiological conditions, and that their individual structures could be identified with AFM.

5.4.1 Sample Preparation

Prior to the initiation phase of RNA synthesis, open promoter complexes (OPCs) are formed when RNAP binds to a specific promoter sequence on template DNA. To 10nM 550 bp DNA containing a promoter sequence (a high salt buffered solution of 25 mM hepes, 10 mM NaOAc, 5 mM $MgCl_2$, pH 7.8), 20 nM RNAP (holoenzyme containing σ) from *E. coli* was added. The DNA-protein mixture was incubated at 37°C for 10 minutes to maximize OPC formation. After the solution was allowed to return to room temperature, 10 μL of the OPC mixture was deposited onto a section of Corning No.1 glass cover slip that had been sonicated in ethanol for 1 hr at 65°C. The deposition droplet was allowed to incubate on the glass surface for approximately 30 seconds before removal via the minimal force method. Three minimal force rinses with ddI H_2O were conducted to ensure the prevention of salt. Residual moisture was dried from the sample with a very light stream of N_2. The glass sample was fixed to the imaging piezo of our Digital Instruments Nanoscope IIIa (Santa Barbra, CA) atomic force microscope. Both topographic and phase (see section 4.5.2) images were captured of homogeneous areas in the imaging surface.

5.4.2 Results

We show the first high resolution AFM images of unstretched protein-DNA complexes deposited onto smoothed glass under physiologically relevant buffer conditions are in Figure 5.9a. Figure 5.9b is a 3-D topographic rendition of the OPCs deposited onto glass. In our OPC images on glass, the DNAs are unaligned, and the RNAP surface coverage is quite high. We observe several examples of protein DNA complexes in Figure 5.9.

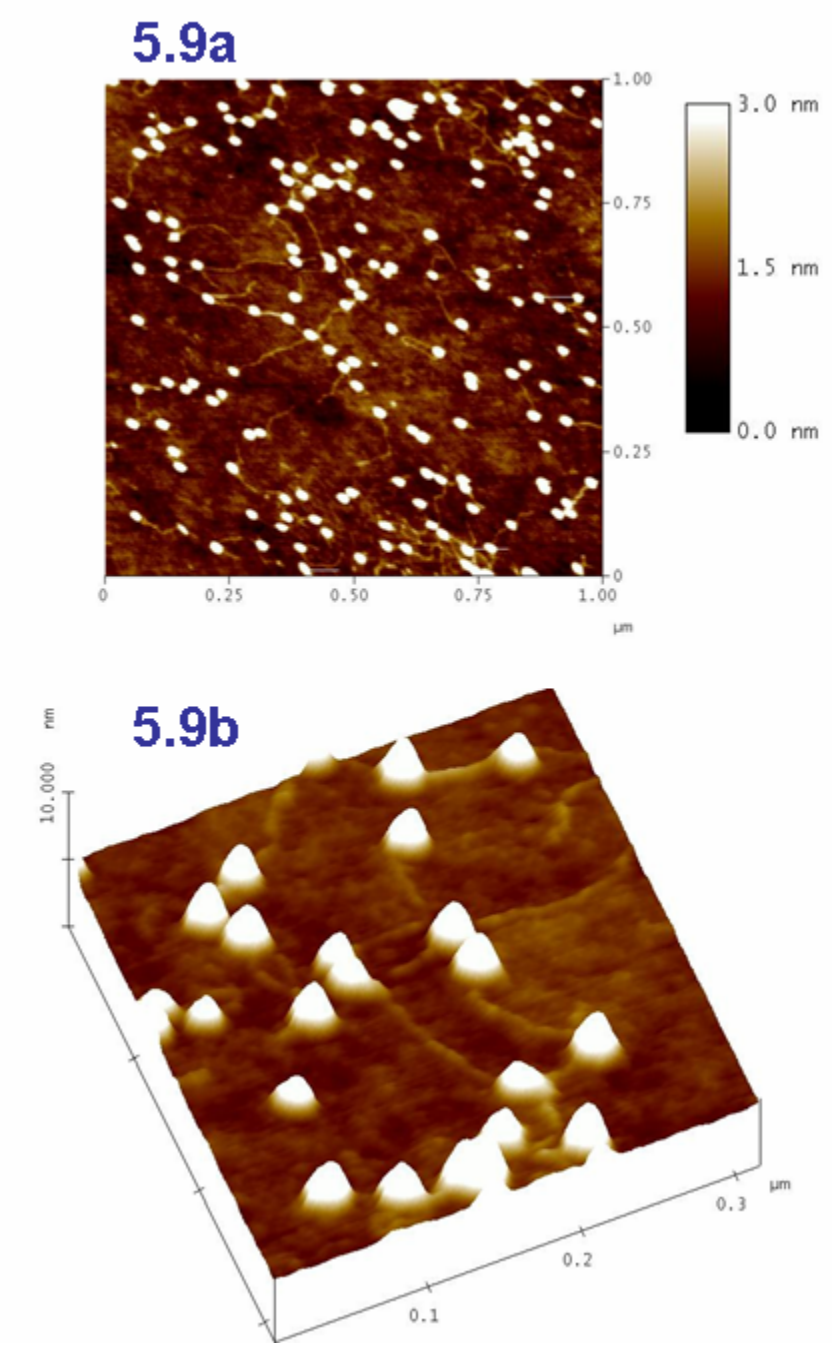

Figure 5.9 The First High Resolution AFM Images of Protein-DNA Complexes Deposited onto Smoothed Glass Under Physiological Condition. Figure 5.9a is a 1 μm^2 oscillating mode AFM image. We have rendered topography in 3-D in Figure 5.9b, and zoomed-in to ~300 nm^2. The light colored bumps are RNAP, the yellow/orange colored structures are DNA, and the glass background is dark brown.

5.4.3 Discussion

We conclude that that several of the transcription complex experiments from the literature could have been performed on glass. Specifically, the structural molecular recognition quality is comparable to similar published AFM images of OPCs on mica (Rees *et al.*, 1993; Guthold *et al.*, 1994; Rippe *et al.*, 1997; Schulz *et al.*, 1998). The ability to collect high quality images of transcription complexes on smoothed glass will undoubtedly lead to a myriad of new AFM-SMF experiments and a much deeper understanding of the structure-function relationships of multimeric transcription complexes.

5.5 Topics Unique to AFM on Glass

The study of multimeric biological complexes with combined atomic force microscopy (AFM) and high resolution single molecule fluorescence (SMF) can be brought one step closer to reality by employing smoothed glass for practical use in biological AFM. In support of our AFM-SMF goal, we discuss here a few topics that are unique to oscillating mode AFM imaging on smoothed glass. These topics include the problem of static charge build up with glass imaging in air, the advantage of using phase imaging on glass surfaces, and the future of glass preparation protocols.

5.5.1 A Growing Problem: Static Charges Can Accumulate with Oscillating AFM on Glass

We commonly observed that AFM imaging on glass in oscillating mode could be intermittently unstable (Figure 5.10), probably due to a static charge build up between the insulating glass surface containing mostly silica -$(SiO_2)_n$- and silicon (Si) tip. Within 10 to 30 seconds of tip engagement, the cantilever had vibrated millions of times, and an electrostatic attraction between the probe and the glass may have begun to manifest itself in the false color image relayed to the screen. We often noticed as increase in image noise as the tip was slowly pulled toward the surface.

In Figure 5.10, shown on the left and the right are the same 1.0 μm^2 areas of Corning No.1 rinse in ethanol were scanned at 3Hz at a constant drive amplitude of 25 mV. On the left, we began scanning at the bottom of the image at a rate of 3 Hz, at the lowest practical drive amplitude that produced an image. As a presumptive electrostatic charge drew the cantilever toward the surface with greater force, the tip began to crash. At the start of the 6 min of imaging shown here, the drive amplitude was sufficient to keep the probe in

intermittently contact with the surface. By the end of the scan (Figure 5.10, right), the tip was essentially scraping the surface, probably damaging the probe.

We discovered that raising the amplitude of tip oscillation (drive amplitude) caused imaging to enter repulsive mode. Repulsive mode implies that the some of the energy required to drive the cantilever's pendulum motion is needed to push the probe toward the surface. In attractive mode, the energy provided by the drive amplitude is partially going into pulling the probe away from the surface. In attractive mode, if the drive amplitude is too low, the tip can crash into contact with the surface. When an unchallenged electrostatic charge was allowed to overcome the drive amplitude in attractive mode, imaging as seen in Figure 5.10 was typical.

Unfortunately, using higher than normal drive amplitudes can distort data by physically squashing soft biological molecules due to increased forces tip-sample energy transfer; in order to vibrate the cantilever at a constant frequency with greater amplitude, the pendulum velocity of the cantilever must increase. Therefore, the momentum transferred from the probe to the sample is higher. As a rule of thumb, we suggest that one uses lowest drive amplitude required for effective repulsive mode imaging whenever possible. For the sake of biological structural integrity, the growing attractive forces should only be address when they appear.

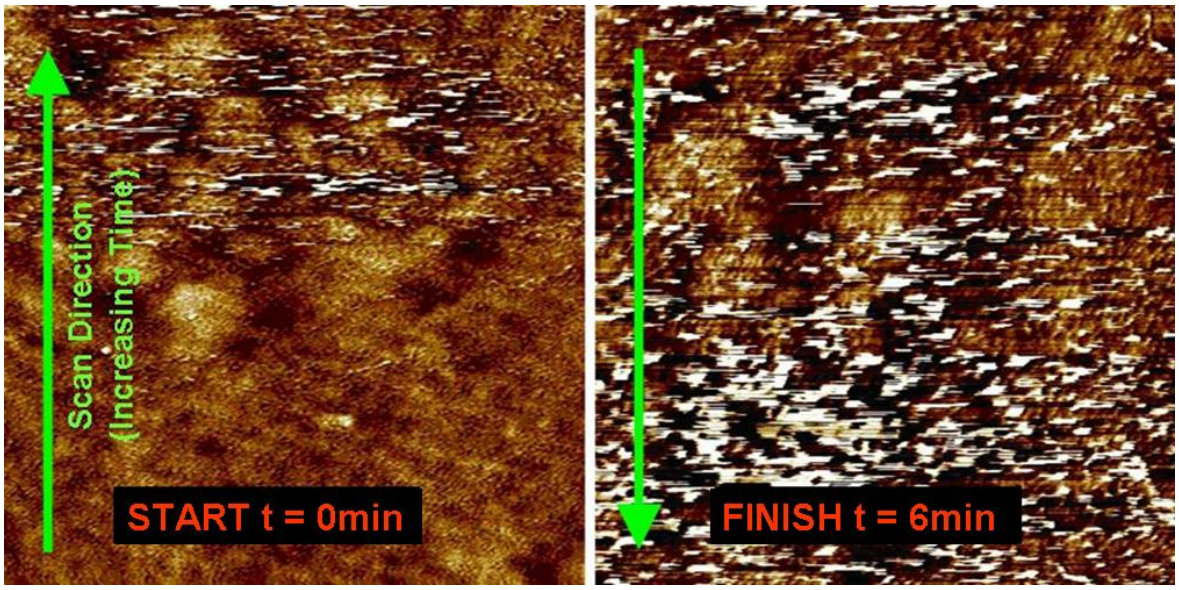

Figure 5.10 An Electrostatic Build Up Between Tip and Surface can be Deleterious to AFM Imaging on Glass. The image on the left is a 1 μm^2 scan of glass that has been ethanol sonicated, scanned from bottom to top. A low drive amplitude (~25 mV) was held constant during scanning. The image on the right is the same area, scanned consecutively from top to bottom.

5.5.2 Phase Imaging: Seeing Samples Differently

In oscillating mode AFM, a flexible cantilever is vibrated at its resonant frequency. The amplitude of tip oscillation is monitored by reflecting a laser beam into a position sensitive diode. As the tip encounters structures on an imaging surface, the oscillation amplitude is clipped. A feedback loop keeps the amplitude constant by moving the stage in the z-direction, and the z-movement is plotted versus x-y position to generate a false color image of the scanned surface topography. The cantilever drive frequency is held constant during oscillating mode AFM. However, changes in the phase of the cantilever oscillation can be related to the intermolecular interactions between tip and sample. During drive voltage tuning, the cantilever's phase is arbitrarily set to zero in air. As the tip approaches the scanning surface, a shift in this phase is observed. As the tip is scanned across a homogeneous surface (no sample deposited), the phase changes very little as the surface topography changes. In the same way that false color images are produced by plotting measuring z-stage movement, the phase shift of cantilever vibration can be plotted versus x-y probe position. Phase data, is in theory, independent of homogeneous topography and z-stage movement.

When imaging homogeneous samples in practice, the phase response plotted versus x-y tip position will closely resemble topographic images due to the minute changes in phase with amplitude clipping. However, when an object on the surface is encountered comprised of material other than that of the surface background, the intermolecular forces between the tip and sample change; the differences in the attractive and repulsive forces manifest themselves as changes in phase. What is most useful is that phase imaging is much more sensitive to sample electrostatic heterogeneity than small changes in topography. With phase

imaging, a dip or bump in the surface topography will likely not be as noticeable as a deposited protein or a hole in a thin film that exposes a different material.

5.5.2.1 Phase Imaging on Glass

Phase imaging can be used to "see" things that cannot be seen in topographic images. The capabilities of phase imaging are seen in the literature, facilitating the capture of DNA in surfaces far to rough to see complete DNA molecules topographically (Kwak *et al.*, 2002). Pulsed force mode (PFM-AFM) can also be used to assay the interaction of tip and surface at every x-y pixel position (Kwak *et al.*, 2003), however, phase imaging does a similar duty with much higher throughput and sample invasion.

5.5.2.2 Our use of Phase Imaging on Glass

In this work, the images on the right in Figures 5.11a and 5.11b are the simultaneously generated phase modulation plots of the same topography captured on the left. In both examples, phase data reduced the apparent heterogeneity of the of the glass substrate background, as phase imaging on detected changes in the tip-sample interactions, in theory. Both images show that DNA can be effectively imaged with phase mode AFM on glass where DNA molecules are sometimes undetectable in height mode. Additionally, the identification of RNAP in 5.11b was easier to that in the height mode where debris on the surface could sometimes be mistaken for protein.

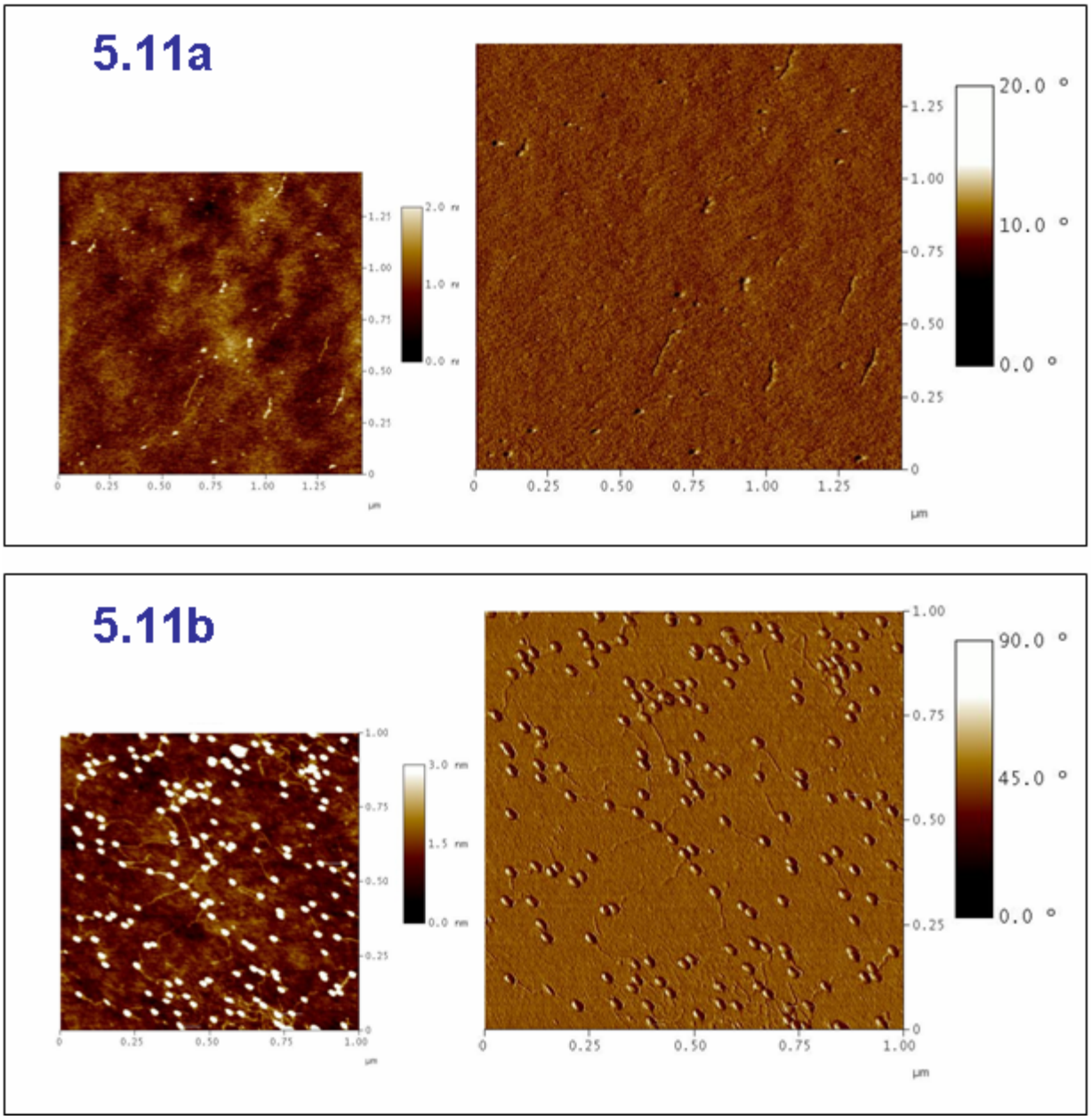

Figure 5.11 Phase Imaging with AFM Selectively Reveals Biological Constructs and Not Background topography. In 5.11a, DNA deposited onto HMDS/O_2-plasma glass is shown on the left (small) in height AFM (topography) mode, and in phase mode on the left. Similarly, the images in 4.11b are topography (left, small) and phase (right, large) of OPCs deposited onto sonicated glass using the minimal force method.

5.5.2.3 The Future Use of Phase Imaging on Glass

With the capability to "filter" out topographic noise of the glass background, the conformations of proteins and DNA could be more easily characterized. Phase data cannot be substituted for actual topographic height, making volume analysis by AFM not possible with phase images. However, some of the structural attributes of single biological molecules and complexes can be supplemented with the aid of phase AFM. While glass will likely not be made as smooth as atomically flat mica any time soon, the use of phase imaging with glass will help capture much of the same quality information.

The phase data captured with the instrument are not much more than qualitative. Veeco, the suppliers of our Digital Instruments Multimode Nanoscope IIIa AFM, make no claims that the phase shift data captured with their instruments vary linearly with the actual repulsive and attractive forces between tip and surface. Our newly acquired MFP-3D^{TM} instrument from Asylum, however, has phase and force mode capabilities that may allow us to more quantitatively characterize attractions and repulsions between tip and sample. It would be interesting to see if proteins with different surface electrostatics can be discriminated with the MFP-3D^{TM}.

5.5.3 The Future of Glass Preparation Protocols

In Figure 5.8a, we show DNA deposited onto a TMS monolayer that had been plasma cleaned. Its Rq is 0.130 nm; examples of lower glass Rq cannot be found elsewhere in the literature. However, the minimal force deposition method could not reduce the alignment of DNA molecules enough to characterize the structure-function relationships of DNA conformations on HMDS-O_2-plasma cleaned glass. Yet, proteins with hydrophobic surfaces

may readily stick to the ultra-flat HMDS-O^2-plasma surfaces. Molecular stretching is not as much of an issue with proteins alone. Multimeric protein assemblies may be more easily characterized via AFM-SMF on HMDS-O_2 plasma glass than any other surface.

Approaches have been explored that incorporate the gas phase deposition of mixed monolayer reagents that put some percentage of hydrophilic and hydrophobic groups onto a glass surface (Kwak *et al.*, 2003). Gas phase HMDS and APTES reactions with Corning No.1 glass cover slips might yield surfaces that are more homogeneous that we find (Figure 5.7). If further investigations with multi-component monolayers combined with plasma cleaning on Corning No.1 provide glass that is ultra flat with decreased hydrophobicity, perhaps the structure-function characteristics of complexes containing DNA could more efficiently probed with AFM-SMF.

Lastly, there may be ways to employ plasma cleaning without the deleterious affects to glass (Figure 5.5) and monolayer (Figure 5.8) homogeneity at the nanoscale. O_2-plasma cleaning modifies surfaces chemically with reactive oxygen radical ions, and thermal via the physical particle bombardment. Since O_2-plasma cleans a surface physically and chemically, the mechanism of TMS monolayer alteration in our work was unclear. Alternative plasma cleaning process gases such as inert Argon (Ar) will act on the surface via thermal mechanisms only because significant populations of reactive radical species are not produced in Ar-plasmas. Characterizing the effects of Ar-plasma cleaning on glass should be done if a wider variety of glass surfaces are desired for AFM-SMF.

5.5.4 The Future of AFM on Glass

With the issues we addressed in this chapter, the only step remaining to perform combined microscopy is image alignment. Our work has shown that good quality images can be taken of proteins and DNA deposited on smoothed glass in lieu of mica. Our lab has recently acquired a MFP-3D^{TM} stand alone AFM from Asylum Research (Santa Barbara, CA) that can be place directly on top of an inverted total internal reflectance fluorescence (TIRF) microscope. In this configuration, alignment of AFM and SMF data will be made easier (and near simultaneous), and work can be made towards a FRET-AFM. The use of our robust sample deposition protocol on glass will greatly aid in the assembly of the combined AFM-SMF microscope designs.

BIBLIOGRAPHY

Allen, M. J., X. F. Dong, T. E. O'Neill, P. Yau, S. C. Kowalczykowski, J. Gatewood*, et al.* (1993). "Atomic force microscope measurements of nucleosome cores assembled along defined DNA sequences." Biochemistry **32**(33): 8390.

Bensimon, A., A. Simon, A. Chiffaudel, V. Croquette, F. Heslot and D. Benisimon (1994). "Single Molecule Analysis of DNA Replication by Molecular Combing." Science **265**(9): 2096.

Binnig, G., C. F. Quate and C. Gerber (1986). "Atomic Force Microscope." Phys Rev Lett **56**: 930.

Bustamante, C., D.A.Erie and D. Keller (1994). "Biological and Structural Applications of Scanning Force Microscopy." Curr Opin Struct Biol **4**(5): 750.

Dederich, D. A., G. Okwuonu, T. Garner, A. Denn, A. Sutton, M. Escotto*, et al.* "Glass Bead Purification of Plasmid Template DNA for High Throughput Sequencing of Mammalian Genomes." Nucleic Acids Res. **30**(7): 5.

Ebenstein, Y., T. Mokari and U. Banin (2004). "Quantum-Dot-Functionalized Scanning Probes for Fluorescence-Energy-Transfer-Based Microscopy." J. Phys. Chem. B **108**(12): 93.

Ebenstein, Y., E. Nahum and U. Banin (2002). "Tapping Mode Atomic Force Microscopy for Nanoparticle Sizing: Tip-Sample Interaction Effects." Nano Letters **2**(9): 945.

Erie, D. A., G. Yang, H. C. Schultz and C. Bustmante (1994). "DNA Bending by Cro Protein in Specific and Nonspecific Complexes: IMplications for protein Site Recognition and Specificity." Science **266**(12): 1562.

Guthold, M., M. Bezanilla, D. A. Erie, B. Jenkins, H. G. Hansma and C. Bustamante (1994). "Following the Assembly of RNA Polymerase-DNA Complexes in Aqueous Solutions with the Scanning Force Microscope." Biophysics **91**(12): 12927.

Kwak, K. J., H. Kudo and M. Fujihira (2003). "Imaging Stretched Single DNA Molecules by Pulsed-Force-Mode Atomic Force Microscopy." Ultramicroscopy **97**(12): 249.

Kwak, K. J., S. Yoda and M. Fujihira (2002). "Observation of stretched single DNA molecules by Kelvin probe force microscopy." Applied Surface Science **210**(6): 73.

Liu, X., Z. Wu, H. Nie, Z. Liu, Y. He and E. S. Yeung (2007). "Single DNA molecules as probes for interrogating silica surfaces after various chemical treatments." analytica chimica acta **602**(9): 229.

Lyubchenko, Y. L., P. I. Oden, D. Lampner, S. M. Lindsay and K. A. Dunker (1993). "Atomic force microscopy of DNA and bacteriophage in air, water and propanol: the role of adhesion forces." Nucleic Acids Res **21**(5): 1117.

Nakao, H., H. Hayashi, T. Yoshino, S. Sugiyama, K. otobe and T. Ohtani (2002). "Development of Novel Polymer-Coated Substrates for Straightening and Fixing DNA." Nano Letters **2**(5): 475.

Pastre, D., O. Pietrement, S. Fusil, F. Landousy, J. Jeusset, M.-O. David*, et al.* (2003). "Adsorption of DNA to Mica Mediated by Divalent Counterions: A Theororetical and Experimental Study." Biophys J **85**(10): 2507.

Rees, W. A., R. W. Keller, J. P. Vesenka, G. Yang and C. Bustamante (1993). "Evidence of DNA Bending in Transcription Complexes Imaged by Scanning Force Microscopy." Science **260**: 1646.

Reynolds, O. (1883). "An experimental investigation of the circumstances which determine whether the motion of water shall be direct or sinuous, and of the law of resistance in parallel channels." Philosophical Transactions of the Royal Society **174**(6): 935.

Rippe, K., M. Guthold, P. H. von Hippel and C. Bustamante (1997). "Transcriptional activation via DNA-looping: visualization of intermediates in the activation pathway of *E. coli* RNA polymerase x sigma 54 holoenzyme by scanning force microscopy." J Mol Biol **270**(2): 125.

Sacho, E. J., F. A. Kadyrov, P. Modrich, T. Kunkel and D. A. Erie (2008). "Direct Visulaization of Asymmetric Adnine Nucleotide-Induced Conformational Changes in MutLa." Molecular Cell **29**(1): 112.

Schulz, A., N. Mucke, J. Langowski and K. Rippe (1998). "Scanning Force Microscopy of *E. coli* RNA Polymerase-sigma Holoenzyme with DNA in Buffer and in Air." J. Mol. Biol. **283**: 821.

Sweetser, D., M. Nonet and R. A. Young (1987). "Prokaryotic and Eukaryotic RNA Polymerases have Homologous Core Subunits." Proc Natl Acad Sci U S A **84**(5): 1192.

Wang, W., J. Lin and D. C. Schwatrz (1998). "Scanning Force Microscopy of DNA Molecules Elongated by Convectiv Fluid Flow in an Evaporating Droplet." Biophys J **75**(7): 513.

Yang, Y., H. Wand and D. A. Erie (2003). "Quantitative Characterization of Biomolecular Assemblies and Interactions using Atomic Force Microscopy." Methods **29**: 175.

Yildiz, A., J. N. Forkey, S. A. McKinney, T. Ha, Y. E. Goldman and P. R. Selvin (2003). "Myosin V walks hand-over-hand: single fluorophore imaging with 1.5-nm localization." Science **300**(5628): 2061.

Yildiz, A., M. Tomishige, R. D. Vale and P. R. Selvin (2004). "Kinesin walks hand-over-hand." Science **303**(5658): 676.

APPENDIX A:

SOURCES OF PROTEINS AND TEMPLATE DNA

A.1 Proteins and DNA

Wild-type His_6-tagged RNAP was prepared and purified from log phase *E. coli* strain RL916 (a gift from Robert Landick) using published procedures (Uptain *et al.*, 1997). Wild-type His_6-tagged *Taq*MutS was prepared and purified from the BL21 cell strain using the previously published protocols (Biswas *et al.*, 1999; Clark *et al.*, 1999; Schofield *et al.*, 2001) The 550 bp DNA template was derived from pDE13 plasmid and purified by a Qiagen Miniprep Kit (Qiagen). Transcription template DNA was amplified by PCR and contains the λP_R promoter. The 550 bp PCR product was biotinylated on one end using modified primers.

BIBLIOGRAPHY

Biswas, I., C. Ban, K. G. Fleming, J. Qin, J. W. Lary, D. A. Yphantis*, et al.* (1999). "Oligomerization of a MutS mismatch repair protein from Thermus aquaticus." J Biol Chem **274**(33): 23673.

Clark, A. B., M. E. Cook, H. T. Tran, D. A. Gordenin, M. A. Resnick and T. A. Kunkel (1999). "Functional analysis of human MutSalpha and MutSbeta complexes in yeast." Nucleic Acids Res **27**(3): 736.

Schofield, M. J., S. Nayak, T. H. Scott, C. Du and P. Hsieh (2001). "Interaction of Escherichia coli MutS and MutL at a DNA mismatch." J Biol Chem **276**(30): 28291.

Uptain, S. M. and M. J. Chamberlin (1997). "*Escherichia coli* RNA Polymerase Terminates Transcription Efficiently at Rho-independent Terminators on Single-stranded DNA Templates." Proc Natl Acad Sci U S A. **94**(25): 13548.

APPENDIX B:

RevMAPP CONTROLS

B.1 Boiling Control

Once SECs were eluted from the matrix, we found it necessary to briefly boil the complexes in formamide to ensure that the RNA and NTPs dissociated from the RNAP. In early experiments, we commonly noticed that multiple bands appeared near the migrating NTPs on 8 M urea-20 % polyacrylamide gels. We hypothesize that the NTPs were being thermally degraded into NDPs and NMPs. Figure B.1 shows where [α-^{32}P]-UTP could have been broken into UDP and free phosphate. Compared with UTP, the decrease in phosphate moieties on UDP was consistent with shorter migration away from the negative electrode. In figure 3.2, we show that boiling NTPs for 30 sec in transcription buffer and formamide at 90°C did not severely degrade the molecules, while longer boiling times (90 sec) clearly broke the NTPs into multiple fragments. The same behavior was observed alpha phosphate labeled with ATP and GTP. With [γ-^{32}P]-NTPs, the fragments were not observable, as expected. When released, the radiolabeled gamma phosphate ran down the gel much faster than the remaining nucleotide. We determined that over boiling of gamma labeled NTPs especially needed to be avoided so that NTP-SEC stoichiometries were not underestimated.

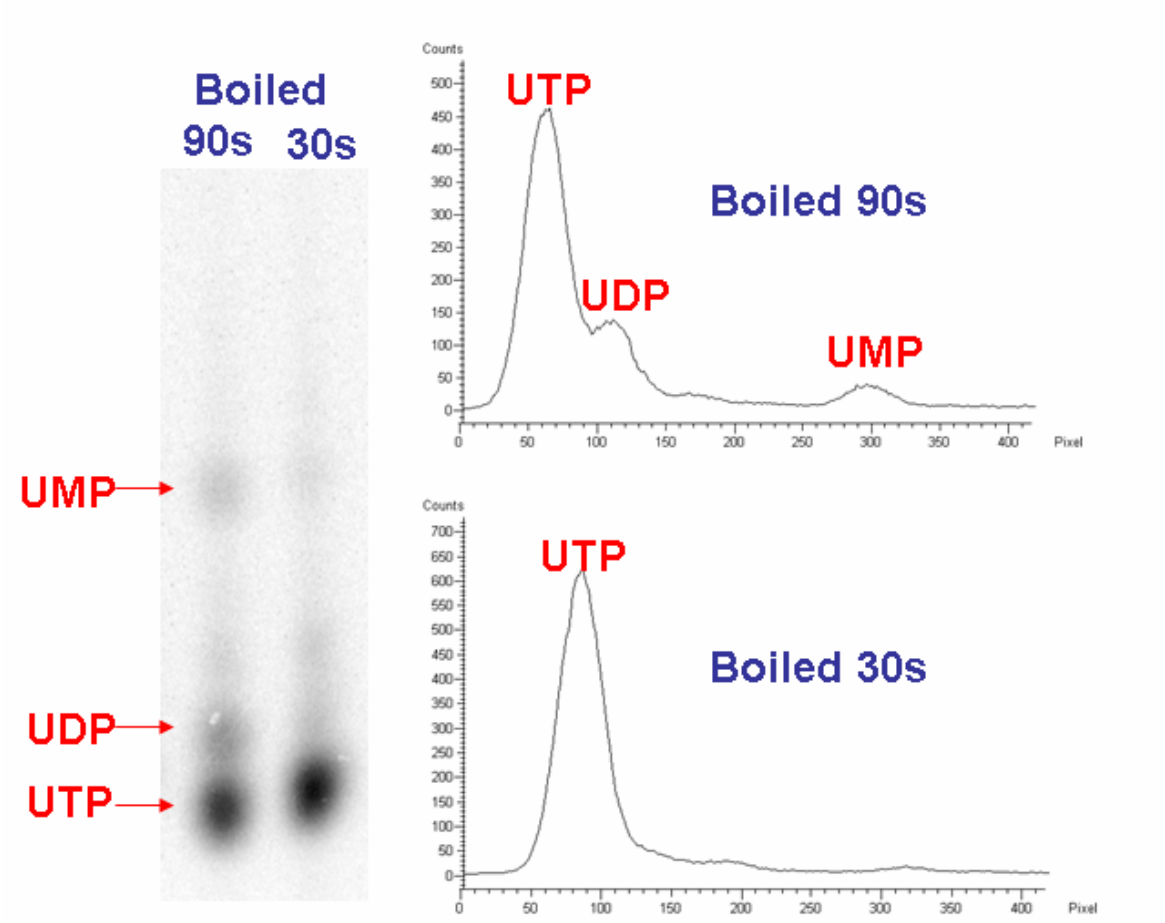

Figure B.1 Over Boiling Thermally Degrades NTPs. We observe multiple peaks with PAGE analysis of UTP that has been boiled longer than 30 sec.

B.2 RNAP(-) Controls

As with all bead matrices, we found that NTPs nonspecifically bind to the UltraLink monomeric avidin coated support. These NTPs would slough off from the beads into solution under conditions typically used to dissociate SECs for PAGE analysis, including formamide quench, 1 M hydrochloric acid (HCl) quench, and elevated temperature conditions (above 70°C). Before quenching or boiling of any type.

We determined that the original reaction test tube was also a significant source of background. Scraping the walls of the test tube with a pipette tip was sufficient to liberate non-specifically absorbed radioactive NTPs into the analyte solution. Along with delicate sample care, we always transfer the purified matrix into a second reaction tube that had not been exposed to a high quantity of radionucleotides.

The acceptor (*A*) in this work was the stalled elongation complex, which could not be formed without RNAP. Since the sources of nonspecific background were often unidentifiable (beads, tips, tubes etc), we found it necessary to validate every experiment we report here with a simultaneous RNAP- control. Figure B.2 shows a gel from an experiment that passed the RNAP- control, and one of many that failed. Greater than 75 % of the experiments in this work are not reported due to RNAP- control failure. Each of these failures assisted us in identifying detrimental sources of background and helped to solidify the basic RevMAPP method. Lanes 1 through 4 in the gel in figure 3.3 correspond to line graphs 1 though 4. Lanes 1 and 2 are SECs synthesized with [α-^{32}P]-ATP. We calculated ATP-SEC ratio in lane 1 to be 0.93. The ATP-SEC stoichiometry experiment was performed simultaneously with a control solution not containing RNAP. Lane 3 is the RNAP- control for the lane 1 experiment. The lane 3 RNAP- control revealed a noticeable source of

background signal, therefore the ATP-SEC ratio from lane 1 over estimated the amount of ATP bound to the SECs. The ATP-SEC ratio from lane 2 however, is 0.24. The accompanying RNAP- control for the lane 2 experiment is shown in lane 4, which revealed no observable ATP over the noise.

We found that in some cases, the RNAP- control signal in could be subtracted from the observed stoichiometry. Lane 3 was subtracted from lane 1 to reveal an ATP-SEC stoichiometry of 0.25 in figure B.2, validating the consistency of the RNAP- control. In most cases however, RNAP- control failure revealed background NTP noise much higher than shown in lane 3, preventing us from regularly making a confident background subtraction.

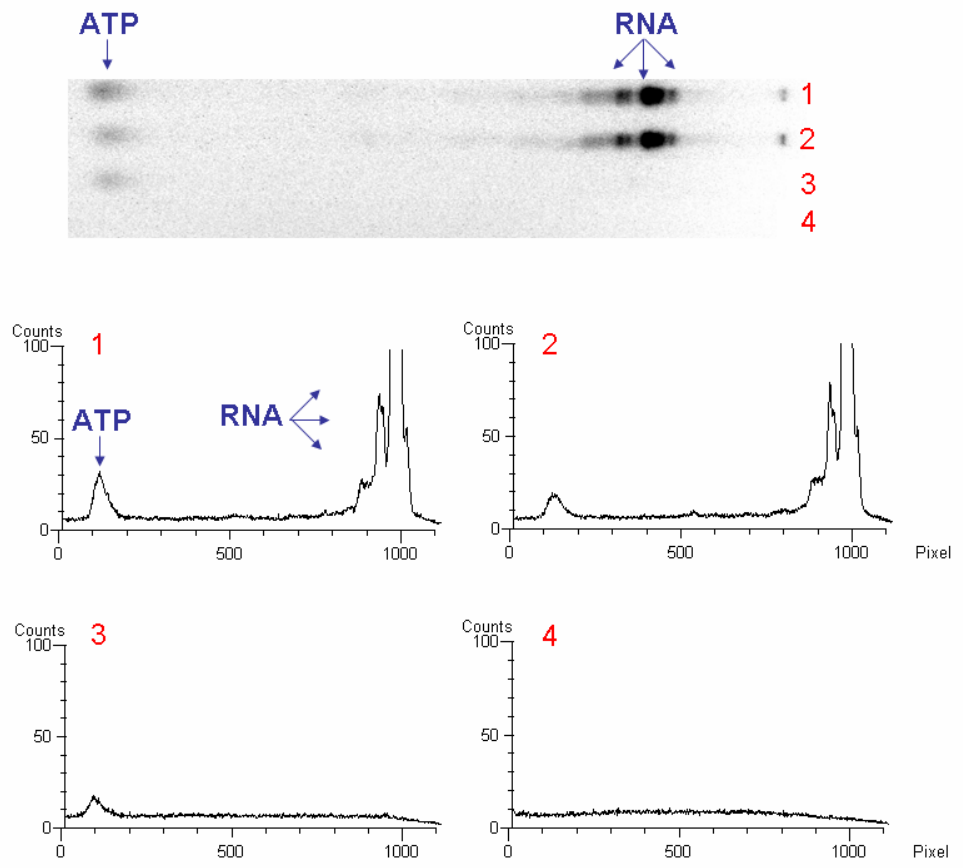

Figure B.2 The RNAP- Control Validates the RevMAPP Protocol. Lanes 1 and 3 are the ATP-SEC analysis and RNAP- control, respectively. The lane 1 experiment does not pass the lane 3 control. Lanes 2 and 4 show an ATP-SEC experiment with no observable background contribution.

B.3 Staggered Gel Loading and Transcript Distribution Controls

Analysis of the RNA chain length was also important for all types of NTP-SEC analysis. At position 25 of the DE13 template, C then A are the next templated nucleotides. As described earlier, the *i*+1 and *i*+2 nucleotides have direct roles in the states of transcription (Holmes, 2002; Kennedy, 2007). We needed to verify in every experiment that that the majority of the ternary complexes were in the same downstream template DNA sequence context to guarantee acceptor homogeneity. Figure B.3 displays the motif for all PAGE analyses in our work. To analyze the RNA chain length of denatured SECs, an 8 M urea 20 % polyacrylamide gel was run for 8 hrs at 55 W. After 4 hrs of transcript separation, we loaded additional fractions of the same samples on the gel to separate the bulk transcript form nucleotides. Our staggered loading strategy allowed us to comprehensively quantify the ternary complex template positions while simultaneously analyzing the NTP-SEC ratios. Only ternary complex preparations containing more than 75 % of stalls at a C-A sequences were included in our quantitative measurements; all other SEC batches were disqualified from analysis. Many batches of SECs showed the misincorporation of U for C at positions 25 and sometimes 28, leaving populations of complexes stalled at positions 27 and 29. It happens that positions 30-31 are also C-A: we considered these to be the "same" acceptor as those stalled at position 24 due to their similar downstream DNA sequence contexts. Staggered gel loading also assisted us in developing corollaries between catalytic actively, irreversible NTP binding and NTP displacement. For example, in figure B.3 we observed about 45 % of the SECs incorporated CMP in lane 2. A corresponding ~45 % of bound ATP was no longer present after walking with CTP as seen in lane 7.

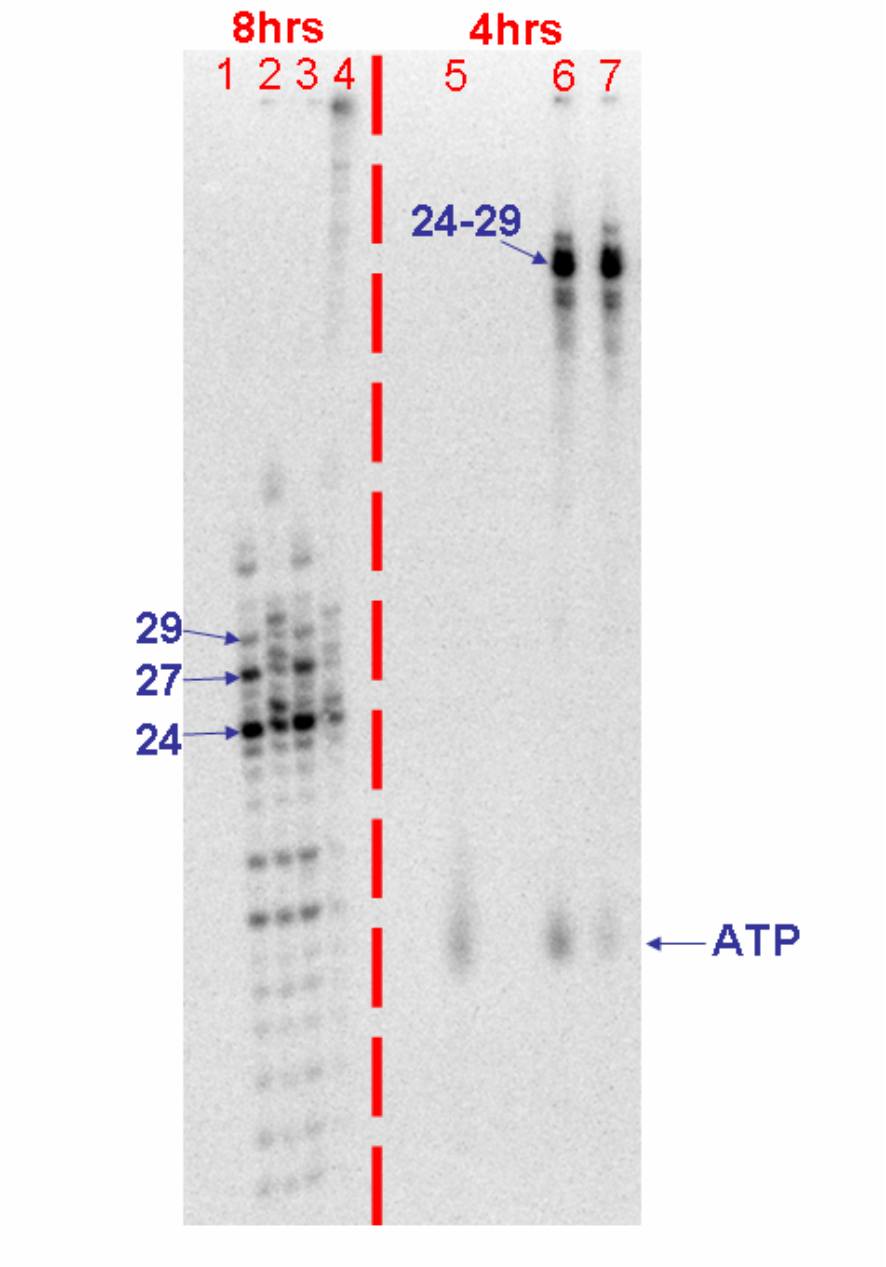

Figure B.3 Simultaneous Analysis of RNA Chain Length Distribution and NTP-SEC ratios. The lanes on the left were run twice as long as the lanes on the right. Lanes 1, 3 and 7 are all the same [α-^{32}P]-ATP labeled RevMAPP purified SECs. Lanes 2 and 7 are SECs that have been walked to position 26 *via* the addition of 30μM CTP. Lane 5 is a dilute sample of ATP only to help identify the bands in lanes 6 and 7. Lane 4 contains SECs that had been given high concentrations of all four NTPs to assay that enzyme's ability to

transcribe the sequence all the way to completion. Staggered gel loading identified SEC batches that were no primarily stalled at C-A template positions and allowed for the disqualification of about 50 % of experiments.

B.4 Equilibrium Binding Control

The passive rates of GTP dissociation observed in Table 3.2 suggest that the addition of GTP to SECs during a titration could not possibly reach equilibrium in one minute of incubation. Still, we observed a binding dependence on GTP concentration that suggested equilibrium binding. To determine whether or not the K_D experiment was in fact assaying a *different* site that which GTP is tightly bound to SECs after initial purification, we followed the classic "cold competition" check describe frequently. The addition of a high concentration of cold competitor will actively displace labeled bound to an acceptor in a specific manner, provided the incubation time is shorter that the time needed to reach equilibrium binding (Winzor *et al.*, 1995).

We prepared two aliquots of ATP labeled, purified SEC as shown in Figure 3.6. We added 30 μM radiolabeled GTP into the first aliquot, allowed the solution to incubate for one min and followed the remained for the Figure 3.6 protocol. To the second fraction, we added 30 μM GTP, waited one minute, and then added 1 mM unlabeled GTP. After one min, we washed the SEC and followed the remained of the protocol in Figure 3.6. We found that no GTP was bound to the complexes that we tested with the classic cold competitor experiment.

In addition, we picked the order of titration at random to avoid any possible experimental error associated with the various times SEC fractions sat on ice. To identify potential variances related to complexes waiting on ice for > 2 hrs, we performed the 25 μM concentration first, and repeated the 25 μM data point after the titration was complete (Figure 3.15). More than one hour elapsed between the elapsed between the first and final additions of 25 μM GTP.

BIBLIOGRAPHY

Holmes, S. (2002). Downstream DNA Sequence Effects on Transcription Elongation: NTP Binding Induces Translocation Via A Ratchet Motion. Chemistry. Chapel Hill, University of North Carolina at Chapel Hill. **Ph.D.**

Kennedy, S. R. (2007). Modulation of Transcription Elongation via the Main Channel in Eschericia coli RNA Polymernase. Chemistry. Chapel Hill, NC, University of North Carolina at Chapel Hill. **Ph.D.:** 162.

Winzor, D. J. and W. H. Sawyer (1995). Quantitative Characterization of Ligand Binding. New York, John Wiley and Sons, Inc.